2020 年度 課程博士学位論文

Defect in chromosome alignment is a novel mechanism underlying ALK inhibitor-induced suppression of cell proliferation

染色体整列異常は ALK 阻害により誘導される
細胞増殖阻害の新規メカニズムである

Sirajam Munira

Department of Biochemistry & Molecular Biology
Kyoto Pharmaceutical University

This thesis (Chapter 1, 2, 3) contains the data from the following paper:

Sirajam Munira, Ryuzaburo Yuki, Youhei Saito and Yuji Nakayama.
ALK Inhibitors-Induced M Phase Delay Contributes to the Suppression of Cell Proliferation.
Cancers, 2020, *12*, 1054,
doi: 10.3390/cancers12041054.

Table of contents

Abbreviations

A/T	Anaphase/Telophase
ALCL	Anaplastic large-cell lymphoma
ALK	Anaplastic lymphoma kinase
APC/C	Anaphase promoting complex/cyclosome
BubR1	Budding uninhibited by benzimidazole related 1
Bub3	Budding uninhibited by benzimidazole 3
BSA	Bovine serum albumin
Cdc	Cell division cycle
CDK1	Cyclin-dependent kinase 1
CIN	Chromosomal instability
Cyto	Cytokinesis
DMEM	Dulbecco's modified Eagle's medium
DMSO	Dimethyl sulfoxide
EGFR	Epidermal growth factor receptor
EML4	Echinoderm microtubule-associated protein-like 4
ERK	Extracellular-signal-regulated kinase
FBS	Fetal bovine serum
FDA	The Food and Drug Administration
HA	Human influenza hemagglutinin
HRP	Horseradish peroxidase
IC_{50}	Half maximal inhibitory concentration
IF	Immunofluorescence
IGF1R	Insulin-like growth factor 1 receptor
IR	Insulin receptor
JAK2	Janus kinase 2
Knl1	kinetochore scaffold 1
KRAS	Kirsten rat sarcoma (oncogene homolog)
LDL	Low-density lipoprotein
M	Metaphase
MAD2	Mitotic arrest defect
MAPK	Mitogen-activated protein kinase
MCC	Mitotic checkpoint complex
Mps1	Monopolar spindle 1
NB	Neuroblastoma

NPM1	Nucleophosmin1
NSCLC	Non-small cell lung carcinomas
ORF	Open reading frame
ORR	Overall response rate
P/PM	Prophase/Prometaphase
PBS	Phosphate-buffered saline
PFS	Progression-free survival
PI3K	Phosphoinositide 3-kinase
PLK1	Polo-like kinase 1
PVDF	Polyvinylidene difluoride
RTK	Receptor-type tyrosine kinase
SAC	Spindle assembly checkpoint
SDS	Sodium dodecyl sulfate
siRNA	Small interfering RNA
TM	Trans-membrane domain
UTR	Untranslated region
WB	Western blotting
WST-8	Water soluble tetrazolium-8
WT	Wild-type

Abstract

Introduction

Receptor-type tyrosine kinases are the most prevalent therapeutic targets in anti-cancer drug development as they are aberrantly activated in a wide range of cancers. The receptor-type tyrosine kinase, anaplastic lymphoma kinase (ALK) is a member of the insulin receptor superfamily and is especially highly expressed in neonates and in the developing central and peripheral nervous system. Genetic alterations of ALK, such as gene amplification, fusion, and mutation, have been found in different cancers and ALK inhibitors have been approved for the treatment of non-small-cell lung carcinoma. Although these inhibitors suppress proliferation and induce apoptosis of cancer cells via the inhibition of the MEK/ERK and the PI3K/AKT pathways, resistance to these treatments is generally developed. Understanding the precise mechanism for suppressing the proliferation will enable an improved polytherapy to overcome the resistance. Therefore, novel mechanisms that suppress cell proliferation were explored. In this study, the effects of ALK inhibition by various inhibitors as well as ALK-targeted siRNAs (siALKs) on cell division were evaluated and the mechanism of action in neuroblastoma and lung cancer cells was investigated.

Chapter 1: ALK inhibition by inhibitors and knockdown causes delay in the early M phase

The ALK inhibitors, crizotinib, ceritinib, and TAE684 showed a concentration-dependent reduction in the proliferation of the neuroblastoma SH-SY5Y cells. To examine the effect on M-phase progression, cells were treated with inhibitors at around IC_{50} concentration for 1 h after release from arrest at the G2/M border caused by the CDK1 inhibitor RO-3306. The M phase is a process in which duplicated chromosomes are divided equally into two progeny cells and comprises 5 subphases: prophase (P), prometaphase (PM), metaphase (M), anaphase (A), and telophase (T), and followed by cytokinesis (Cyto) that splits cytoplasm. Based on microtubule and chromosome morphologies, the cells were classified into four groups: P/PM, M, A/T, and Cyto. Most control cells progressed to cytokinesis in an hour after release from the arrest at the G2/M border whereas the M-phase progression of ALK inhibitors-treated cells was largely delayed in P/PM. Interestingly, a significant percentage of cells showed the misalignment of chromosomes upon inhibitor treatment, indicating the involvement of ALK in chromosome alignment. The western blotting analysis revealed that the autophosphorylation of ALK was almost completely abolished by inhibitors, indicating an inhibition of the kinase activity. Three different siALKs were used to knockdown ALK expression and caused delay in P/PM/M, excluding the off-target effects of inhibitors. Furthermore, the ALK knockdown-induced delay

was suppressed via the re-expression of siALK-resistant ALK. Taken together, these results suggest that ALK is involved in the chromosome alignment in M phase and that ALK inhibition-induced delay in the early M phase may partly contribute to the suppression of cell proliferation.

Chapter 2: Delays in the early M phase and anaphase onset are accompanied by SAC activation

Proper chromosome segregation is achieved through several critical processes, such as the duplication of sister chromatids, spindle formation, kinetochore-microtubule attachment, and alignment of chromosomes at the mitotic equator. To find out the mechanism of ALK knockdown-induced delay in the early M phase, inhibitor- or siALK-treated cells were synchronized with RO-3306 and subsequently observed every 3 min for 5 h under time-lapse imaging. Hoechst 33342 was used to stain DNA for monitoring chromosome movement. The M-phase cells were classified into three stages based on chromosome morphology: P/PM, M, and A/T. In the control cells, the average duration of P/PM and M were 31 and 26 min, respectively. In sharp contrast, crizotinib treatment extended the duration of P/PM and M to 74 and 83 min, respectively. Likewise, it took siALK-treated cells 63 and 40 min to complete P/PM and M, respectively. 16% of siALK-treated cells failed to complete the M phase within 5 h. These results suggest that ALK downregulation hampers the chromosome alignment and thereby delays the onset of anaphase. Moreover, abnormal M-phase characteristics, such as spindle misorientation and chromosome misalignment were observed. Chromosome misalignment can be caused bt a defect in spindle formation and can activate the spindle assembly checkpoint (SAC). To confirm whether the delay in the early M phase was accompanied by SAC activation, the SAC components, the Mps1 kinase and the MAD2, were inhibited by an inhibitor and siRNA, respectively, and then cells were treated with crizotinib. In both conditions, crizotinib-induced delay in the anaphase onset was not observed and most of the cells progressed to cytokinesis within 1 h after release from the G2/M arrest. These findings indicate that SAC is responsible for the delay in the anaphase onset in ALK-inhibited cells.

Chapter 3: Inhibition of the EML4-ALK fusion protein causes delay in the M phase

The EML4-ALK fusion protein is one of the major oncoprotein identified in non-small-cell lung cancer. The non-small-cell lung cancer H2228 cells express the EML4-ALK fusion and have been used in preclinical cancer research. These cells are relatively resistant to crizotinib compared to EML4-ALK-expressing H3122 cells. In general, EML4-ALK triggers both the PI3K-AKT and MEK/ERK pathway and sustains this survival and proliferative signaling. However, the MEK/ERK pathway is activated independently of EML4-ALK in H2228 cells.

Therefore, as a model of drug-resistant cancer cells, H2228 cells were used to examine whether ALK inhibitor affected the M-phase progression.

H2228 cells were treated with TAE684 at around IC_{50} and observed under time-lapse imaging for 12 h. The average duration of P/PM in control cells was 30 min, whereas this was prolonged to 130 min in TAE684-treated cells. Furthermore, the M phase was completed by only 40% of the cells, while the remaining cells either continued the M phase during the observation, prematurely exited, or died in the M phase. Western blotting analysis showed that the phosphorylation of EML4-ALK was suppressed. These results suggest that inhibition of EML4-ALK causes the defect of the M-phase that may partly contribute to the suppression of the H2228 cell proliferation.

Conclusion

The inhibition of ALK or EML4-ALK disrupts cell division through delays in the early M phase and anaphase onset. The latter is caused by SAC activation to which defects in chromosome alignment and spindle orientation lead. These results conclude that ALK is a novel regulator of the M phase and the delay in the M-phase progression is a novel mechanism that underlies the ALK inhibitor-caused suppression of cell proliferation. Understanding the mechanism of action of ALK inhibitors will undoubtedly support to the develop new therapeutic approaches.

Introduction

Anaplastic lymphoma kinase (ALK) contributes to the oncogenesis

Anaplastic lymphoma kinase (ALK), a receptor-type tyrosine kinase (RTK), belongs to the insulin receptor (IR) superfamily. It possesses a typical RTK structure that consists of an extracellular ligand-binding domain, a transmembrane domain (TM), and an intracellular kinase domain [1,2]. The tyrosine kinase domain of ALK shows a high level of similarity with that of the IR, whereas ALK extracellular domain is unique among the RTK family as it consists of a glycine-rich region (G-rich), a low-density lipoprotein receptor domain (LDL), as well as two receptor protein tyrosine phosphatase mu (MAM) domains (Fig. 1) [2,3]. The human *ALK* gene is located at chromosome 2p and encodes a 180-kDa polypeptide. The polypeptide undergoes post-translational modification, such as N-glycosylation, generating approximately 220-kDa ALK containing 1620 amino acids [2,4–6].

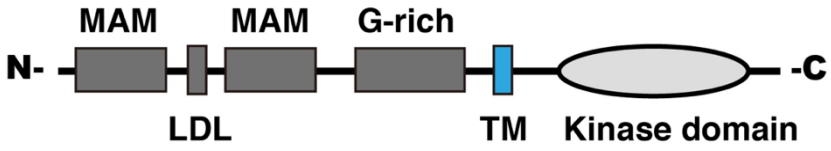

Figure 1. Structure of full-length ALK. Full-length ALK consists of 1620 amino acid residues. The extracellular domain of ALK consists of an N-terminal signal peptide (1–18 amino acids), two MAM domain (264–427, 480–626 a.a), an LDL domain (453–471 a.a), and a glycine-rich region (816–940 a.a). The intracellular domain is composed of a tyrosine kinase domain (1116–1392 a.a) and the juxtamembrane region (1060–1115 a.a.).

ALK is expressed in neonates during the development of the nervous system [4]. It is found in discrete areas of the developing central and peripheral nervous systems [1]. Conversely, in an adult mammal, ALK expression is found at a relatively low level in a certain region of few organs such as the hippocampus within the brain [4,7]. Consistent with its expression profile, mammalian ALK plays a regulatory role in the function of the nervous system during the development [4,8]. ALK may also regulate mammalian behavior [8]; however, it's direct biological role is still not completely clarified. Like other RTKs, the activation of ALK is presumed to occur through ligand binding and receptor dimerization. Several proteins have been reported as a ligand of ALK such as pleiotrophin, midkine, augmentor-α and β [9–11]. As the expression of ALK is predominant in the nervous system, it was suggested by researchers that ALK can serve as a receptor for neurotrophic factors [12].

In 1994, ALK was first discovered as an NPM1-ALK fusion protein in the anaplastic large-cell lymphoma (ALCL) cell line [13]. Chromosomal translocation between nucleophosmin 1 (*NPM1)* and the *ALK* gene generates oncogenic ALK fusion proteins. Although the ALK expression cannot be found in normal lymphoid cells, the vast majority of pediatric ALCL patients are ALK-positive [13,14]. Later in 2007, EML4-ALK, another prominent ALK fusion was discovered in non-small-cell lung carcinoma (NSCLC) by a group of Japanese researchers[15]. Expressions of aberrant ALK in the form of amplification, gene fusion, and mutation with gain of function have been identified in different cancers. Activating mutations in the kinase domain at R1275, F1174, and F1245 positions, and gene amplification have been reported in pediatric cancer neuroblastoma (NB) [16,17]. Other than NSCLC, ALK gene fusion is also identified widely in inflammatory myofibroblastic tumors, diffuse large B-cell lymphoma, and esophageal squamous cell, colorectal, breast carcinomas [14,18]. Moreover, alternative ALK transcript (ALK^{ATI}) is found in melanomas [19].

Though the exact mechanism of activation of full-length ALK is still not completely understood, genetically altered ALK remains constitutively active via activating mutations or the dimerization of their fusion partners. There are similarities and differences in ALK-triggered signaling among different forms of ALK where the signaling depends on subcellular localization, protein stability, the difference in fusion partners, and tumor cell types [20,21]. In general, ALK activates multiple signaling pathways, such as the RAS/MEK/ERK [22], PI3K-AKT [23], CRKL-C3G [24], JAK-STAT [25], and the MEKK2/3-MEK5-ERK5 pathways (Fig. 2).

Moreover, activation of adaptor proteins and other cellular proteins, such as PTPN11, Src, FRS2, Shc-GRB2, IRS2, GSK-3a, and FAK, has been observed as downstream signals of ALK, suggesting that ALK may play roles in alternative pathways [26]. ALK regulates several cellular functions, such as cell proliferation [27], survival [28], migration [29], cytoskeletal rearrangement [30], and so on. In neuroblastoma, activating ALK mutations lead to greater cell proliferation, resistance to apoptosis, and the enhancement of DNA synthesis [17,31], thereby contributing to oncogenesis.

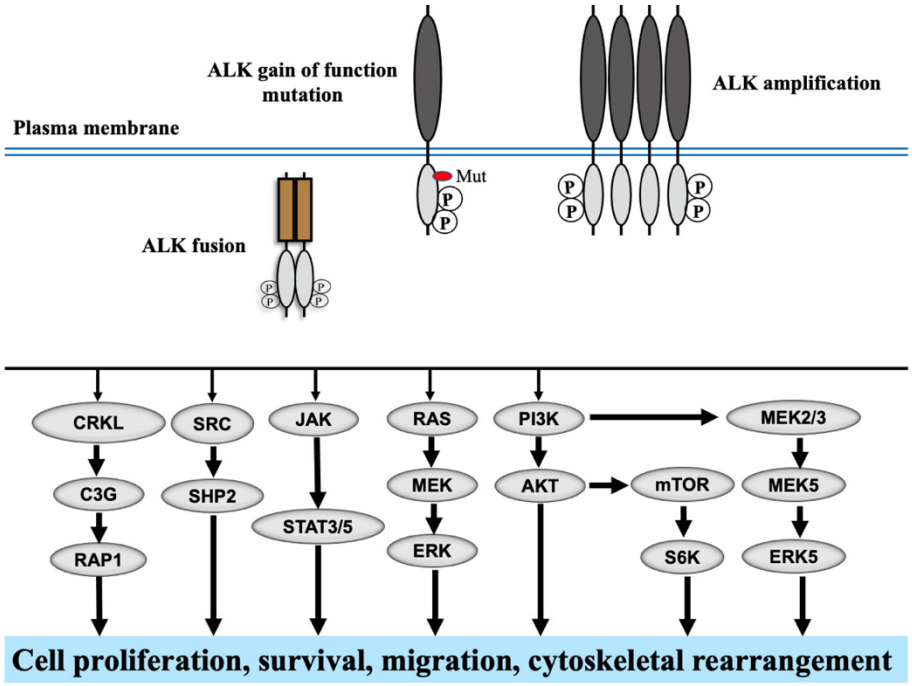

Figure 2. ALK-mediated cellular signaling pathways. Activated ALK stimulates several downstream signaling pathways and thereby regulates different cellular processes such as cell proliferation, survival, migration, cytoskeletal rearrangement, and so on.

Targeting ALK with inhibitors to treat cancer and the development of resistance against inhibitors

Over the last decade, ALK has become an attractive target for the development of small-molecule inhibitor-based anticancer drugs. The discovery of oncogenic EML4-ALK in NSCLC brought a new possibility of an effective clinical therapy through targeting ALK with inhibitors. Recently, ALK inhibitors showed a great breakthrough in the treatment of NSCLC. Gene profiling in the ALK inhibitor-treated NSCLC xenograft model identified modulation of gene expression involved in several critical cellular processes. The downregulation of genes regulating different aspects of cell cycle such as the *CDC2, CDC7*, and *CDK4* (involved in promoting the G1 to S phase transition), *TOP2A* (chromosome condensation), *PTTG* (chromatid separation), *BUBs* (spindle checkpoint functions) was observed, while the upregulation of the expression of proapoptotic proteins was also identified [32]. In preclinical studies, ALK kinase inhibitors showed downregulation of survival signaling pathways and apoptosis in EML4-ALK expressing NSCLC [33,34]. Crizotinib, an ATP analog inhibitor of ALK was the first inhibitor approved by the U.S. Food and Drug Administrator (FDA) for the treatment of ALK-positive NSCLC in 2011 [35]. It was reported that crizotinib was superior to the standard first-line chemotherapy using pemetrexed and cisplatin. Crizotinib significantly improved the overall

response rate (ORR) and progression-free survival (PFS) [36,37]. Although crizotinib shows excellent activity in NSCLC patients, a resistance that leads to disease progression is developed within a year after crizotinib treatment. In these patients, mutations that lead to the development of resistance in EML4-ALK are frequently observed. Approximately 30% of crizotinib-resistant NSCLC patients possess a mutation in the tyrosine kinase domain [38]. Most crizotinib-resistant tumors still depend on ALK-triggered signaling and are sensitive to more potent, second-generation ALK inhibitors having distinct structures [14]. The second-generation ALK inhibitors, ceritinib, alectinib, brigatinib were developed to be effective against tumors having resistance to crizotinib. These ALK inhibitors show potent and durable activity in NSCLC. Ceritinib showed 20 times more potency to inhibit ALK compared to crizotinib. In preclinical studies, ceritinib efficiently inhibits ALK having mutations developed by crizotinib treatment [39]. Despite that, the development of resistance against second-generation inhibitors promoted the invention of the third-generation inhibitors having a more potent ability to inhibit mutants generated in response to second- generation inhibitors. One such inhibitor is Loratinib that is capable of overcoming all existing ALK mutants resistant against ALK inhibitors [40].

In general, cancer cells develop resistance against ALK inhibitors through several mechanisms. The mutation and amplification of ALK are most frequently observed in ALK resistant cancer cells [41,42] . Activation of other signaling pathways, such as the activation of other tyrosine kinases including EGFR [43] and IGF1R, bypasses the requirement of ALK. Besides, focal amplification of KRAS and reduced levels of MAPK phosphatase DUSP6 [22] have been reported to impart resistance against ALK inhibitors (Fig. 3). Overcoming resistance is a critical challenge to ALK-targeted therapies and most studies have focused on the development of next-generation ALK inhibitors. However, understanding the regulatory role of ALK in critical cellular processes, such as cell proliferation will enable the development of novel strategies of ALK-targeted therapy.

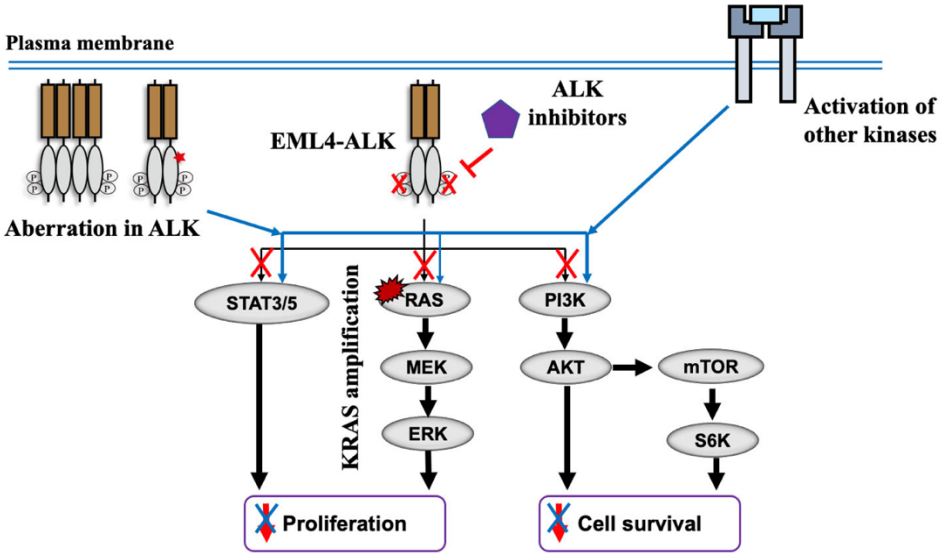

Figure 3. Mechanisms of development of acquired resistance. Cancer cells can develop resistance against ALK inhibitors through one or more resistance mechanisms including aberration in ALK (amplification or additional mutation), activation of other receptor tyrosine kinases (EGFR, IGFR, PDGFR, etc.), focal amplification of KRAS. Cancer cells achieving such resistance can proliferate over inhibitor treatment.

Purpose of this study

As ALK is expressed exclusively in the nervous system during development but not abundantly in adults, it becomes a promising molecular target for targeted-therapy in cancers expressing oncogenic ALK. To date, several small molecule inhibitors of ALK have been developed and used for cancer therapy, especially in the treatment of NSCLC. These inhibitors mainly suppress cell proliferation and/or induce apoptosis. However, resistance is developed against ALK-targeting inhibitors due to the heterogeneous nature of the cancer cells. Though several approaches have been taken into account to eliminate resistance; achieving potential therapeutic outcomes is still far behind. In this context, understanding the molecular mechanisms of ALK regulating cellular processes such as cell proliferation is required to improve the treatment of these cancers, for instance, to develop effective polytherapy against cancers.

In our laboratory, a wide screening of active compounds including small molecule inhibitors of RTKs has been performed to find out compounds affecting M-phase progression. This screening shows that crizotinib, a small molecule inhibitor of ALK, delays the M-phase progression. The M phase is the most crucial event of the cell cycle and is required for cell proliferation. Based on the effect of ALK inhibitor on the M phase, it was assumed that ALK may regulate cell proliferation by regulating M phase. Therefore, the purpose of this study is to demonstrate the effect of ALK inhibition on M phase and the underlying mechanisms for understanding the precise mechanisms underlying the ALK-induced suppression of cell proliferation.

Chapter 1: ALK inhibition by inhibitors and knockdown causes delay in the early M phase

1-1. Introduction

SH-SY5Y is a type of human neuroblastoma (NB) cell line. NB is a malignancy of the sympathetic nervous system accounting for about 9–10% of pediatric cancer mortality [44]. A genome-wide analysis of primary NB revealed a high level of amplification and mutation of the *ALK* gene, which may contribute to oncogenicity [16]. Mutation in the tyrosine kinase domain of ALK accounts for 8–10% of NB [44]. SH-SY5Y cells harbor both wild-type (WT) ALK and ALK F1174L mutation activating the kinase [16,45]. These cells are sensitive to ALK inhibitors and suppression of ALK expression results in apoptosis and impaired cell proliferation [16].

Our screening of active compounds showed that crizotinib affects M-phase progression. Crizotinib is a multi-targeted RTK inhibitor and able to inhibit ALK, c-Met, and ROS1 tyrosine kinases. However, crizotinib showed 20 times more selectivity toward ALK compared to c-Met and other RTKs [46]. The role of ALK in the pathophysiology of many cancers is well recognized. Inhibition of ALK kinase activity using small molecule inhibitors has been found to have potent antitumor efficiency [39,47,48]. Until now, the efficacy of ALK inhibitors has been widely investigated through targeting fusion ALK such as NPM-ALK and EML4-ALK. However, the effect of ALK inhibitors on mutants having oncogenic gain-of-function mutation and amplified ALK has not been sufficiently investigated yet. We hypothesized that crizotinib caused M-phase delay through the inhibition of ALK. To investigate this, the effects of ALK inhibition using inhibitors and siRNAs on M-phase progression were evaluated in SH-SY5Y cells.

Cell division is a process in which a parent cell divides into two genetically identical daughter cells. It comprises the division of replicated chromosomes, cytoplasm, and organelles through a series of regulated events. Among the cell cycle phases (G1, S, G2, and M), the M phase is the most dramatic period consisting of 5 subphases: prophase, prometaphase, metaphase, anaphase, and telophase, followed by cytokinesis. Each subphase has distinguishing features regarding the chromosome and microtubule morphologies. A representative illustration of each subphase is shown in Figure 4.

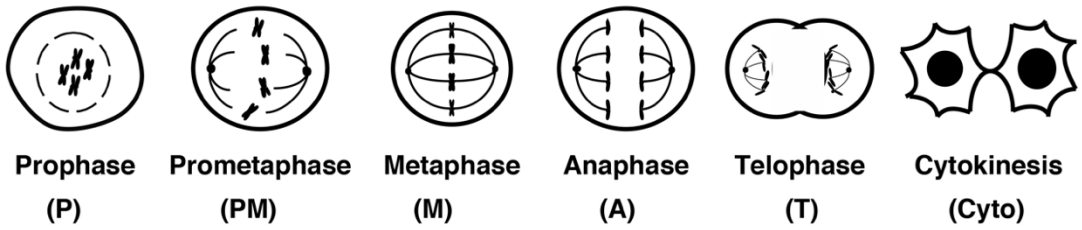

Figure 4. Morphological changes of chromosomes and microtubules in different subphases from mitotic entry to the division of cytoplasm. Illustration of cells in 5 subphases and cytokinesis.

Prophase can be defined by condensed and visible chromosomes. In prometaphase, kinetochore is formed around the centromere and spindle formation begins. Chromosomes are moving to the equatorial region of cells by motor proteins and microtubule dynamics. Metaphase is characterized by that all chromatids are lined up at the cell equator and attached to the microtubules emanated from both poles. Then, the sister chromatids are separated and pulled to the opposite sides of the cell in anaphase. Telophase is characterized by the de-condensation of chromosomes, the formation of two nuclei in opposite sides of the cell, and broken spindle. The cell begins to split into two at cytokinesis where cytoplasmic components are divided into two daughter cells.

To analyze the M phase, cells can be synchronized by inhibiting CDK1 that is essential for mitotic entry and progression through the M phase [49]. RO-3306 is a reversible inhibitor of CDK1. When cells are treated with RO-3306, cells are arrested in the G2/M border. After release from the arrest by washing RO-3306 out, cells can synchronously enter the M phase. Approximately 30% of cells can be synchronized in the M phase through this method. After the release, fixation of cells at different times allows the evaluation of the M-phase progression and the visualization of cells in different subphases [50]. For instance, at 30, 45, and 60 min after the release from RO-3306 treatment, the M phase mainly progresses to metaphase, anaphase, and cytokinesis, respectively, as shown in the following illustration in Figure 5. Several advantages are taken into account for RO-3306 synchronization over other synchronization methods, such as simple single-step protocol, efficient synchronization, immediate entry into mitosis after release, and no effect on the microtubule dynamics [51].

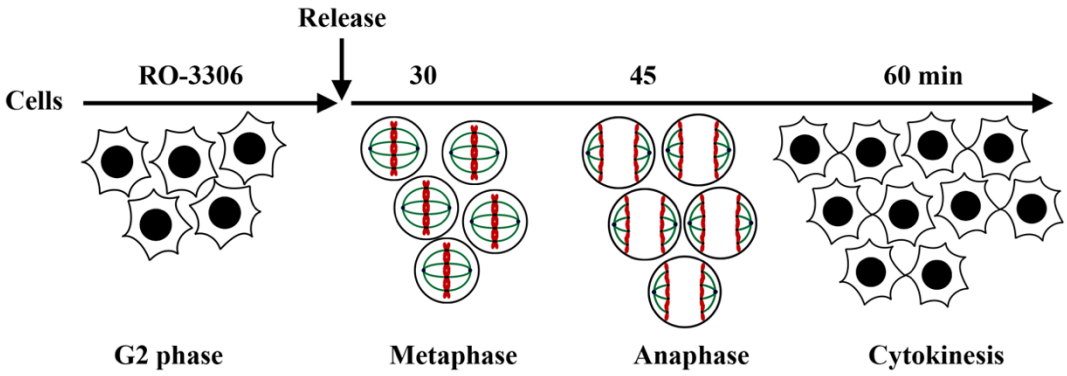

Figure 5. Synchronization of cells with the CDK1 inhibitor RO-3306. Cells are treated with RO-3306 to synchronize cells at G2 to M phase border. At different times, such as 30, 45, and 60 min after release, the majority of the M-phase cells are found in metaphase, anaphase, and cytokinesis, respectively.

1-2. Materials and methods

1-2-1. Cell culture

SH-SY5Y human neuroblastoma cells were obtained from the European Collection of Cell Cultures (Salisbury, UK). IMR-32 human neuroblastoma cells, HeLa S3 cervical carcinoma cells, and MCF7 breast cancer cells were purchased from the Japanese Collection of Research Bioresources (JCRB, Osaka, Japan). Lenti-X 293T cells were obtained from Clontech Laboratories (Mountain View, CA, USA). All cells were cultured in Dulbecco's modified Eagle's medium (DMEM) supplemented with 20 mM HEPES-NaOH (pH 7.4) and 5% fetal bovine serum (FBS) (AusGeneX, CA, USA) in a humidified 5% CO_2 incubator at 37°C.

1-2-2. Chemicals

The inhibitors of ALK, crizotinib was obtained from LC Laboratories (Woburn, MA, USA), ceritinib and TAE684 were purchased from Selleck Chemicals (Houston, TX, USA). The reversible inhibitor of CDK1 RO-3306 was purchased from Selleck Chemicals. All these inhibitors were dissolved in dimethyl sulfoxide (DMSO, Nacalai Tesque, Kyoto, Japan). DMSO was used as a solvent control in the experiments.

1-2-3. The primary and secondary antibodies

The primary antibodies were used for Western blotting analyses (WB) and immunofluorescence (IF) listed as follow:

Rabbit monoclonal antibody

anti-ALK (WB, 1:500–1000; IF, 1:200; #3333S, Cell Signaling Technology, Danvers, MA, USA)
anti-pALK-Y1507 (WB, 1:1000; #14678, Cell Signaling Technology)
anti-c-Met (WB, 1:1000; #8198, Cell Signaling Technology)

Rat monoclonal antibody

anti-α-tubulin (WB, 1:1000; IF, 1:800; MCA78G, Bio-Rad Laboratories, Hercules, CA, USA)
anti-HA (WB, 1:1000; IF, 1:400; 3F10, Roche, Basel, Switzerland)

Goat polyclonal antibody

anti-Lamin B (WB, 1:200–500; sc-6216, Santa Cruz Biotechnology, Dallas, TX, USA)

Mouse monoclonal antibody

Anti-Actin (WB, 1:2000; A3853, MilliporeSigma, Burlington, MA, USA)

Secondary antibodies used for IF

Alexa Fluor 555-labeled goat anti-rat IgG (1:1000; Cat. No. A21434, Life Technologies, Waltham, MA, USA)

Alexa Fluor 488-labeled donkey anti-rat IgG (1:800; Cat. No. A21208, Life Technologies)

Secondary antibodies conjugated with horseradish peroxidase (HRP) were used for WB

Donkey anti-rabbit IgG antibody (1:4000; 711-035-152, Jackson Immuno Research, West Grove, PA, USA)

Donkey anti-rat IgG antibody (1:4000; 712-035-153, Jackson Immuno Research)

Donkey anti-mouse IgG antibody (1:4000; 715-305-151, Jackson Immuno Research)

Bovine anti-goat antibody (1:4000; sc-2350, Santa Cruz Biotechnology)

1-2-4. siRNA transfection

Lipofectamine 2000 (Invitrogen, Carlsbad, CA, USA) was used for the transfection of small interfering RNA (siRNA) diluted with Opti-MEM (Gibco, Thrermofisher). For ALK knockdown, 20 pmol of the following siRNAs were used. Commercially available siALKs, Hs_ALK_6329_s (5'-GUCAUUACGAGGAUACCAUTT-3', siALK #1), and Hs_ALK_6330_s (5'-GAAGUGAAUAUUAAGCAUUTT-3', siALK #2) were purchased from MilliporeSigma (Burlington, MA, USA). Another siALK (5'-GUGAUAAAUACAAGGCCCATT-3', siALK #3) targeting the 3'-UTR of ALK was synthesized by MilliporeSigma. Seventy-two hours after transfection, protein levels were examined by Western blotting analysis, and M-phase progression was analyzed by immunofluorescence analysis.

Similarly, to knockdown c-Met, two commercially available siMet were purchased from MilliporeSigma. These were Hs_MET_9694_s (5'-CACCUUUGAUAUAACUGUUTT-3', siMet #1) and Hs_MET_9695_s (5'-CGGAUAUCAGCGAUCUUCUTT-3', siMet #2). siMet #3 (5'-AAGCCAAUUUAUCAGGAGGTT-3') was customized by MilliporeSigma. Suppression of c-Met expression in HeLa S3 cells was obtained after 48 h of siRNA transfection and examined by Western blotting analysis.

1-2-5. Evaluation of the effect on M-phase progression

To synchronize in the M phase, both SH-SY5Y and HeLa S3 cells were arrested at the G_2/M border with the CDK1 inhibitor RO-3306. SH-SY5Y and HeLa S3 cells were treated with 4 and 8 μM RO-3306, respectively, for 20 h. The cells were then washed with pre-warmed (37°C) PBS containing Ca^{2+} ($CaCl_2$) and Mg^{2+} ($MgCl_2$) [PBS(+)] four times and released into pre-warmed DMEM. At different times after release from the RO-3306 arrest, cells were fixed and

stained for DNA and α-tubulin. M-phase cells were classified into subphases. More than 190 cells were examined in each experiment.

1-2-6. Western blot analysis

Cells were lysed in an SDS-sample buffer. The SDS-sample buffer was prepared containing the following chemicals: leupeptin (2 μg/mL, Nacalai Tesque), aprotinin (2 μg/mL, Seikagaku Kogyo, Tokyo, Japan), pepstatin A (0.8 μg/ml, Wako Pure Chemicals, Osaka, Japan), β-glycerophosphate (20 mM, MilliporeSigma), PMSF (2 mM, Nacalai Tesque), NaF (50 mM, Wako) and Na_3VO_4 (10 mM, Wako). Cells were then denatured at 40°C for 20 min and at 100°C for 5 min in the block incubator for detection of ALK and c-Met kinases, respectively. Equal amounts of cell lysates were run in the polyacrylamide gel (7-9%). The proteins were then transferred onto the polyvinylidene difluoride (PVDF) membranes (Pall Corporation, Port Washington, NY, USA). Blocking One (Nacalai Tesque) was used to block the membranes for 1 h at room temperature. Membranes were then incubated with the primary antibody diluted in tris-buffered saline containing Tween20 (0.1%) and Blocking One (5%) for 1 h at room temperature or overnight at 4°C. Secondary antibodies were diluted similarly and exposed to the membrane for 1-3 h at room temperature. After incubation with each antibody, the membrane was washed with tris-buffered saline containing Tween20. Chemiluminescence by using either Chemi-Lumi One L (07880-70, Nacalai Tesque) or Clarity (#1705061, Bio-Rad, Hercules, CA, USA) was detected for 1-5 min using an image analyzer ChemiDoc XRS+(Bio-Rad).

1-2-7. Immunofluorescence microscopy

For immunofluorescence staining, cells were seeded in either a 35-mm dish or 24-well plate. Cells on the glass cover slip were fixed using 4% formaldehyde (HCHO) in PBS(-) at room temperature for 20 min. For permeabilization and blocking, PBS containing saponin (0.1%) and bovine serum albumin (BSA 3%) was added to the cells for 30 min. Cells were then exposed to the primary antibody diluted in 3% BSA-0.1% saponin in PBS at room temperature for 1 h. Similarly, cells were treated with secondary antibody and Hoechst 33342 (Merck-Millipore, Darmstadt, Germany) for 1 h in dark. Cell images were captured through fluorescence microscope (Olympus). Different optical systems were used to observe Hoechst 33342, Alexa Fluor 488, and Alexa Fluor 555 fluorescence such as a U-FUNA filter cube (excitation and emission, 360–370 and 420–460 nm, respectively), a U-FBNA filter cube (excitation and emission, 470–495 and 510–550 nm, respectively), and a U-FRFP filter cube (excitation and emission, 535–555 and 570–625 nm, respectively. Software such as ImageJ (National Institutes of Health, Bethesda, MD, USA), Adobe Illustrator CC, and Photoshop CC (San Jose, CA, USA) were used to edit the captured images.

1-2-8. Cell viability assay

Cell viability of SH-SY5Y cells was assessed using Cell Counting Kit-8 (Dojindo, Kumamoto, Japan) according to the manufacturer's instructions. Ten thousand cells were seeded with 100 μL of media in each well of 96-well plates and were cultured for 48 h after treating with crizotinib (0.01, 0.1, 1, and 10 μM), ceritinib (0.001, 0.01, 0.1, and 1 μM), and TAE684 (0.0001, 0.001, 0.01, 0.1, and 1 μM). As a solvent control, DMSO (0.1%) was used. WST-8 (10 μL) was added to each well and after 1 h absorbance at 450 nm was taken using a microplate reader (Bio-Rad). The number of viable cells was estimated based on the absorbance of reduced 2-(2-methoxy-4-nitrophenyl)-3-(4-nitrophenyl)-5-(2,4-disulfophenyl)-2H-tetrazolium monosodium salt (WST-8) at 450 nm. IC_{50} values were estimated from the website https://mycurvefit.com/

1-2-9. Plasmids

The plasmid R777-E008 Hs.ALK-nostop was a gift from Dominic Esposito (plasmid 70292; Addgene, Watertown, MA, USA) and the lentiviral plasmid pLIX_402 was a gift from David Root (plasmid 41394; Addgene) [52]. Through Gateway LR reaction, R777-E008 Hs.ALK-nostop was recombined with pLIX_402 according to the manufacturer's instructions (Invitrogen, CA, USA). When expressed from the pLIX_402 vector, ALK was tagged with hemagglutinin at the C-terminus (HA) (ALK-HA). pCAG-HIVgp and pCMV-VSV-G-RSV-Rev, lentiviral packaging plasmids were a gift from Dr. Hiroyuki Miyoshi [Rikagau Kenkyusho Foundation (RIKEN) BioResource Center, Ibaraki, Japan].

1-2-10. Establishment of stable cell lines by lentiviral transduction

A stable cell line, which is capable of inducible overexpression of wild-type ALK, was established by lentiviral transduction. Lenti-X 293T cells were seeded in a 60 mm dish. For co-transfection PEI Max (Polysciences, Warrington, PA, USA) was used. A mixture of PEI Max, pLIX_402 vector (1.2 μg) harboring the ALK-HA construct, pCAG-HIVgp (0.8 μg), and pCMV-VSV-G-RSV-Rev (0.8 μg) was made in Opti-MEM and kept for 30 min at room temperature. Forskolin (10 μM) (Wako) was added to the mixture. Cells were incubated with this Opti-MEM solution for approximately 16 h to generate lentivirus harboring wild-type ALK. The virus-containing media was filtered through a 0.45 μm filter.

Mag4C LV magnetic kit (OZ Biosciences, San Diego, CA, USA) was added to the microtube containing virus and kept for 20 min at room temperature. The microtube was placed in a magnetic separation rack for approximately 15 min to collect the virus bound to the magnet. After removing the supernatant, precipitate was washed with PBS. Viruses from more than one tube were gathered through diluting with Opti-MEM. Polybrene (8 μg/mL) (MilliporeSigma) was added to the virus before infecting SH-SY5Y cells that were seeded in a 35 mm dish. After

incubation at 37°C for approximately 12 h, SH-SY5Y cells were translocated into a 60 mm dish. Infected cells were selected 1.5 μg/mL puromycin (StressMarq Biosciences, Victoria, BC, Canada) for 7 days.

1-2-11. Statistics

The results obtained from more than three independent experiments were statistically analyzed with the Statcel add-in program for Microsoft Excel (OMS Publishing, Tokorozawa, Japan). For evaluation of the homogeneity of variance, the Bartlett test was used. One-way ANOVA was used to analyze among groups with equal variance, followed by the Tukey Kramer multiple comparisons test. When two groups were compared, the Student's *t*-test was used. The results were considered as significant when the *p* value was lower than 0.05.

1-3. Results

1-3-1. Detection of the ALK expression in cancer cells

ALK is predominantly found to be expressed in neuroblastoma cell lines, such as SH-SY5Y (WT/ F1174L-ALK) and IMR-32 (WT-ALK). The breast cancer MCF7 cells were reported as ALK-negative cells [10], and some studies report very low or no expression of ALK in HeLa S3. In this study, at first, the expression of ALK was evaluated in these cell lines. Western blotting analysis using anti-ALK antibody showed several bands (Fig. 6A) in these cell lines. The bands at around 220 kDa and 140 kDa represent glycosylated full-length ALK and truncated ALK generated by extracellular cleavage, respectively. This finding is consistent with other studies showing that a doublet 220 kDa bands corresponding to full-length ALK and a band at 140 kDa representing the cleaved form are detected in both SH-SY5Y and IMR3-32 cells [53,54]. However, the anti-p-ALK antibody was detected only two bands in SH-SY5Y and IMR-32 cells but not in MCF7 and HeLa S3 (Fig. 6B). This result indicates that ALK is expressed in SH-SY5Y and IMR-32 but not MCF7 and HeLa S3 cells. For further confirmation, MCF7 and SH-SY5Y cells were treated with siALKs as a mixture of three different siALKs targeting the different ALK region for complete knockdown (Fig. 6C). In MCF7 cells, siALK did not affect the appearance of any bands, indicating that they are non-specific bands. In SH-SY5Y cells, the 220 kDa ALK was completely abolished; but, the reduction of the 140 kDa band was partial (Fig. 6C), indicating that the non-specific band is overlapped with the 140 kDa band. As the overall expression of ALK is higher in SH-SY5Y than that in IMR-32 cells, SH-SY5Y cells were further investigated.

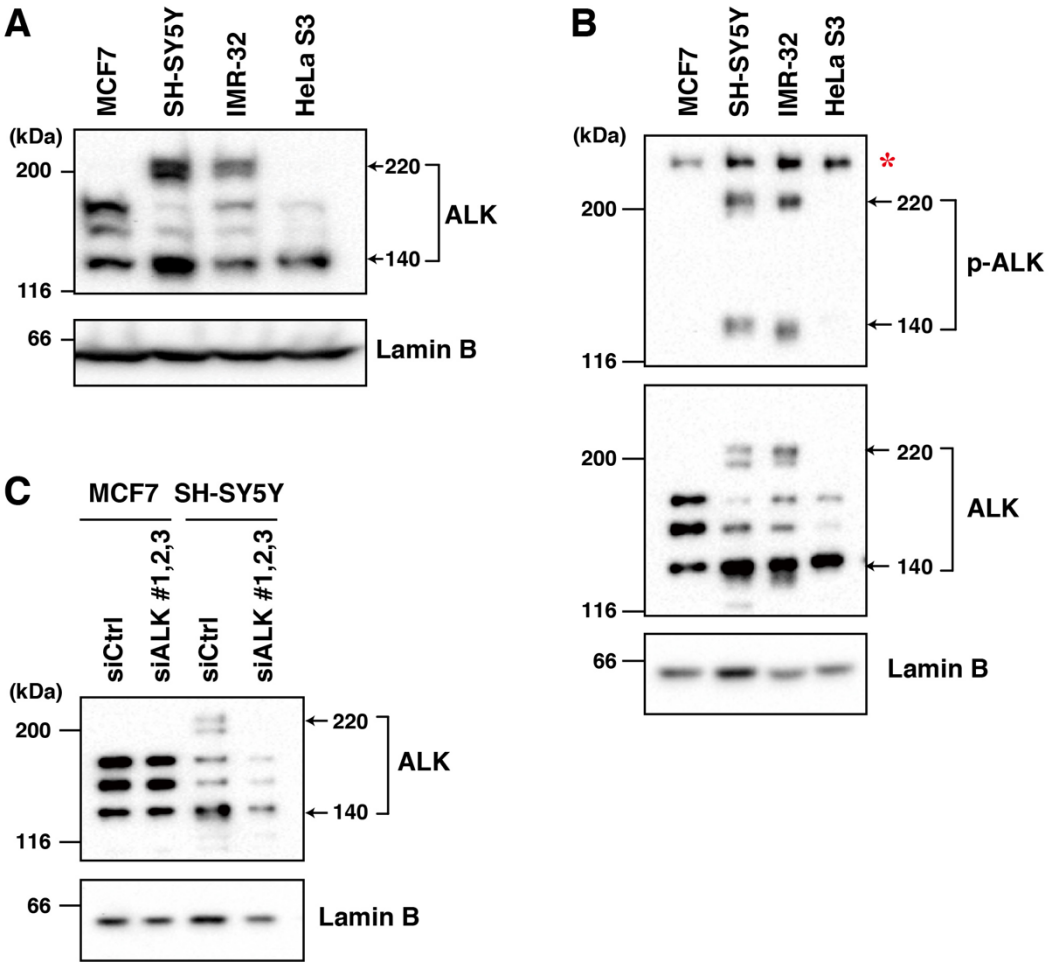

Figure 6. Detection of the ALK expression in different cancer cell lines. Whole-cell lysates were obtained from MCF7, SH-SY5Y, IMR-32, and HeLa S3 cells and analyzed by Western blotting using anti-ALK, anti-p-ALK, and anti-Lamin B antibodies (**A, B**). An asterisk indicates non-specific bands. (**C**) MCF7 and SH-SY5Y cells were transfected with a mixture of three siALK (#1, #2, #3, total 60 pmol) or non-targeting siCtrl (60 pmol). At 70 h after transfection, whole-cell lysates were prepared and Western blotting analysis is performed with anti-ALK and anti-Lamin B (loading control) antibodies.

1-3-2. Determination of IC_{50} values of ALK inhibitors in SH-SY5Y cells

To determine the IC_{50} values of ALK inhibitors, WST-8 assay was performed. SH-SY5Y cells were seeded in 96-well plates (1x 10^4 cells/well) and the next day treated with crizotinib, ceritinib, and TAE684 in different concentrations. After 2 days, WST-8 was added (10 µL/well) and incubated for 1 h. The absorbance of reduced 2-(2-methoxy-4-nitrophenyl)-3-(4-nitrophenyl)-5-(2,4-disulfophenyl)-2H-tetrazolium monosodium salt was measured at 450 nm. Data are plotted as concentration vs absorbance ratio to solvent control. The result shows that the ratio of absorbance is decreased in a concentration-dependent manner for all three inhibitors (Fig. 7), suggesting the reduction of viable cells upon treatment with a high concentration of inhibitors. The IC_{50} values were calculated from three independent experiments as described in the Materials and methods section 1-2-8 and showed as mean ± SD.

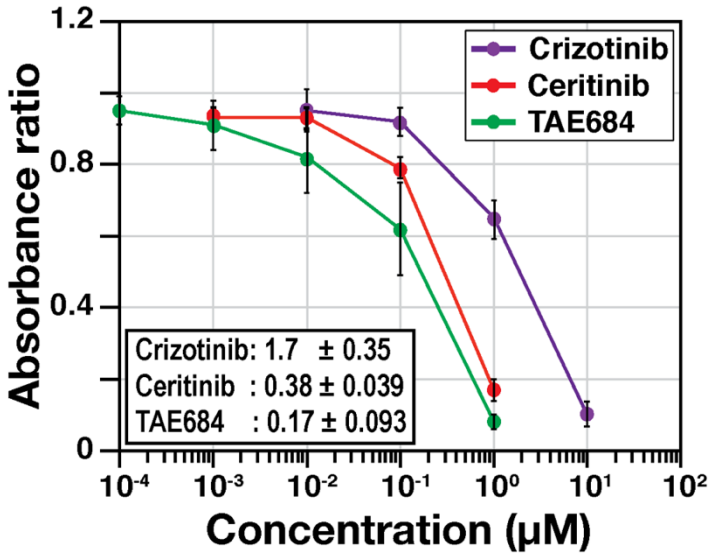

Figure 7. Evaluating IC_{50} values of ALK inhibitors. SH-SY5Y cells were treated with crizotinib (0.01, 0.1, 1, and 10 µM), ceritinib (0.001, 0.01, 0.1, and 1 µM), and TAE684 (0.0001, 0.001, 0.01, 0.1, and 1 µM) in different concentrations. After 48 h viable cells were determined by WST-8 assay. Relative values of absorbance to solvent control (DMSO) are shown as mean ± SD, calculated from three independent experiments.

1-3-3. Delay in the early M phase in ALK inhibitor-treated cells

To determine the effect of ALK inhibitors on cell division, SH-SY5Y cells were first synchronized with the CDK1 inhibitor RO-3306. RO-3306 treatment arrests cells at the G2/M border and approximately 30% of cells can synchronously enter the M phase after release from the arrest. Fixation at different times after release allows evaluation of M phase progression [51]. After 20-h RO-3306 treatment, cells were released for 1 h in a medium containing either DMSO, 1 μM crizotinib, 0.5 μM ceritinib, or 0.3 μM TAE684. The experimental protocol is shown in Figure 8A. Cells were fixed by 4% formaldehyde and permeabilized with PBS containing 3% BSA and 0.1% saponin. Anti-α-tubulin and Hoechst 33342 were used to stain α-tubulin and DNA. Based on microtubule and chromosome morphologies observed under the fluorescence microscope, M-phase cells were classified into four groups: prophase/prometaphase (P/PM), metaphase (M), anaphase/telophase (A/T), and cytokinesis (Cyto). Such classification showed that most solvent control cells (Fig. 8B, DMSO) progressed to cytokinesis in 1 hour after the release. On the other hand, in ALK inhibitors-treated cells, accumulation of P/PM cells was observed, indicating that M-phase progression was largely delayed in P/PM. The percentage of M phase cells, which is represented as the mitotic index, showed no significant change by inhibitor treatment (Fig. 8C). These results suggest that inhibition of ALK delays M-phase progression without affecting mitotic entry.

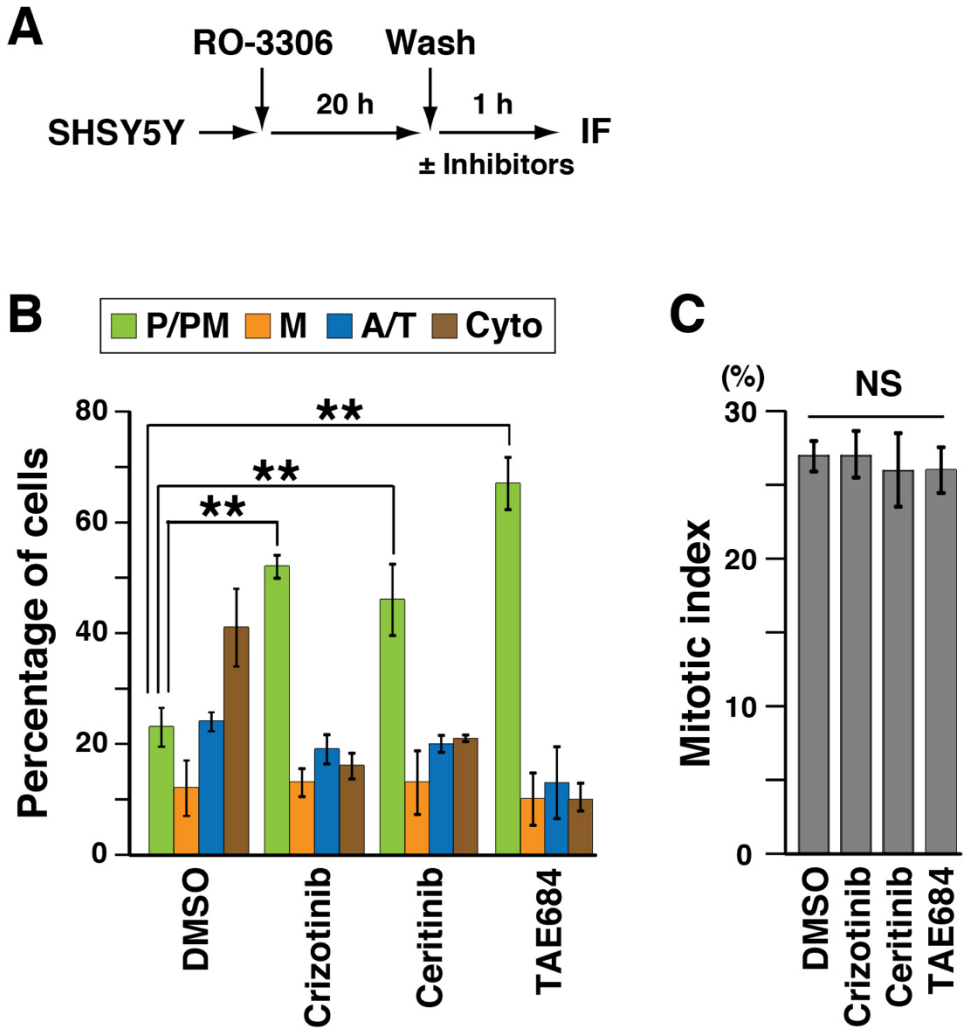

Figure 8. Inhibition of ALK with small-molecule inhibitors causes delay in the M phase. SH-SY5Y cells were synchronized with 4 μM RO-3306 for 20 h. After release, cells were treated with 1 μM crizotinib, 0.5 μM ceritinib, and 0.3 μM TAE684 for 1 h and stained for α-tubulin and DNA. (**A**) Schematic representation of the experimental protocol. (**B**) M-phase cells were classified into four groups: prophase/prometaphase (P/PM), metaphase (M), anaphase/telophase (A/T), and cytokinesis (Cyto). The percentages of cells of each group (n > 246 in each experiment) are plotted as the mean ± SD, calculated from three independent experiments. (**C**) Mitotic indices (n > 453 in each experiment) are plotted as the mean ± SD, calculated from three independent experiments. The Tukey–Kramer multiple comparison test was used to calculate *p* values. $^{**}p < 0.01$; NS, non-significant.

1-3-4. ALK inhibitors cause the misalignment of chromosomes

Chromosome alignment at the cell equator is the predominant event of metaphase, which is required for proper chromosome segregation in anaphase. Microscopic observation of cells showed that metaphase chromosomes were completely aligned at the cell equator in control cells (Fig. 9A). However, in crizotinib- and TAE684-treated cells at around IC_{50} concentration for 1 h, few chromosomes remain scattered although most of the chromosomes were aligned, and these misaligned chromosomes were frequently observed (Fig. 9A). In control cells (DMSO), less than 10% of cells had misaligned chromosomes (Fig. 9B). On the other hand, crizotinib- and TAE684-treatment increased this percentage to 18% and 21%, respectively (Fig. 9B). These results suggest that defects in chromosome alignment may be one of the mechanisms of the M-phase delay in ALK inhibitor-treated cells.

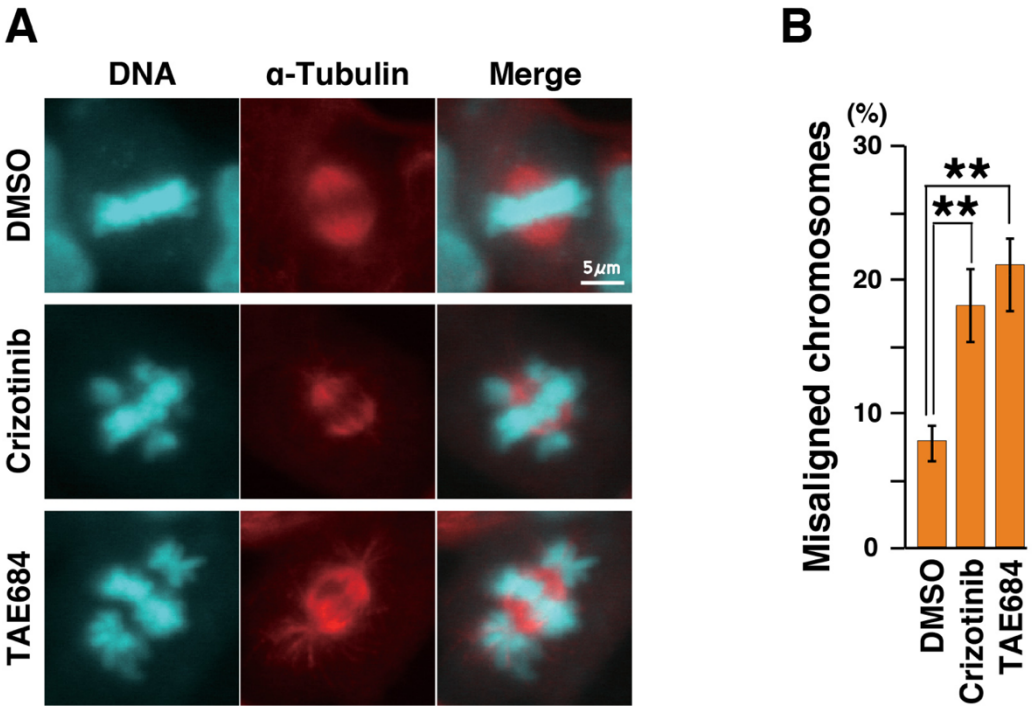

Figure 9. The inhibition of ALK affects chromosome alignment. SH-SY5Y cells were synchronized and treated with crizotinib and TAE684 as described in the section 1-3-3. Cells were fixed with 4% HCHO and stained for α-tubulin and DNA. Cells were observed under a fluorescence microscope and representative images of cells with misaligned chromosomes are shown in (**A**). Scale bar = 5 μm. (**B**) The number of cells with misaligned chromosomes was counted and plotted as a percentage to metaphase cells. The Tukey–Kramer multiple comparison test was used to calculate *p* values. $^{**}p < 0.01$.

1-3-5. Inhibition of ALK kinase activity

To check the effect of ALK inhibitors on the kinase activity, auto-phosphorylation of ALK at Tyr1507 was analyzed by WB analysis. The tyrosine residue at 1507 is localized in the c-terminal tail of ALK and its phosphorylation depends on the kinase activity. After 1-h treatment of inhibitors, whole-cell lysates were probed with indicated antibodies. Inhibitor treatment caused suppression of ALK phosphorylation, while total ALK expression did not change (Fig. 10). Lamin B was detected as loading control. Based on this result, it could be proposed that the kinase activity of ALK might be responsible for regulating the M phase.

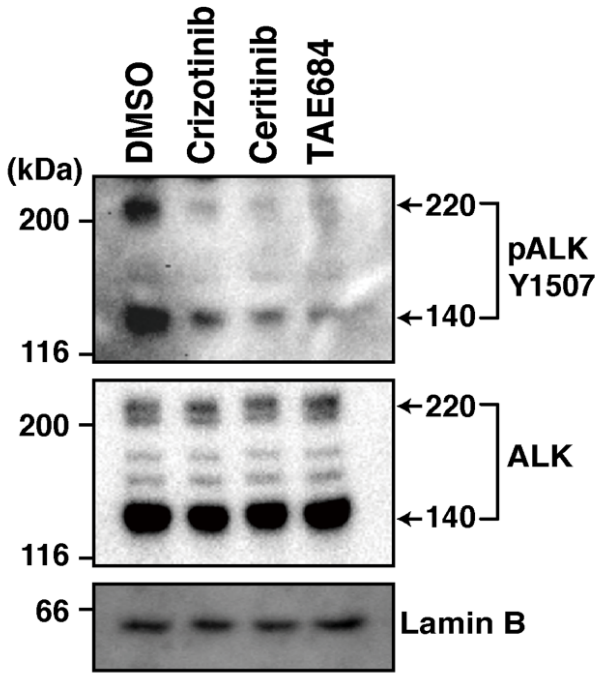

Figure 10. The auto-phosphorylation of ALK is suppressed by inhibitor treatment. SH-SY5Y cells were treated with inhibitors in the same concentration as described in the section 1-3-3 for 1 h, and whole-cell lysates were analyzed by Western blotting using anti-pALK-Y1507 and anti-ALK antibodies. Lamin B was analyzed as a loading control.

1-3-6. Delay in the early M phase upon ALK knockdown

One of the drawbacks of small molecule inhibitors is the variable specificity. Although ceritinib and TAE684 show much higher specificity to ALK compared to crizotinib, however, ceritinib shows very little specificity to other RTKs. To exclude the off-target effects of inhibitors specific small interfering RNAs (siRNAs) were used to knockdown ALK. The knockdown efficiency of siALKs was determined by Western blotting analysis (Fig. 11A, B). Three different siALKs, which include siALK #1 and 2 targeting within the open reading frame (ORF) and siALK #3 targeting 3' UTR of ALK, were used for ALK knockdown. The efficiency of siALKs can vary depending on the targeted region or sequence of a protein. Knockdown efficiency was determined in SH-SY5Y cells after 24, 48, and 72 h of transfection using Lipofectamine 2000. Partial knockdown of ALK was observed after 24 and 48 h of transfection (data not shown) while 72 h transfection caused significant knockdown of full-length ALK compared to non-targeting siCtrl (Fig. 11B). Although 140 kDa band showed slight or no change due to siALK treatment. It was speculated that the overlapping non-specific band at 140 kDa position, as described in the section 1-3-1, hindered the observation of downregulation of 140 kDa ALK.

To examine the effect of ALK knockdown on M-phase progression, synchronization experiments were performed in ALK-knockdown cells. SH-SY5Y cells were seeded in a 24-well dish on a coverslip and transfected with siALK (# 1 and #2) for 52 h. Cells were then treated with RO-3306 for 20 h to synchronize at the G2/M phase border. Cells were released through washing with PBS (+) and incubated for 90 min at 37°C. Cells were then fixed and stained for α-tubulin and DNA (Fig. 11A, IF). Based on chromosome and microtubule morphologies, the M-phase cells were divided into two groups: before and after anaphase onset. In siCtrl-treated cells, 67% of cells progressed to or through anaphase (Fig.11C). Whereas in the siALK-treated condition, a significant percentage of cells failed in chromosome segregation and thereby remained before anaphase onset. This result suggests that ALK knockdown causes a delay in the early M phase. Moreover, the mitotic index was also decreased by ALK knockdown (Fig. 11D). This result can be supported by previous findings [55], which shows that the downregulation of ALK causes prolongation of cell cycle through altering the expression of genes involved in G1 phase.

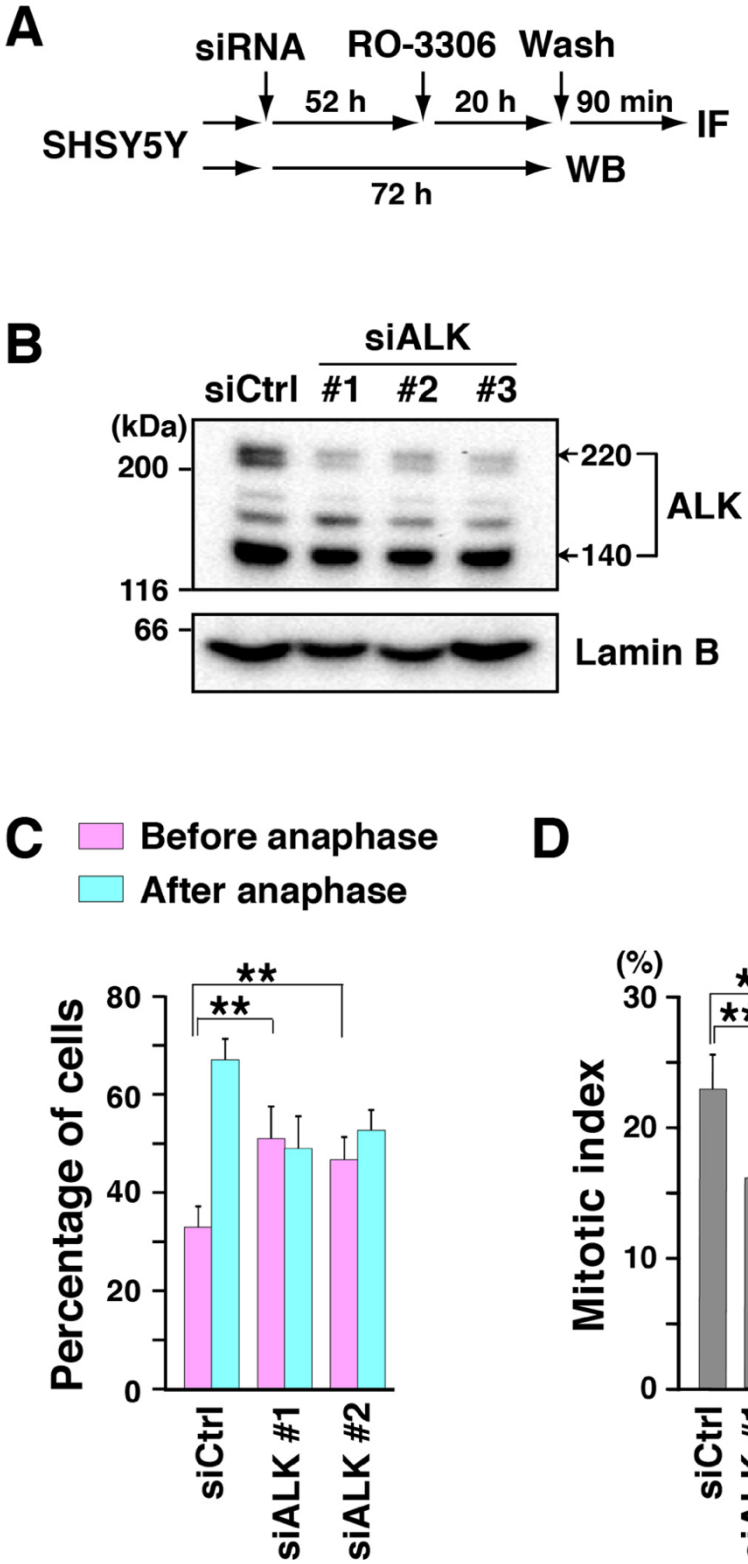
A
siRNA
RO-3306
Wash
52 h
20 h
90 min
IF
SHSY5Y
WB
72 h
B
siALK
siCtrl
#1
#2
#3
(kDa)
200
116
66
220
140
ALK
Lamin B
C
Before anaphase
After anaphase
Percentage of cells
80
60
40
20
0
**
**
siCtrl
siALK #1
siALK #2
D
(%)
Mitotic index
30
20
10
0
**
**
siCtrl
siALK #1
siALK #2

Figure 11. siALK-mediated ALK knockdown delays anaphase onset. SH-SY5Y cells were transfected with 20 pmol of ALK-targeting siRNAs (siALK #1, #2, and #3) or nontargeting siCtrl using Lipofectamine 2000. (**A**) Schematic representation of the experimental protocol. (**B**) At 72 h after transfection, whole-cell lysates were prepared and analyzed by Western blotting using anti-ALK and anti-Lamin B (loading control) antibodies. (**C** and **D**) SH-SY5Y cells were transfected, incubated for 52 h, and then treated with 4 μM RO-3306 for 20 h. After release from RO-3306 treatment, cells were incubated in fresh media for 90 min. Immunofluorescence staining was performed to stain with anti-α-tubulin antibody and Hoechst 33342. Based on microtubule and chromosome morphologies, M-phase cells were classified into two groups: before and after anaphase onset. Percentages of cells ($n > 243$ in each experiment) and mitotic indices ($n > 503$ in each experiment) are plotted as mean ± SD, calculated from three independent experiments. The Tukey–Kramer multiple comparison test was used to calculate p values. $^{**}p < 0.01$.

1-3-7. siALK-induced M-phase delay was rescued by inducible expression of exogenous ALK

To further prove the involvement of ALK in M-phase progression, stable cells, capable of expressing HA-tagged wild-type ALK (ALK-HA) in response to Dox treatment, were established from SH-SY5Y cells (SH-SY5Y/ALK-HA). At first, the expression of endogenous ALK-HA and total ALK were detected by Western blotting analysis (Fig. 12A, B). SH-SY5Y cells were transfected with siALK #3 targeting the 3'-UTR of ALK and incubated for 72 h, resulting in knockdown of both endogenous and exogenous ALK. One group of siALK-transfected cells were exposed to Dox to induce exogenous ALK expression. Whole-cell lysates were obtained and analyzed with anti-HA, anti-ALK, and anti-Lamin B antibodies. ALK-HA was detected only in Dox-treated cells while total ALK expression in Dox-treated cells was comparable to Dox-negative siALK #3-treated cells (Fig. 12B, See 220 kDa band).

To determine the role of endogenous ALK in M-phase progression, SH-SY5Y/ALK-HA cells were transfected with siALK #3 and non-targeting siCtrl for 52 h. Cells were synchronized with RO-3306 and released for 90 min (Fig. 12A, IF). Dox was exposed for 72 h in one group of siALK #3-treated cells. Based on chromosome and microtubule morphologies, M-phase cells were divided into two groups as described in the section 1-3-6. Compared to control cells ALK knockdown caused an increase in the number of cells before anaphase onset (Fig. 12C). On the contrary, re-expression of ALK-HA rescued the ALK knockdown-induced M-phase delay; cells progressed to anaphase or later stages. This result further proves the notion that ALK is involved in M-phase regulation. Although a decrease in the mitotic index was found by ALK knockdown, the re-expression of ALK-HA was unable to rescue the decreased mitotic index (Fig. 12D). It was speculated that ALK may also regulate mitotic entry through a different mechanism involving different downstream signaling molecules. Moderate ALK re-expression may be unable to rescue the target involved in regulating mitotic entry, in spite that re-expression rescued the knockdown-induced M-phase delay. Further investigations are required to prove this phenomenon.

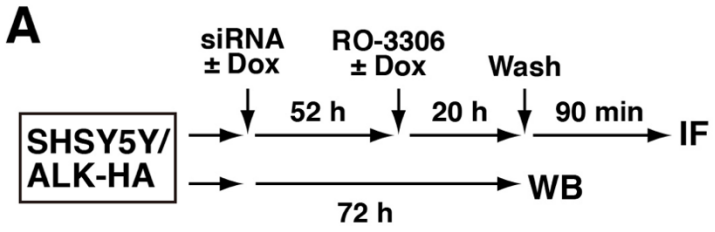
A
siRNA
± Dox
RO-3306
± Dox
Wash
52 h
20 h
90 min
IF
SHSY5Y/
ALK-HA
WB
72 h

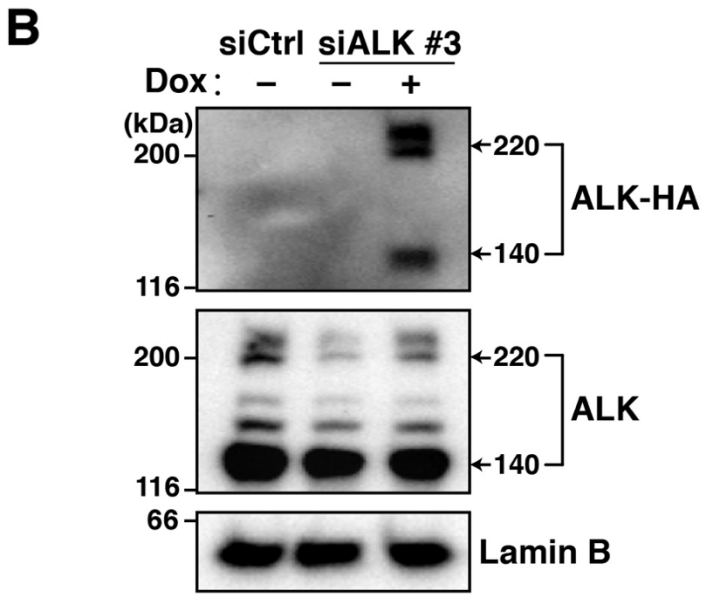
B
siCtrl
siALK #3
Dox: – – +
(kDa)
200
116
220
140
ALK-HA
200
116
220
140
ALK
66
Lamin B

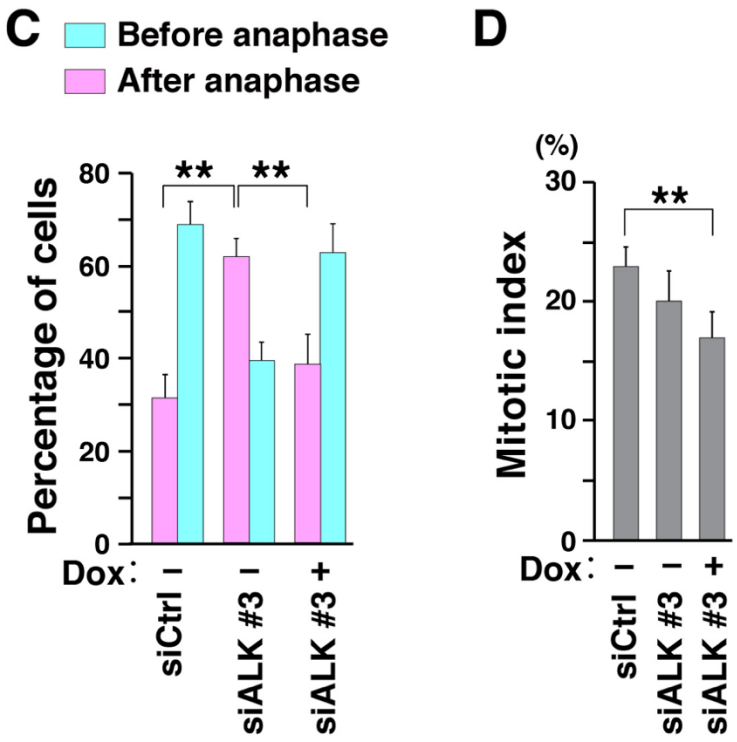
C
Before anaphase
After anaphase
Percentage of cells
80
60
40
20
0
**
**
Dox: – – +
siCtrl
siALK #3
siALK #3
D
(%)
Mitotic index
30
20
10
0
**
Dox: – – +
siCtrl
siALK #3
siALK #3

Figure 12. Inducible expression of endogenous ALK rescues the M-phase delay. SH-SY5Y/ALK-HA cells were transfected with 20 pmol of siALK #3 and non-targeting siCtrl using Lipofectamine 2000 and were simultaneously treated with 5 µg/mL Dox. (**A**) Schematic representation of the experimental protocol. (**B**) Whole-cell lysates were prepared after 72 h of transfection and analyzed by Western blotting with anti-HA, anti-ALK, and anti-Lamin B antibodies. (**C** and **D**) After 52 h of transfection cells were synchronized with 4 µM RO-3306. M-phase cells were classified into two groups: before and after anaphase onset. Percentages of cells ($n > 193$ in each experiment) and mitotic indices ($n > 413$ in each experiment) are plotted as mean ± SD, calculated from three independent experiments. The Tukey–Kramer multiple comparison test was used to calculate p values. $^{**}p < 0.01$.

1-3-8. Detection of c-Met expression in several cell lines

The mesenchymal-epithelial transition factor, c-Met tyrosine kinase is a hepatocyte growth factor receptor and participates in tumorigenesis and malignant progression. c-Met is synthesized as a precursor (pro-Met) and matures through proteolytic cleavage. The mature c-Met is a heterodimeric receptor composed of an extracellular α subunit (50 kDa), which is linked via a disulfide bond to the transmembrane β subunit (145 kDa) [56]. c-MET is one of the prominent targets of crizotinib [57,58]. Crizotinib can bind to the ATP-binding pocket of both ALK and c-Met and inhibit both RTKs. To evaluate that crizotinib inhibited another RTK other than ALK in SH-SY5Y cells, c-Met expression was examined in SH-SY5Y together with HeLa S3, IME-32, and MCF7 cells. Whole-cell lysates were obtained from these cells and subjected to Western blotting using anti-c-Met and anti-Actin antibodies (Fig. 13). c-Met expression is observed in HeLa S3 cells but not in other cell lines. This result is inconsistent with another study showing that c-Met is expressed in HeLa S3 cells and leads to oncogenicity in this cell line [59]. One study reports that, HGF/c-Met signaling promotes the progression of neuroblastoma [60]. However, SH-SY5Y cells did not express c-Met. This result suggests that the target of crizotinib in SH-SY5Y cells is not c-Met and could be solely ALK.

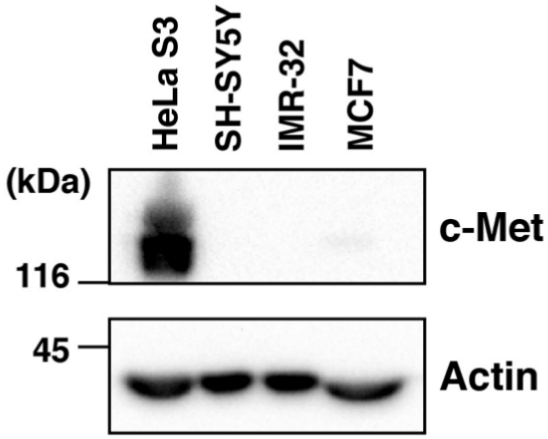

Figure 13. c-Met expression is examined in cancer cells. HeLa S3, SH-SY5Y, IME-32 and MCF7 cells were seeded in a 35-mm dish. The whole-cell lysate was prepared using an SDS-sample buffer. SDS-PAGE was performed using 9% gel. Anti-c-Met antibody was used to detect total c-Met. Actin was detected as the loading control.

1-3-9. Crizotinib delays M-phase progression in HeLa S3 cells

To evaluate whether inhibition of c-Met affected M-phase progression, HeLa S3 cells were treated with crizotinib. Cells were seeded in a 35-mm dish and synchronized with RO-3306 for 20 h. After release form the RO-3306 treatment, cells were incubated with fresh medium containing DMSO (solvent control) or crizotinib for 1 h at 37°C (Fig. 14A). The cells were fixed using 4% HCHO, permeabilized with PBS containing 3% BSA and 0.1% saponin and stained for α-tubulin and DNA using anti-α–tubulin antibody and Hoechst 33342, respectively. M-phase cells were divided into 4 groups and the percentage of cells in each group was calculated (Fig. 14B). In control cells, around 55% of cells were progressed to cytokinesis after 1 h of release from RO-3306 arrest (Fig. 14B, DMSO). On the other hand, crizotinib-treatment largely delayed M-phase progression approximately 66% of cells remained in prophase/prometaphase (P/PM). This result raises the possibility that c-Met may have a role in the regulation of the M-phase progression. The mitotic index indicating the percentage of total mitotic cells showed no significant changes upon crizotinib-treatment (Fig. 14C).

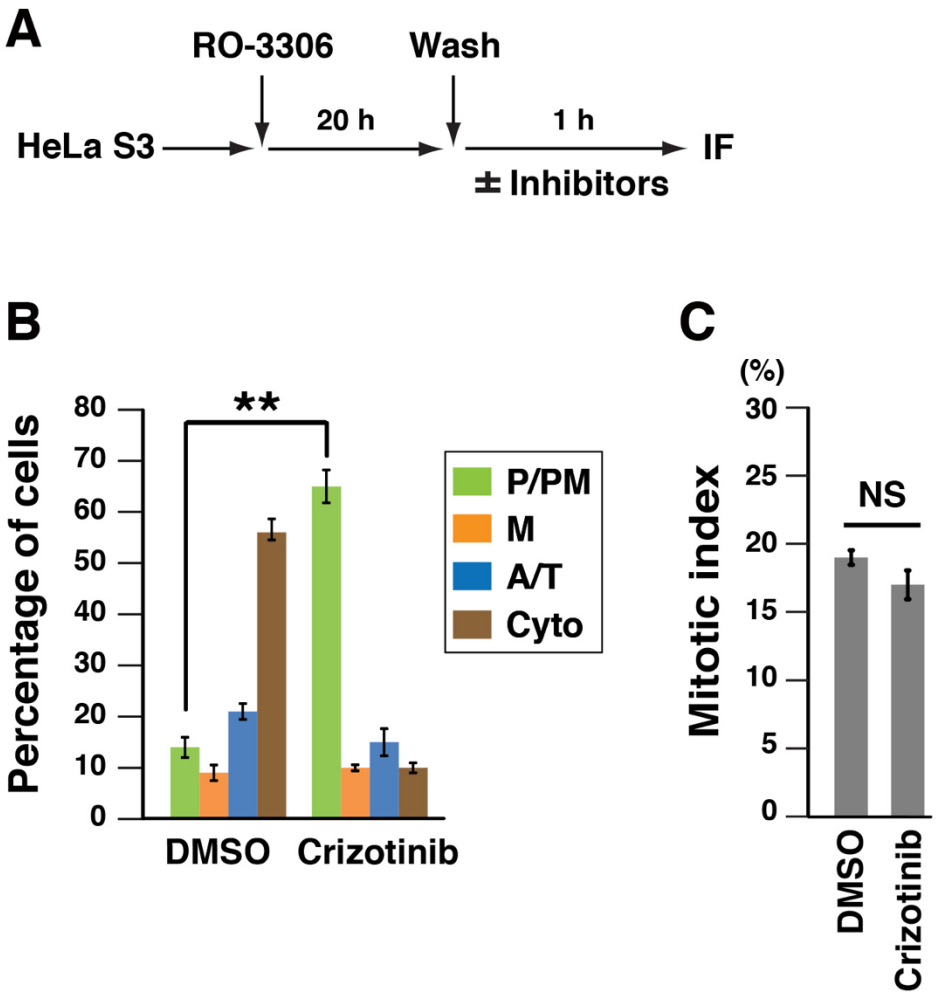

Figure 14. Crizotinib delays M-phase progression in HeLa S3 cells. HeLa S3 cells were seeded in a 35-mm dish on a cover slip and incubated for 24 h. Cells were treated with 6 μM RO-3306 for 20 h. Then cells were released from RO-arrest through washing with PBS (+) 4 times on 37°C and incubated with DMEM containing DMSO or 1 μM crizotinib for 1 h. (**A**) Schematic representation of experimental protocol. (**B** and **C**) Cells were fixed using 4% HCHO, permeabilized with PBA containing 3% BSA and 0.1% saponin. and stained with anti-α-tubulin and Hoechst 33342. Based on chromosome and microtubule morphological, M-phase cells were divided into four groups: prophase/prometaphase (P/PM), metaphase (M), anaphase/telophase (A/T) and cytokinesis (cyto). The percentage of cells of each group ($n > 253$ in each experiment) and mitotic index ($n > 476$ in each experiment) are plotted as the mean ± SD, calculated from three independent experiments. The Tukey–Kramer multiple comparison test was used to calculate *p* values. $^{**}p < 0.01$; NS, non-significant.

1-3-10. Knockdown of c-Met by siRNA showed inconsistent effects on M phase

To confirm the role of c-Met on the M phase, specific knockdown of c-Met is required. Three different siRNAs (siMet, #1, #2 and #3) targeting different regions of c-Met were used to knockdown c-Met. The optimum concentration of siMet (5, 10 and 20 pmol) and transfection time (24, 48 and 72 h) were evaluated, and an efficient knockdown was observed using 20 pmol of siMet for 48 h. After 48 h incubation whole-cell lysates were obtained and subjected to Western blotting using anti-c-Met and anti-Actin (loading control) antibodies (Fig. 15A, B). Compared to siCtrl all three siMet significantly suppress c-Met expression.

M-phase progression of HeLa S3 cells was examined after c-Met knockdown by using all three siMet. Cells were seeded in a 24-well dish with coverslip, transfected with 20 pmol siMet and incubated for 28 h Then, the cells were treated with RO-3306 for 20 h. After release from RO arrest, cells were incubated in fresh medium for 1 h. Cells were then fixed and stained as described in the section 1-3-9. M-phase cells were classified into two groups: before and after anaphase onset (Fig. 15C). The bar graph showed that 58% of control cells were progressed to anaphase, telophase or cytokinesis. On the contrary, siMet #2 delayed M-phase progression as a significant percentage of cells failed in anaphase onset and remained in prophase, prometaphase or metaphase. However, cells treated with siMet #1 and #3 did not exhibit M-phase delay; of siMet #1-treated cells were progressed to anaphase or later phases. siMet #3-treated cells did not show any significant changes compared to siCtrl. Form these results the effect of c-Met knockdown on M-phase progression could not be concluded. Moreover, a vast difference in the mitotic index was observed among siMets-treated cells (Fig. 15D). siMet #2 and #3-treated cells showed a significant reduction in the mitotic index compared to control cells. A high number of dead cells were observed in siMet #2 and #3-treated cells (data not shown). Therefore, it can be speculated that siMet #2 and #3 may cause DNA damage, leading to mitotic cell death. Some studies reported that c-Met is required for G1/S phase transition and also regulates the G2/M phase progression through ERK1/2-dependent activation of key mitotic regulators including CDK1, PLK1, and Aurora A and B [61]. However, based on the present finding the role of c-Met in the M phase remained undermined.

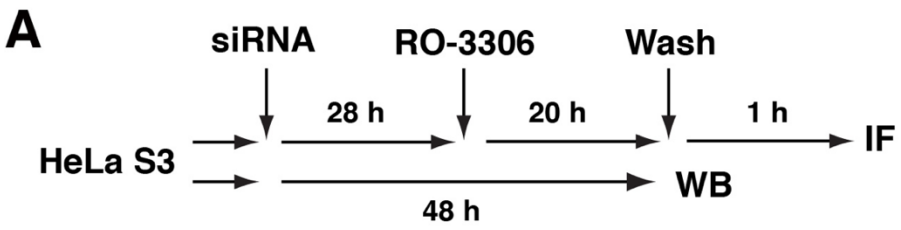
A
siRNA
RO-3306
Wash
28 h
20 h
1 h
IF
HeLa S3
WB
48 h

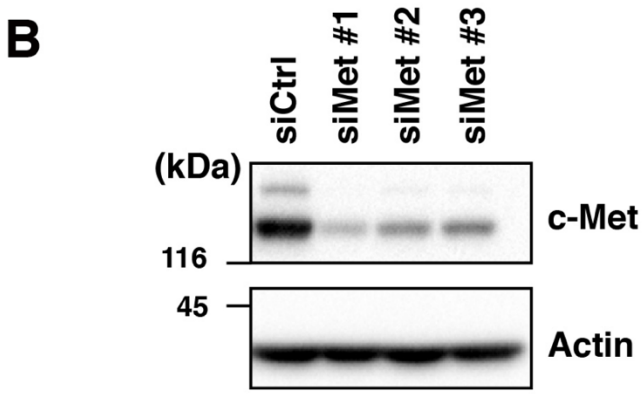
B
siCtrl
siMet #1
siMet #2
siMet #3
(kDa)
116
c-Met
45
Actin

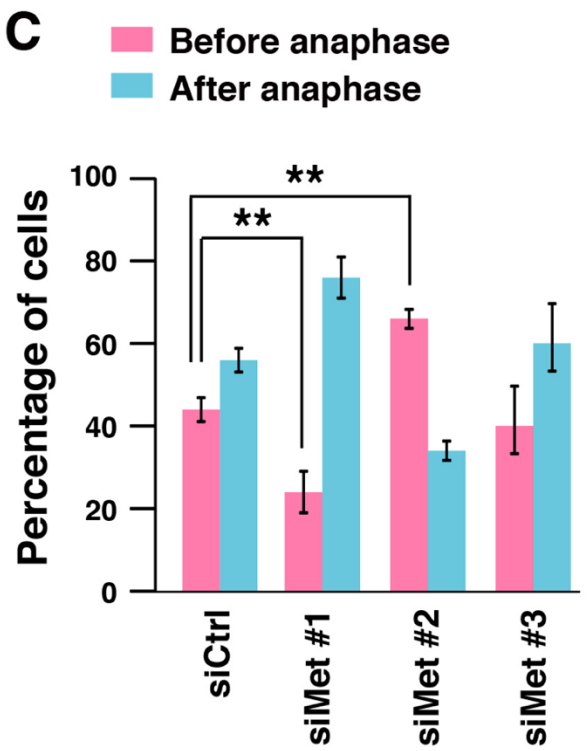
C
Before anaphase
After anaphase
Percentage of cells
100
80
60
40
20
0
**
**
siCtrl
siMet #1
siMet #2
siMet #3

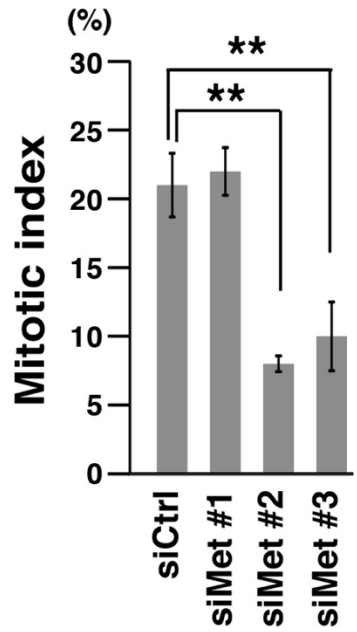
D
(%)
Mitotic index
30
25
20
15
10
5
0
**
**
siCtrl
siMet #1
siMet #2
siMet #3

Figure 15. Effect of c-Met knockdown on M phase. HeLa S3 cells were seeded in a 24-well dish. Using Lipofectamine 2000, cells were transfected with 20 pmol of c-Met-targeting siRNAs (siMet #1, #2, and #3) or nontargeting siCtrl. (**A**) Schematic representation of experimental protocol. (**B**) At 48 h after transfection, whole-cell lysates were prepared and analyzed by Western blotting using anti-c-Met and anti-Actin (loading control) antibodies. (**C** and **D**) HeLa S3 cells were transfected with siMet, incubated for 28 h and then treated with 6 μM RO-3306 for 20 h. Cells were released for 1 h in fresh medium. Cells were stained with anti-α-tubulin antibody and Hoechst 33342. Based on microtubule and chromosome morphologies, M-phase cells were classified into two groups: before and after anaphase onset. Percentages of cells ($n > 247$ in each experiment) and mitotic indices ($n > 507$ in each experiment) are plotted as mean ± SD, calculated from three independent experiments. The Tukey–Kramer multiple comparison test was used to calculate p values. $^{**}p < 0.01$.

1-4. Discussion

The effect of ALK inhibition was assessed using three different inhibitors and siRNAs. These inhibitors are the ATP competitive inhibitors of ALK having different efficacy. All three inhibitors crizotinib, ceritinib, and TAE684 caused a delay in the early M phase through affecting chromosome alignment in the metaphase. Suppression of the auto-phosphorylation of ALK suggests the possibility of the involvement of ALK kinase activity in M-phase delay. To exclude the involvement of the off-target effect of inhibitors, specific siRNAs targeting ALK were used to knockdown ALK. The knockdown of ALK also caused a similar delay in the M phase. Rescue from siALK-induced M-phase delay was achieved through inducible expression of exogenous ALK. These results confirm that ALK has a role in regulating the M phase, mainly chromosome alignment in the early M phase.

Full-length ALK expression was found in 92% of primary neuroblastoma [5]. SH-SY5Y harboring F1174L mutation showed high sensitivity against ALK inhibitors. Through WST-8 assay, suppression of proliferation of SH-SY5Y cells was observed upon inhibitor treatment (Fig. 7). Previously, it was reported that shRNA-mediated ALK knockdown causes a reduction in cell growth and viability [16]. It had been also reported that ALK inhibitors including TAE684 resulted in a 3-12 fold increase in the percentage of apoptotic cells after 24 h in SH-SY5Y cells [16]. The activation of the apoptotic pathway has not been broadly described yet. To determine the involvement of M-phase defect on suppression of cell proliferation, IC_{50} concentrations of the inhibitors were estimated. SH-SY5Y cells showed high sensitivity to TAE684 compared to crizotinib and ceritinib as the IC_{50} value of crizotinib was much higher in this cell line (Fig. 7). When cells were treated with inhibitors at around IC_{50} concentrations, delay in the M phase was observed only after 1 h of treatment (Fig. 8B). This result suggests that delay in the M phase contributes to the suppression of cell proliferation.

ALK shares structural and sequence homology of the catalytic domain and ATP-binding site with other RTKs such as c-Met, ROS1, IGF1R etc. Therefore, ALK targeted inhibitors showed off-target effects. For example, crizotinib can inhibit c-Met and ROS1 [4], while ceritinib targets IGF1R and ROS1[4] in addition to ALK. The targets of inhibitors largely depend on the abundancy of expression of RTK in a particular cell line. The expression of c-Met was examined in several cell lines including SH-SY5Y (Fig. 13); no expression of c-Met was observed in any cell lines other than HeLa S3. This finding was supported by another study that showed that expression of the c-Met protein was undetectable in SH-SY5Y cells [60]. Thus, c-Met can not be the target of crizotinib in SH-SY5Y cells. To eliminate the off-target effects of inhibitors siRNAs were used to knockdown ALK. More than one siALK targeting different sites of ALK were used

in this study. The knockdown of ALK caused delay in the early M phase (Figs. 11C and 12C) similar to ALK inhibitors. This finding proves that ALK has a regulatory role in M phase.

Similar to other RTKs, ALK regulates various cellular processes via activating several downstream pathways that depend on the tyrosine phosphorylation of the kinase domain of ALK [62,63]. The three most important phosphorylation sites in the kinase domain are Tyr1278, Tyr1282, and Tyr1283. Another important phosphorylation site, tyrosine-1507 is located in the c-terminal tail of ALK. This phosphorylation depends on the ALK kinase activity and is critical for the association of the adapter protein Shc [64]. ALK inhibitors at around IC_{50} concentration suppressed phosphorylation of Y1507 (Fig. 10). Therefore, it can be assumed that ALK kinase activity might be responsible for the role in M-phase regulation.

Though the MAPK pathway triggered by ALK regulates cell proliferation by activating several regulatory transcription factors, signaling cascade in M-phase regulation mediated by ALK is yet to be revealed. A previous study reported the involvement of the MEK/ERK/RSK pathway in regulating M-phase progression [65]. Moreover, B-Raf an upstream signaling molecule of MEK/ERK is involved in spindle formation and regulation of mitotic checkpoints [66]. Therefore, it can be assumed that the MAPK pathway may be involved in ALK-mediated M-phase regulation.

One striking feature of full-length human ALK is the cleavage in the extracellular domain. ALK is cleaved possibly through proteolysis, resulting in 140 kDa truncated ALK which remains in membrane-bound form while the smaller fragment of ALK is shed into the extracellular space [4]. Such cleavage phenomenon has been reported to be frequently found in neuroblastoma (NB) cell lines and tissues [16,53,67]. One study reported that 140 kDa isoform of ALK is prominently expressed and highly phosphorylated in tumors showing poor-prognosis [68]. In this study, both 220 and 140 kDa ALK were detected by anti-ALK and anti-phospho-ALK antibodies in NB cell lines (Fig. 6A). It was speculated that siRNAs completely suppress both 220 and 140 kDa ALK in SH-SY5Y cells, though suppression of 140 kDa ALK was not clear due to the presence of overlapping non-specific band (Figs. 6C and 11B). Exogenous expression of full-length ALK-HA resulted in the expression of both 220 and 140 kDa ALK and rescued ALK knockdown-induced M-phase delay (Fig. 12B, C). It can be proposed that both forms of ALK are involved in M-phase regulation. Given that ALK has a role in M-phase regulation in its kinase activity-dependent manner, ALK has to be activated. The full-length ALK is activated by binding its ligands, such as pleiotrophin, midkine, augmentor-β, and augmentor-α. Likewise, 140 kDa ALK fragment also contains ligand-binding domain and is activated by ligand binding. However, it is hard to assume that ALK requires ligand binding for every M-phase progression. It is of note that 140 kDa ALK is reportedly constitutively active [69]. If 140 kDa ALK fragment actually remains in constitutively active form, 140 kDa ALK may play a role in M-phase progression in its ligand-

independent manner. If full-length ALK plays a role in M-phase regulation, how ALK is activated in M phase has to be resolved.

Although the mitotic index did not change in inhibitor-treated cells (Fig. 8C), a significant reduction in mitotic index was observed in siALK-treated cells (Figs. 11D and 12D). Several possible effects of ALK downregulation may lead to a reduction in the mitotic index, such as the impairment of the G_2 to M phase transition, an increase in premature mitotic exit, and extended duration of cell cycle due to defect in cell cycle regulatory proteins. A previous study suggests that the inhibition of ALK can arrest the G1 phase of the cell cycle by altering the expression of genes involved in G1 to S phase transition [55]. ALK inhibition potentially suppresses expression of Cyclin D1, D3, and E2F1 and up-regulates the expression of the p27 [55]. Also, proteins involved in mitotic entry could be dysregulated at transcriptional and translational levels due to ALK knockdown by siALKs for long period. Therefore, ALK knockdown-caused decrease in the mitotic index might be a result of either prolongation of the cell cycle or defect in the mitotic entry. We speculate that a very short exposure to ALK inhibitors can not affect such proteins in transcriptional levels, resulting in no effect on the mitotic index.

In the investigation of the mechanism of M-phase delay caused by ALK downregulation, defect in chromosome alignment was observed (Fig. 9A, B). The alignment of chromosomes at the cell equator during metaphase ensures proper chromosome segregation, which is an important regulatory event. Based on the above results, it can be concluded that inhibition of ALK causes delay in the early the M phase, leading to the suppression of cell proliferation. The graphical presentation of the summary is shown in the following Figure 16.

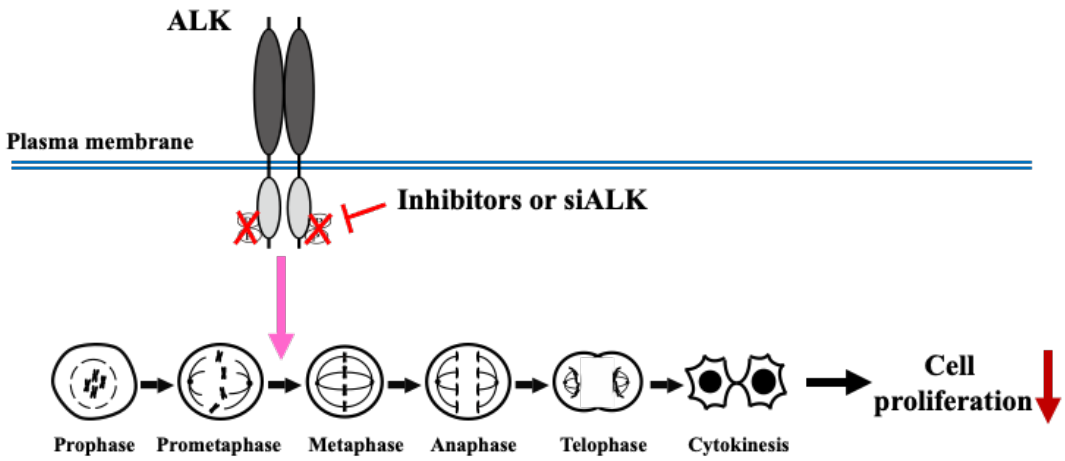

Figure 16. Summary of chapter 1. Inhibition of full-length ALK either by inhibitors or siALKs in SH-SY5Y cells causes delay in the early M phase. Specifically, chromosome alignment was failed. This phenomenon leads to the suppression of cell proliferation, which is a novel mechanism for ALK inhibition-mediated suppression of cell proliferation.

Chapter 2: Delays in the early M phase and anaphase onset are accompanied by SAC activation

2-1. Introduction

M phase is a highly complex event regulated by different kinases and phosphatases to ensure proper chromosome segregation and maintain the genetic fidelity. In the present study it was found that inhibition of ALK delays M-phase progression. Moreover, inhibition of ALK caused misalignment of chromosomes in metaphase. Chromosome misalignment can occur due to various reasons such as defects in spindle formation, chromosome congression error, and defect in kinetochore microtubule attachment [70,71]. Furthermore, defect in chromosome alignment and/or spindle formation can trigger the spindle assembly checkpoint (SAC) activation. To understand the mechanism beyond the ALK-inhibition induced delay in the early M phase, M-phase progression was observed precisely by time-lapse imaging and involvement of SAC was evaluated in this chapter.

The SAC also known as the mitotic checkpoint is the regulatory signal that ensures accurate chromosome segregation between the two daughter cells and thereby maintains the mitotic fidelity [72]. The SAC can prevent chromosome mis-segregation and aneuploidy that is implicated in tumorigenesis. Proper chromosome segregation depends on the successful attachment of chromosomes on its sister kinetochores to microtubules emanated from two opposite poles [73]. The plus end of the microtubules binds to kinetochore through the KMN protein network (consist of Knl1/Mis12/Ndc80 protein complex), a crucial constituent of the outer kinetochore [72,74]. Only when sister kinetochores are attached to the microtubules from opposite poles of the spindle and become bi-oriented, sister-chromatids can be accurately segregated to daughter cells at anaphase (Fig. 17A).

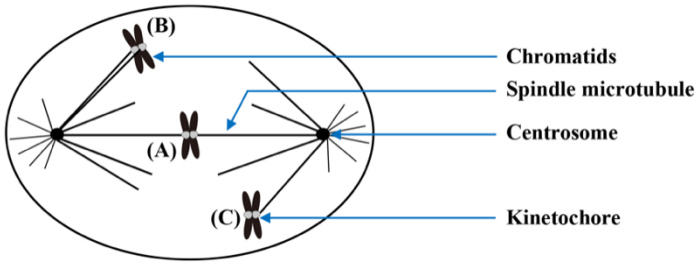

Figure 17. Different forms of attachment between kinetochore and microtubules. Kinetochore and microtubule attachment can occur in different ways depending on several factors. The correct attachment is considered when both sister kinetochores bind microtubules from both poles (**A**). However, when both sister kinetochores bind microtubules emanated from the same spindle pole (**B**) or only one kinetochore binds microtubules and the other remains unbound (**C**), these attachments are considered as an improper attachment.

However, the position of the chromosome within the cell and the relative geometry of the sister-kinetochores relative to the microtubules at the onset of the prometaphase can contribute to the mis-attachment of the kinetochore and the microtubule [75]. Such mis-attachments include the binding of one kinetochore to the microtubules from one spindle pole while its sister is unattached or both sister kinetochores are attached to the microtubules from the same spindle pole [76] (Fig. 17B, C). Incorrect attachment can cause unbalanced tension, the error of the chromosome alignment and lagging chromosome during the anaphase.

The key signal for SAC activation is the presence of unattached or improperly attached kinetochores, which produces an inhibitory signal to prevent the onset of the anaphase. The SAC senses the occupancy of the microtubules at the surface of the kinetochores and the inter-kinetochore tension when the sister-kinetochores are linked to opposite spindle poles [77]. A single unattached kinetochore is capable of activating the SAC signaling cascade and sustaining a mitotic arrest [78]. This signal triggers the formation of the mitotic checkpoint complex (MCC), which is comprised of highly conserved proteins, such as the mitotic arrest defect 2 (MAD2), the budding uninhibited by benzimidazole related 1 (BubR1), Bub3, and cell division cycle 20 (Cdc20) [79] (Fig. 18).

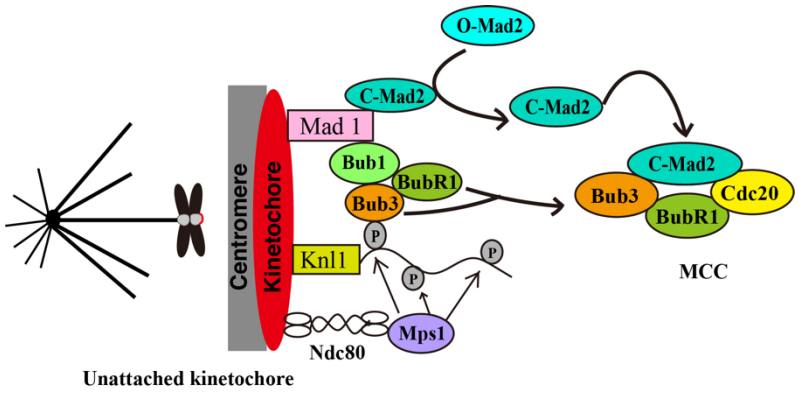

Figure 18. Formation of the MCC complex in response to the signal from an unattached kinetochore. In response to the SAC-on signal, MCC complex, which consists of c-Mad2, BubR1, Bub3 and Cdc20, is formed. All of these SAC components are recruited to the unattached kinetochore in a sequentially.

All checkpoint proteins localize dynamically to unattached kinetochores. The Knl1 protein act as a receptor for the Bub3-Bub1-BubR1 complex as the monopolar spindle 1 (Mps1) phosphorylates the MELT (Met–Glu–Leu–Thr) repeat in Knl1 [80]. Both the Bub1 and BubR1 contain a short motif that plays a role in the localization of Cdc20. Moreover, a complex of Mad1-C-Mad2 acts as a scaffold bound to kinetochore catalyzes conformational conversion of Mad2 protein from the open form (O-Mad2) to closed form (C-Mad2) [81,82]. The direct interaction

between Bub1 and Mad1 has also been reported [83]. Mad2 induces conformational changes of Cdc20 and allow it to bind with the N terminus of BubR1 bound to Bub3 to generate the MCC complex[84].

When MCC is formed, Cdc20 which serves as a co-activator of APC/C, is unable to activate APC/C, resulting in inhibition of anaphase onset [85]. Inhibition of APC/C leads to inhibition of ubiquitination of both securin and cyclin B1. Therefore, separase remains bound with securin in an inactive form and is unable to cut cohesion connecting two sister chromatids. As a result, the sister chromatids separation is failed. Once all chromosomes align at the equator with proper attachment of the kinetochores to the microtubules, SAC becomes silenced and MCC is disassembled [86]. The active APC/C catalyzes the ubiquitination of cyclin B1 and securin [87]. Degradation of securin, an inhibitor of the protease separase, leads to cohesin proteolysis, sister-chromatid separation, and progression to anaphase. Degradation of cyclin B1 results in the inactivation of the CDK1, leading to the dephosphorylation of proteins that are phosphorylated at the mitotic entry. This is required for the exit from M phase. In the Chapter 1, ALK inhibition caused defect in chromosome alignment, which is enough to activate SAC and delay the anaphase onset. In this Chapter 2, to explore the mechanisms underlying ALK inhibitor-caused M-phase delay, M-phase progression was observed precisely by time-lapse imaging, and effects of inhibition of SAC components on this M-phase delay was investigated.

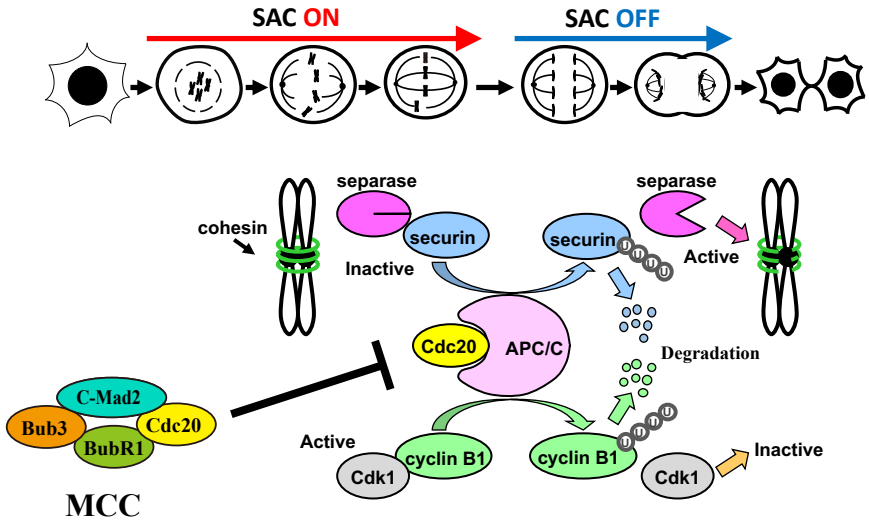

Figure 19. The Spindle assembly checkpoint halts M-phase progression until all chromosomes are bound to the microtubules. Unattached kinetochore triggers MCC formation, which inhibits the ubiquitin ligase APC/C. As a result, separase cannot be released from securin and remains in an inactive form. Consequently, cohesin degradation by separase is halted and sister chromatids are not separated. This phenomenon leads to delay in the anaphase onset.

2-2. Materials and methods

2-2-1. Cell culture

Cell culture was performed as described in Chapter 1, Section 1-2-1.

2-2-2. Chemicals

AZ3146, an Mps1 inhibitor was purchased from Adooq Bioscience (Irvine, CA, USA) and dissolved in DMSO (Nacalai Tesque, Kyoto, Japan).

2-2-3. siRNA transfection

siMAD2 (Hs01_00042213, 5'-GUUGGAAGUUUCUUGUUCATT-3') was purchased from MilliporeSigma (Burlington, MA, USA). To knockdown MAD2, 20 pmol of siMAD2 was transfected into SH-SY5Y cells using Lipofectamine 2000 (Invitrogen, Carlsbad, CA, USA).

2-2-4. Synchronization of cells using RO-3306

SH-SY5Y cells were synchronized as described in Chapter 1, Section 1-2-5.

2-2-5. Time-lapse imaging

Time-lapse imaging was performed in both crizotinib- and siALK-treated conditions. SH-SY5Y cells were seeded in 24-well plates, and the cell cycle was synchronized with 4 μM RO-3306 for 20 h. After cells were washed with pre-warmed PBS (+) four times at 37°C on a water bath, cells were immediately cultured with DMEM containing 1 μM crizotinib or DMSO. Hoechst 33342 was also added to the cultures and the cells in 24-well plates were then set in the live cell chamber of an Operetta imaging system (Perkin Elmer, Waltham, MA, USA), which was maintained at 37°C under 5% CO_2 atmosphere. The live-cell images of brightfield and fluorescence of Hoechst 33342 were captured every 3 min for 5 h. Likewise, SH-SY5Y cells were seeded in 24-well plates and transfected with 20 pmol of siCtrl and siALK #1 using Lipofectamine 2000. Cells were then synchronized with RO-3306 as mentioned above. Immediately after release from RO-3306, cells were cultured in pre-warmed DMEM containing 5% FBS and 0.1 μM Hoechst 33342 and live-cell images were obtained.

The duration of each phase was measured by observing individual cells until the end of the imaging. The duration of prophase/prometaphase was defined as from mitotic entry (chromosomes condensation/cell round up) to the timing just before metaphase (chromosomes alignment at the cell equator). The time from chromosomes alignment to the beginning of their separation and from chromosomes separation to cleavage furrow completion were defined as metaphase and anaphase/telophase, respectively.

The bar graph was prepared to show the duration of each phase of each individual cell from mitotic entry to furrow completion. A line graph was prepared to clearly understand the percentage of cells remained in each phase at a specific time. Captured images were processed using the ImageJ (National Institutes of Health, Bethesda, MD, USA), Adobe Illustrator CC (San Jose, CA, USA) software.

2-2-6. Immunofluorescence microscopy

Immunofluorescence microscopy was performed as described in Chapter 1, Section 1-2-7.

2-2-7. Statistics

Statistical analysis was performed as described in Chapter 1, Section 1-2-11. For analysis among more than three independent groups, the Bartlett test was used to determine the homogeneity of variance. For groups with equal variance, data were analyzed by one-way analysis of variance (ANOVA) and then by the Tukey–Kramer multiple comparisons test. A p value lower than 0.05 was considered as significant.

2-3. Results

2-3-1. Crizotinib treatment prolongs prophase/prometaphase and metaphase due to defect in chromosome alignment

To clarify the mechanisms for the ALK inhibitor-induced M-phase delay, time-lapse imaging was performed. SH-SY5Y cells were seeded in a 24-well dish without coverslip to monitor live cell images. Cells were then treated with 4 μM RO-3306 for 20 h to synchronize in the G2/M phase border. Immediately after release from RO-3306, fresh DMEM containing DMSO or crizotinib was added to the cells. Also, Hoechst 33342 was added to the cells to observe chromosome movement. Live-cell images were observed every 3 min for 5 h using an Operetta imaging system. The M phase was divided into three stages: prophase/prometaphase (P/PM), metaphase (M), and anaphase/telophase (A/T), which are indicated by green, red and blue colors, respectively. Representative images of cells treated with DMSO or crizotinib are shown in Figure 20A. It took the DMSO-treated cell 60 min to complete the M phase (from mitotic entry to cleavage furrow completion) while the duration of both P/PM and M were 18 min, and that of A/T was 24 min. On the other hand, crizotinib-treated cells failed to complete the M phase and showed a prolonged P/PM and M until 5 h of observation time. It took this crizotinib-treated cell 60 min to complete chromosome alignment, During the rest of the time, most chromosomes were partly aligned; however, few chromosomes unaligned. Moreover, chromosomes scattering and alignment were fluctuated within a very short time. Through the observation of the morphology of chromosomes in brightfield and fluorescence images, it can be said that the spindle was misoriented during prolonged metaphase.

The duration of each subphase of the individual cell was determined through observation of chromosome morphology and cell shape as described in the materials and methods section 2-2-5. The bar graphs were plotted as the duration of subphases over time (Fig. 20 B). Moreover, cells showing abnormal M-phase characteristics, such as misalignment of chromosomes, misorientation of the spindle, and cell death during mitosis were indicated in the graphs. Almost all (36/37 cells) control cells (DMSO) completed the M phase, and the average duration was 60 min. The average duration of P/PM and M were 31 and 26 min, respectively. In contrast, 31% of crizotinib-treated cells failed to complete the M phase due to prolonged P/PM and M, while few cells were dead. On average, P/PM and M were 74 and 83 min, respectively. Additionally, abnormal M-phase characteristics, including misoriented spindle (23/39 cells) and misaligned chromosomes (20/39 cells), were frequently observed in crizotinib-treated cells. These results suggest that crizotinib caused prolongation of the early M phase through chromosome misalignment and spindle misorientation.

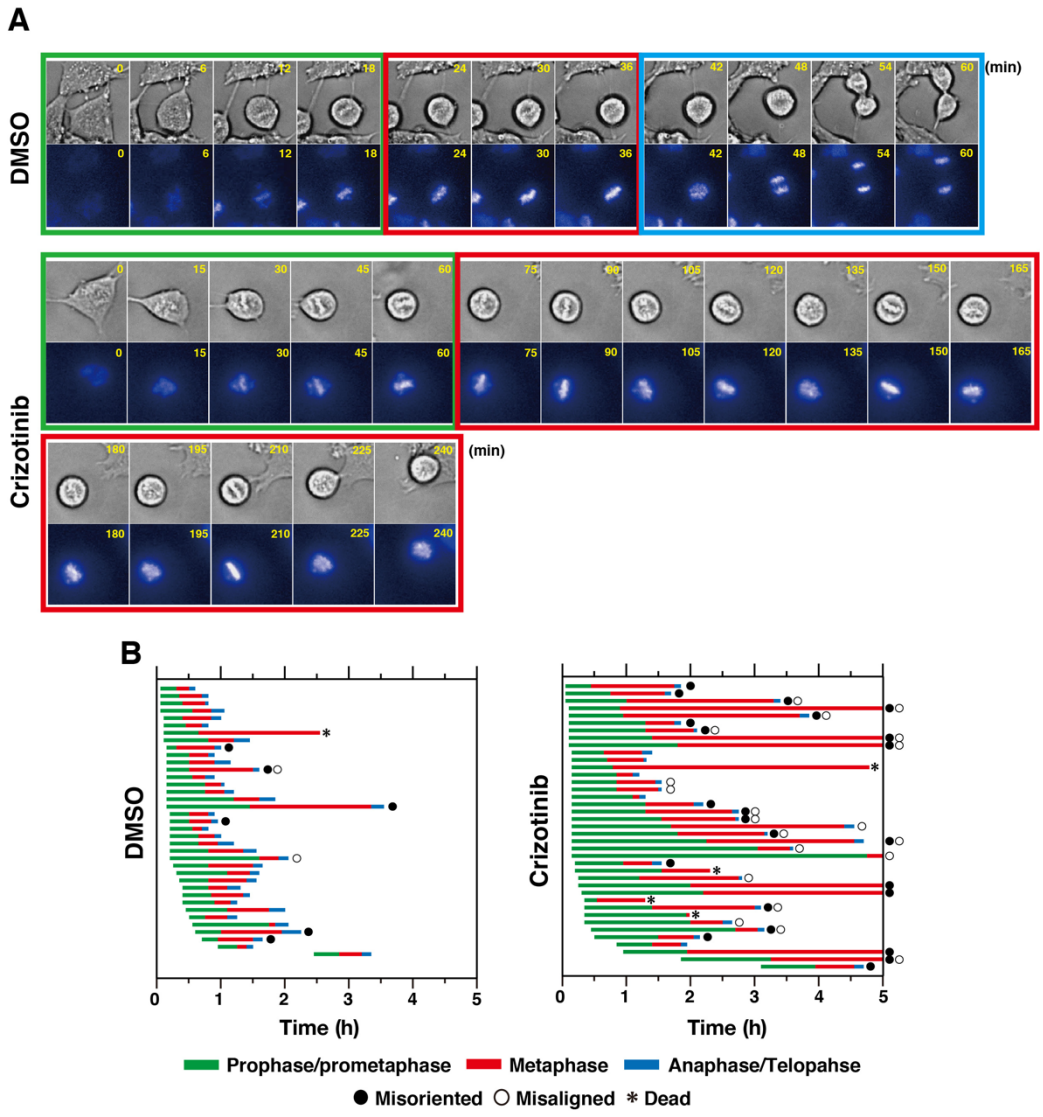

Figure 20. Delay in prophase/prometaphase and metaphase is observed in crizotinib-treated cells. SH-SY5Y cells were seeded in a 24-well dish and incubated for 24 h. Then cells were treated with 4 µM RO-3306 for 20 h. After release, DMEM containing DMSO or 1 µM crizotinib was added together with 0.1 µM Hoechst 33342. The dish was then immediately set in the live cell chamber of the Operetta imaging system. Live-cell images were observed every 3 min for 5 h. (**A**) Representative images of solvent control (DMSO) and crizotinib-treated cells are shown. Scale bar = 10 µm. Different subphases were indicated as follows: P/PM-*green*, M-*red* and A/T-*blue* (**B**) Durations of prophase and prometaphase (P/PM), metaphase (M), and anaphase and telophase (A/T) in 37 control and 39 crizotinib-treated cells are shown in the graph. Cells exhibiting misoriented spindle (closed circle), misaligned chromosomes (open circle), and cell death (asterisk) are indicated.

2-3-2. ALK knockdown prolongs M phase

To precisely understand the mechanism for the ALK knockdown-induced M-phase delay, time-lapse imaging was performed. SH-SY5Y cells were transfected with 20 pmol of siALK #1 or nontargeting siCtrl using Lipofectamine 2000. After 52 h cells were treated with 4 μM RO-3306. After release, cells were cultured in DMEM containing 5% FBS and Hoechst 33342 and then observed in the Operetta imaging system every 3 min for 5 h. Representative brightfield images of cells were shown in Figure 21A. The siCtrl-treated cells completed the M phase in only 63 min whereas it took the siALK #1-treated cells 135 min. Cell morphology observed in the brightfield images showed that the duration of prophase/prometaphase and metaphase was prolonged in siALK #1-treated cells.

The duration of each subphase of individual cells was monitored based on chromosome morphology as described in the Materials and Methods. The M phase was divided into three stages, as described in 2-3-1. Moreover, abnormal M-phase characteristics were monitored and indicated similarly to Figure 20B. The duration of each subphase was plotted in the bar graph (Fig. 21B). This graph clearly shows that it took ALK knockdown cells a longer time to complete the M phase compared to control cells. On average the duration from mitotic entry to furrow completion in control cells was 60 min, while those of P/PM and M were average 29 and 23 min, respectively. On the other hand, the average duration of P/PM and M in siALK-transfected cells was far more prolonged compared to control cells. It took these cells an average of 63 and 40 min to complete P/PM and M, respectively. The abnormal M-phase characteristics were more prominent in ALK knockdown cells exhibiting misalignment of chromosomes (9/31 cells) and misorientation of the spindle (14/31 cells). A fraction of ALK knockdown cells (16%) failed to complete the M phase until the observation time.

The line graph (Fig. 21C) was prepared based on the bar graph and shows the percentage of cells in each phase to clearly understand the progression of cells through the M phase. The black dot line indicates the percentage of M-phase cells. In siCtrl-treated cells, each line graph possesses a peak and declined to zero, indicating that cells entered each subphase after a particular time and all cells completed M phase. Unlikely, the line graph for ALK-knockdown cells shows that the red line (metaphase) starts at 30 min and possesses a lower peak, indicating prolongation of P/PM compared to control cells. Moreover, as few siALK-treated cells failed to complete the M phase, the line graph representing P/PM and M don't decline to zero.

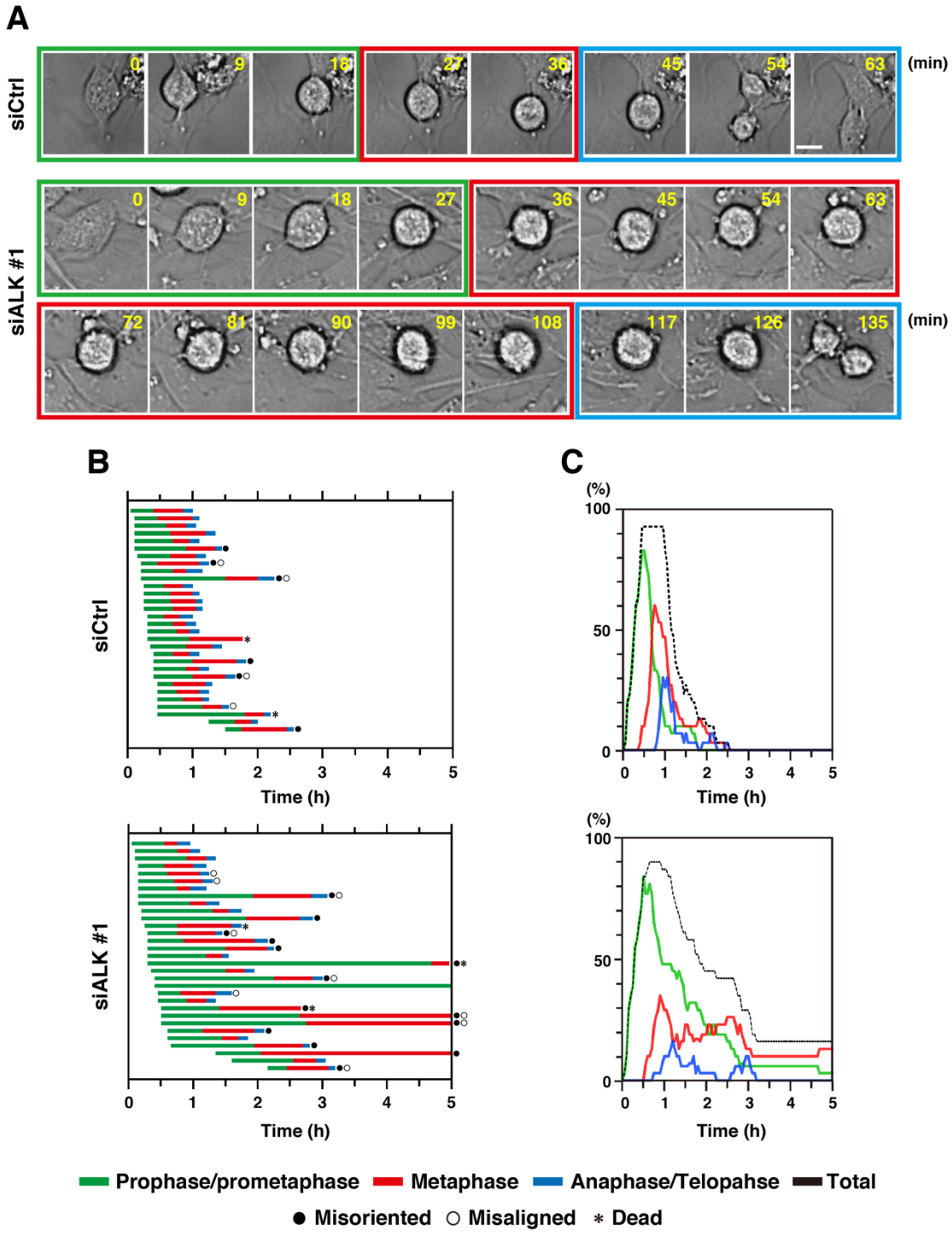
A
siCtrl
0
9
18
27
36
45
54
63
(min)
siALK #1
0
9
18
27
36
45
54
63
72
81
90
99
108
117
126
135
(min)
B
siCtrl
siALK #1
Time (h)
C
(%)
100
50
0
Time (h)
Prophase/prometaphase
Metaphase
Anaphase/Telopahse
Total
Misoriented
Misaligned
Dead

Figure 21. Prophase/prometaphase and metaphase are delayed in ALK-knockdown cells. SH-SY5Y cells were seeded in 24-well plate without cover glass and transfected with 20 pmol of ALK-targeting siRNA (siALK #1) or nontargeting siCtrl using Lipofectamine 2000. After 52 h, cells were treated with 4 μM RO-3306 to synchronize cells at the G2/M border. After release from the RO-3306 treatment, fresh DMEM containing Hoechst 33342 was added to the cells and the dish was immediately set in the live cell chamber. Time-lapse imaging was performed every 3 min for 5 h. (**A**) Representative brightfield images of cells transfected with siCtrl or siALK are shown. Scale bar = 10 μm. (**B**) The bar graph shows durations of prophase and prometaphase (P/PM, *green*), metaphase (M, *red*), and anaphase and telophase (A/T, *blue*) for 30 and 31 individual cells treated with siCtrl and siALK, respectively. Cells showing misoriented spindle, misaligned chromosomes and dead cells are indicated by a closed circle, open circle and asterisk, respectively. (**C**) Percentages of total mitotic cells (*black*), and cells in P/PM (*green*), M (*red*), and A/T (*blue*) are shown in a line graph.

2-3-3. SAC activation accompanies the ALK inhibition-induced M-phase delay

SAC is activated by the signal triggered by the unattached kinetochore and can halt M-phase progression in metaphase to ensure proper chromosome segregation. Inhibition of ALK delayed progression in the early M phase and increased the number of cells exhibiting abnormal M-phase characteristics, including a defect in chromosome alignment. Hence, to investigate whether ALK inhibition was accompanied by SAC activation, the SAC component Mps1 kinase was inhibited by the inhibitor AZ3146 together with crizotinib. SH-SY5Y cells were seeded in a 35-mm dish with cover glass and incubated for 24 h. Cells were then synchronized with RO-3306, and after release from the RO-3306 treatment, cells were exposed to 0.5 μM crizotinib alone or in combination with the AZ3146 for 45 min (Fig. 22A). Cells were fixed with 4% HCHO and permeabilized by PBS containing 3% BSA and 0.1% saponin. Cells were then stained with anti-α-tubulin antibody and Hoechst 33342 to observe microtubule and chromosome morphologies under a fluorescence microscope (Fig. 22B). M phase was divided into four groups: prophase/prometaphase (P/PM), metaphase (M), anaphase/telophase (A/T), and cytokinesis (Cyto) (Fig. 22C). In the solvent control (DMSO), 38% of cells were progressed to cytokinesis after 45-min release. Upon AZ3146 treatment, most of the cells progressed to cytokinesis, indicating inhibition of SAC by AZ3146 treatment. Inhibition of ALK by crizotinib-treatment caused accumulation of 52% of cells in P/PM, indicating delay in the early M phase. On the contrary, simultaneous AZ3146-treatment with crizotinib decreased the accumulation of cells in P/PM, and most of the cells were found to progress in cytokinesis. The mitotic index representing the percentage of M-phase cells showed no significant changes among different groups, indicating no effects on mitotic entry (Fig. 22D). These results suggest that SAC is activated in ALK inhibitor-treated cells and participates in M-phase delay.

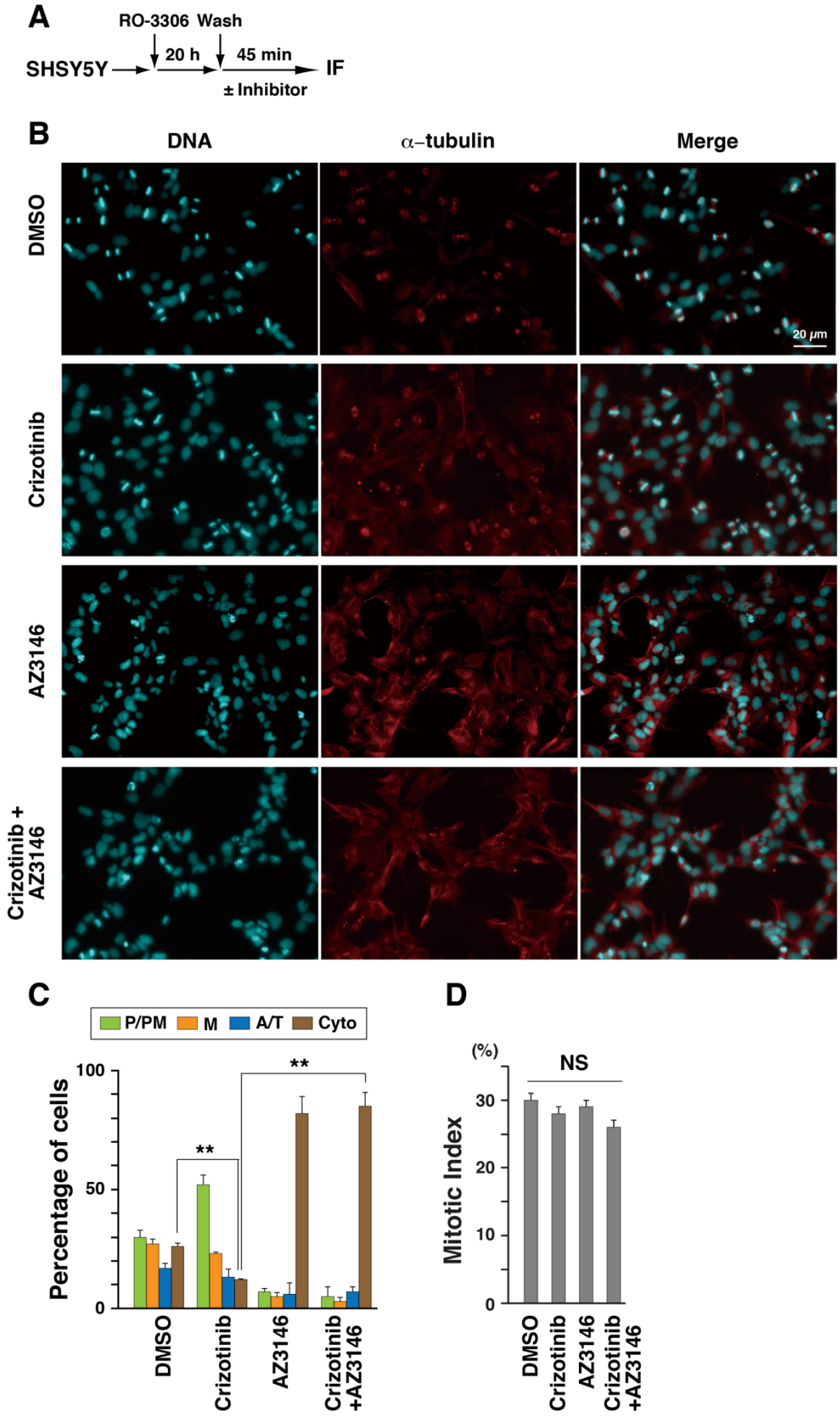
A
RO-3306 Wash
20 h
45 min
SHSY5Y
IF
± Inhibitor
B
DNA
α–tubulin
Merge
DMSO
Crizotinib
AZ3146
Crizotinib + AZ3146
20 μm
C
P/PM
M
A/T
Cyto
Percentage of cells
100
50
0
**
**
DMSO
Crizotinib
AZ3146
Crizotinib +AZ3146
D
(%)
NS
Mitotic Index
30
20
10
0
DMSO
Crizotinib
AZ3146
Crizotinib +AZ3146

Figure 22. SAC contributes to the crizotinib-induced M-phase delay. SH-SY5Y cells were seeded in a 35-mm dish and then treated with 4 μM RO-3306 for synchronization. After release from RO-arrest, DMEM was added to the cells containing DMSO, 0.5 μM crizotinib, 4 μM AZ3146, or a combination of both for 45 min. (**A**) Schematic representation of experimental protocol. (**B**) Representative images of cells were captured using a 20× objective, indicating the abundance of cells in P/PM on crizotinib treatment and in Cyto under AZ3146 treatment and its combination with crizotinib. Scale bar = 20 μm. (**C**) M-phase cells were classified into four groups: prophase/prometaphase (P/PM), metaphase (M), anaphase/telophase (A/T), and cytokinesis (Cyto). The graph shows the percentages of cells in subphases ($n > 256$ in each experiment) as mean ± SD, calculated from three independent experiments. (**D**) The percentage of mitotic cells was plotted ($n > 464$ in each experiment) as mean ± SD, calculated from three independent experiments. *P* value was calculated by using the Tukey–Kramer multiple comparison test. $^{**}p < 0.01$; NS, non-significant.

2-3-4. Knockdown of MAD2 confirms SAC activation in ALK inhibitor-treated cells

MAD2 is another core component of SAC and plays a critical role in MCC complex formation, which inhibits APC/C-cdc20 complex and thereby delays the anaphase onset. To support the inference of SAC activation upon ALK inhibition, MAD2 was knocked down using siRNA. In this experiment, SH-SY5Y cells were seeded in a 24-well plate with cover glass. Cells were then transfected with 20 pmol of siMAD2 using Lipofectamine 2000, and after 28 h cells were synchronized with RO-3306. During release from RO-3306 treatment, cells were treated with crizotinib for 45 min (Fig. 23A). Immunofluorescence staining was performed and based on microtubule and chromosome morphologies; M-phase cells were divided into four groups as described in section 2-3-3. Consistent with previous result, 42 % of solvent control DMSO-treated cells progressed to cytokinesis (Fig. 23B). Upon MAD2 knockdown, 62% of cells were progressed to cytokinesis, indicating SAC inactivation in MAD2-knockdown cells. ALK inhibition by crizotinib treatment showed a similar delay in the M phase. However, 48% of cells progressed to cytokinesis after 45-min of treatment upon MAD2 knockdown in crizotinib-treated cells, confirming that SAC is activated in crizotinib-treated cells. These observations suggest that SAC participates in ALK inhibitor-induced delay in the onset of anaphase. The mitotic index showed no change among the different groups (Fig. 23C), indicating crizotinib treatment alone or in combination with MAD2 knockdown did not affect the mitotic entry.

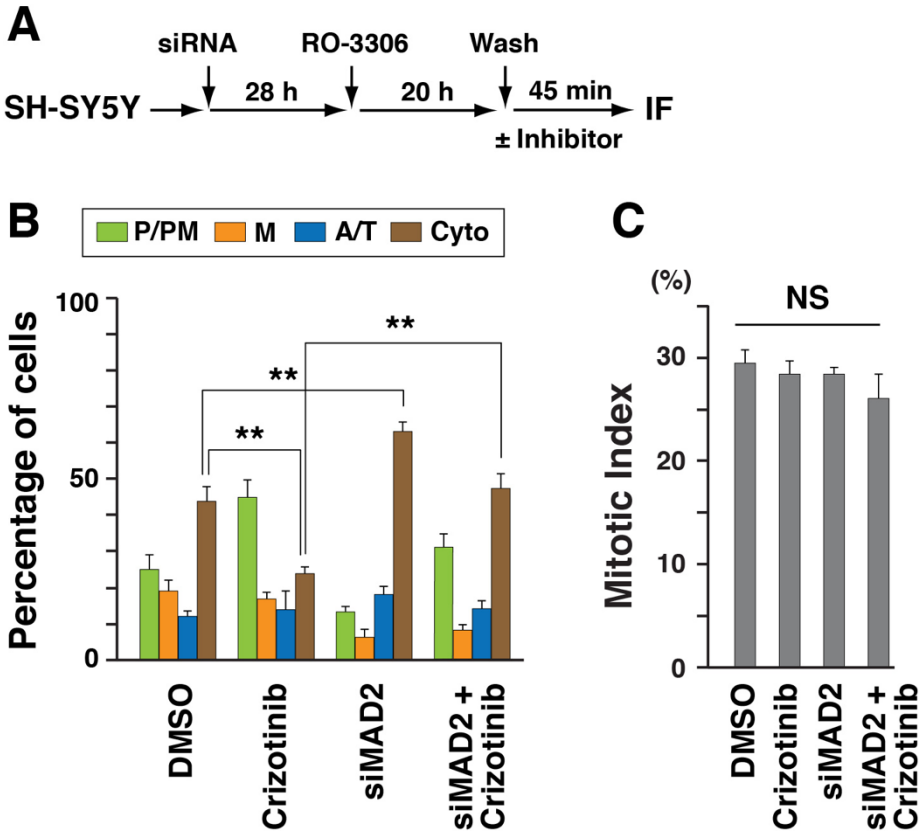

Figure 23. MAD2 knockdown rescues crizotinib-induced M-phase delay. SH-SY5Y cells were seeded in a 24-well plate with cover glass. Cells were transfected with siMAD2 using Lipofectamine 2000. RO-3306 was added to the cells to be synchronized. After release, cells were treated with DMSO or 0.5 μM crizotinib separately or in MAD2 knockdown cells for 45-min. (**A**) Schematic representation of experimental protocol. (**B** and **C**) Immunofluorescence staining was performed with anti-α-tubulin antibody and Hoechst33342. Cells were observed under a fluorescence microscope and M-phase cells were divided into four groups: prophase/prometaphase (P/PM), metaphase (M), anaphase/telophase (A/T), and cytokinesis (Cyto). The percentage of cells in each subphase ($n > 240$ in each experiment) and mitotic indices ($n > 470$ in each experiment) are plotted. The mean ± SD was calculated from three independent experiments. The Tukey–Kramer multiple comparison test was used to calculate *p* values. $^{**}p < 0.01$; NS, non-significant.

2-4. Discussion

In this chapter, detailed investigation of the M phase after ALK inhibition revealed the underlying mechanism of M-phase delay. An abnormality in chromosome alignment and spindle orientation was mainly observed upon ALK inhibition in cells exhibiting M-phase delay before anaphase onset. Such abnormalities trigger SAC activation that halts cells in metaphase, contributing to the delay of anaphase onset.

Chromosome alignment at the cell equator and spindle orientation during metaphase are two fundamental events required for proper cell division. Chromosome alignment ensures equal segregation of chromosomes, and proper spindle positioning determines the cleavage plane and size of the daughter cells. Both of these events also determine cell fates, since errors in these processes lead to aneuploidy or polyploidy progeny of cells through asymmetrical chromosome segregation. In this study, it was found that almost all crizotinib- and siALK #1-treated cells exhibited either chromosome misalignment and/or spindle misorientation (Figs. 20B and 21B). These cells either resolved such defects by taking a long time and progressed to anaphase or continuously tried to align all chromosomes until 5 h of observation time. Although the fate of these cells was not determined, it is assumed that those cells may be unable to resolve mitotic errors and may face cell death.

Error in chromosome alignment triggers spindle misorientation by dysregulating cortical localization of motor protein LGN, a component of dynein–dynactin complex regulating spindle positioning [88,89]. Moreover, chromosome misalignment resulted in improper segregation of chromosomes [90,91]. Increased levels of chromosome mis-segregation can cause cell death and suppression of cell proliferation via inducing chromosomal instability (CIN) [92]. In ALK-inhibited cells only 10% of cells were found to be dead (Figs. 20B and 21B). Therefore, it can suggest that ALK-inhibition may induce CIN lower than the threshold level, giving rise to the generation of genetic diversification without causing cell death. Broad genetic diversity can generate resistance to inhibitors in cells treated with inhibitors for a long period [93].

The kinetochore of each chromatid plays a key role in the binding with microtubules through the KMN network [94]. Defect in kinetochore-microtubule attachment and/or spindle orientation can lead to SAC activation [95] that inhibits APC/C-cdc20 complex and inhibit chromosome segregation. SAC is an important regulator of M phase that plays a key role in ensuring proper chromosome segregation. Inhibition of SAC components causes premature mitotic exit with chromosome mis-segregation. In ALK inhibitor-treated cells, misalignment of chromosome and/or spindle misorientation triggered SAC activation that accompanies the M-phase delay (Figs. 22C and 23B). Therefore, a combination of crizotinib with SAC inhibitor caused premature mitotic exit, leading to higher CIN and generation of aneuploid cells. These

cells may either become senescence or undergo apoptosis depending on the degree of DNA damages.

From these observations, it can be summarized that ALK-induced delay in the early M phase is achieved due to defects in the chromosome alignment and spindle misorientation. These defects stimulate SAC activation. Active SAC signal inhibits anaphase onset and hence hinders chromosome segregation. Therefore, ALK-inhibition induced M-phase delay is accompanied by SAC, resulting in suppression of cell proliferation. The summary of this observation is illustrated in the following Figure 24.

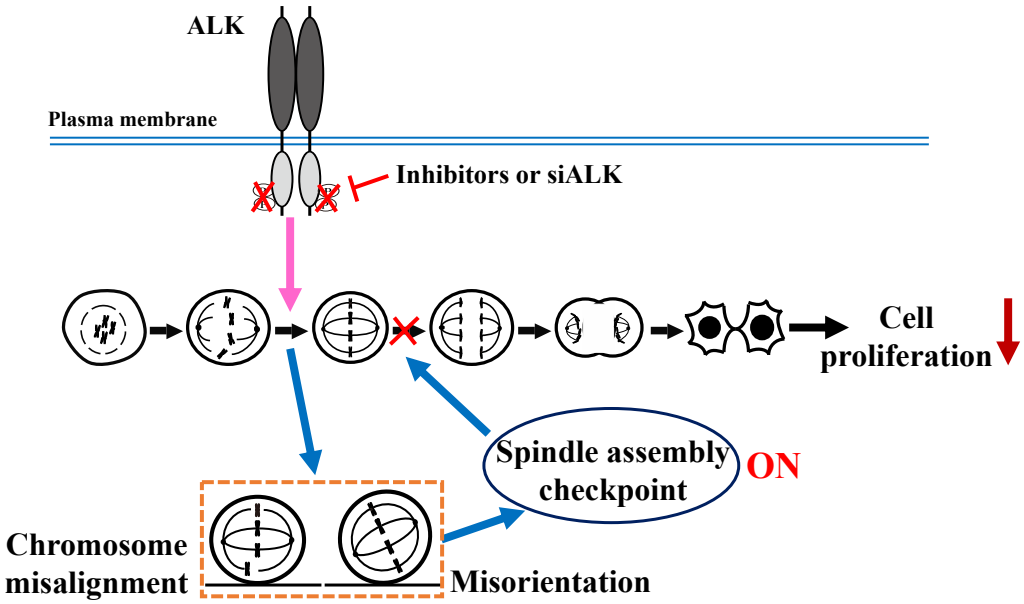

Figure 24. Summary of chapter 2. Inhibition of ALK either by inhibitors or siRNA causes defects in chromosome alignment and spindle misorientation. Such defects can lead to SAC activation. The SAC inhibits progression from metaphase to anaphase. Therefore, SAC activation is one of the mechanisms that participate in ALK inhibition-induced M-phase delay and suppression of cell proliferation.

Chapter 3: Inhibition of the EML4-ALK fusion protein causes delay in the M phase

3-1. Introduction

The echinoderm microtubule-associated protein-like 4 (EML4) is a microtubule-associated protein expressed in most cell types and is essential for cell proliferation and survival [96,97]. EML4 is a member of the EML-family proteins and is localized at the mitotic spindle [98]. EML4 exhibits a regulatory role in mitotic progression as it is required for the organization of mitotic spindle and for the attachment of microtubule to kinetochore [97,98]. The fusion between EML4 and ALK was the first identified ALK fusion in the solid tumor, non-small-cell lung carcinoma (NSCLC). NSCLC is the most common type of lung cancer cases, accounting for 85% of all cases [99]. Studies reported that around 3-7% of lung tumors harbor an EML4-ALK fusion [32]. The EML4-ALK oncoprotein has been also identified in several other types of cancer, such as breast and colorectal cancer [100]. Both the *EML4* and *ALK* genes are located in chromosome 2p. The paracentric inversion of the short arm of chromosome 2 leads to the formation of the EML4-ALK fusion oncoprotein [101] (Fig. 25).

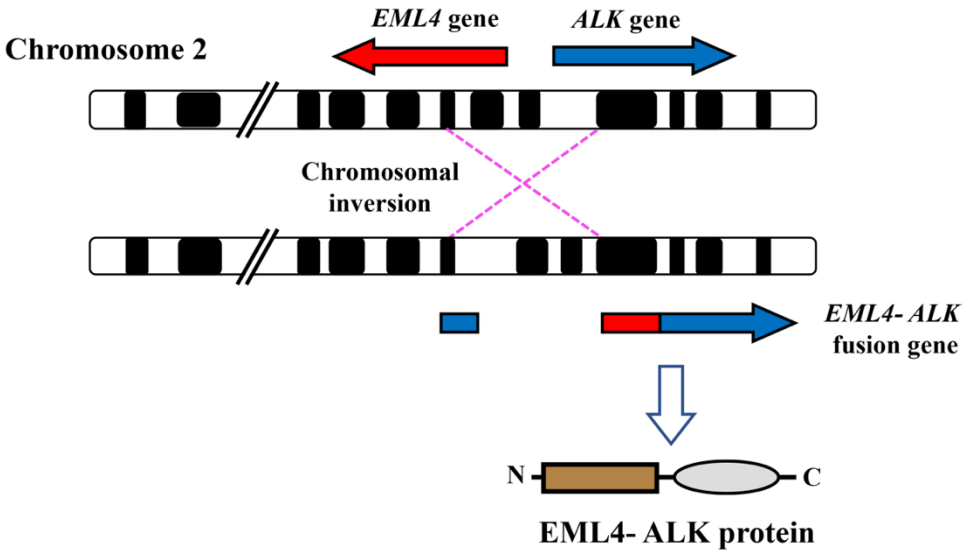

Figure 25. Inversion of chromosome 2p generates EML4-ALK fusion protein. The chromosomal inversion occurs at the short arm of chromosome 2, leading to the formation of the EML4-ALK fusion protein.

The breakpoint in the ALK gene lies near to the 5' end of exon 20. Therefore, the cytoplasmic domain containing the tyrosine kinase domain is only incorporated in EML4-ALK fusion [102]. While the amino-terminal part of EML4 is incorporated in the fusion. The amino-terminal coiled-coil domain of EML4 is responsible for the dimerization of the fusion proteins, which is necessary for the transforming activity of EML4-ALK [15]. The breakpoints of the EML4 gene are more variable. The alternative breakpoint of the EML4 gene results in multiple EML4-ALK variants, while all variants contain the intracellular tyrosine kinase domain of ALK encoded by exon 20. To date, at least 15 variants of EML4-ALK has been identified [18,101]. The localization and stability of these variants are different because of their slightly varying structural differences. Different EML4-ALK variants exhibit different responses against ALK inhibitors as they may have varying biological and clinical significance in NSCLC [103]. Similar to NPM-ALK fusion oncoprotein, EML4-ALK remains constitutively active and drives downstream signaling pathways such as Ras/ERK, PI3K/Akt and JAK/STAT pathways, resulting in enhanced proliferation and reduced apoptosis of transformed cells.

In clinical, cell proliferation is suppressed by inhibition of EML4-ALK in the ALK fusion-expressing NSCLC. The first patient-based study that was carried out in 2010 showed an approximately 57% of response ratio to crizotinib, which is extremely high compared to the second-line chemotherapy (docetaxel and pemetrexed) by which response ratio was below 10% [35]. Despite these encouraging results, development of the resistance, which is due to the activation of bypass pathways to growth signals, limits the effectiveness of these inhibitors. Lung cancer H3122 and H2228 cells have been widely used in preclinical cancer research. Treatment of these cells with the ALK inhibitors results in a potent suppression of Akt and Erk1/2 phosphorylation and induces cytotoxic or cytostatic responses [34]. Compared to H3122 cells, H2228 cells show resistance against inhibitors. This is due to that ERK phosphorylation is triggered by another receptor-type tyrosine kinase and is not suppressed by ALK inhibitors alone [104]. Indeed, a combination of ALK inhibitor with Met inhibitor suppresses ERK phosphorylation and suppresses cell proliferation, indicating that the MEK/ERK pathway, whose activation is independent of ALK, is responsible for the proliferation of H2228 cells [104,105].

Like other chemotherapies, resistance to ALK inhibitors is developed in clinical. To combat the resistance, to identify a novel mechanism underlying the inhibitor-caused suppression of cell proliferation remains in high demand. In the Chapter 1 and 2, the effects on M-phase progression was investigated in full-length ALK-expressing SH-SY5Y cells. However, whether inhibition of EML4-ALK affected M-phase progression was unknown. In the Chapter 3, the effect of EML4-ALK inhibition by TAE684, an ALK-specific inhibitor, on the M-phase progression was analyzed in H2228 cells, as a model for drug-resistant cancer cells.

3-2. Materials and methods

3-2-1. Cell culture

Non-small lung cancer H2228 cells were obtained from ATCC (American Type Culture Collection, Manassas, VA, USA) and were cultured in Dulbecco's Modified Eagle's Medium (DMEM). This culture media was enriched with HEPES-NaOH (20 mM, pH 7.4) and fetal bovine serum (5% FBS) at 37°C in a 5% CO_2 atmosphere.

3-2-2. Antibodies

The following antibodies were used for the Western blotting analysis, as mentioned in Chapter 1: rabbit monoclonal anti-ALK and anti-pALK Y1507 antibodies, and goat anti-Lamin B antibody. Moreover, HRP-conjugated donkey anti-rabbit IgG (1:4000; 711-035-152) and bovine anti-goat (1:4000; sc-2350) secondary antibodies were also used.

3-2-3. Western blotting analysis

Western blotting was performed as described in Chapter 1, Section 1-2-6.

3-2-4. Cell viability assay

Viability assay was performed using Cell Counting Kit-8 as described in Chapter 1, Section 1-2-8. H2228 cells (1.2×10^4 cells per well) were seeded in 96-well plates and subsequently cultured with crizotinib, ceritinib and TAE684 (0.001, 0.01, 0.1, 1, and 10 μM conc.) for 3 days. As a solvent control, 0.1% of DMSO was used. The number of viable cells was estimated based on the absorbance of reduced WST-8 at 450 nm.

3-2-5. Time-lapse imaging

H2228 cells were seeded in 24-well plates without cover glass and were incubated for 24 h. Cells were subsequently treated with DMEM containing DMSO or 0.7 μM TAE684. Hoechst 33342 was added to the cell to observe chromosome movement. The plate was placed in the live cell chamber of an Operetta imaging system (as mentioned in Chapter 2, Section 2-2-5). The live-cell images of the brightfield and the fluorescence of Hoechst 33342 were captured every 5 min for 12 h. The duration of each phase was determined based on the method as described in Chapter 2, Section 2-2-5. Cell death during mitosis was recognized by DNA fragmentation or the blebbing of the plasma membrane. The mitotic exit was morphologically judged by the re-attachment of M-phase cells to the dish.

3-3. Results

3-3-1. Determination of the IC_{50} values of inhibitors in H2228 cells

To determine the IC_{50} values of ALK inhibitors in H2228 cells, WST-8 assay was performed. Cells were seeded in 96-well plates (12,000 cells/well). Cells were treated with crizotinib, ceritinib, and TAE684 in different concentrations. After 3 days of incubation, 10 µL of WST-8 was added to each well and cells were incubated for 1 h at 37°C. The absorbance of the reduced 2-(2-methoxy-4-nitrophenyl)-3-(4-nitrophenyl)-5-(2,4-disulfophenyl)-2H-tetrazolium monosodium salt was measured at 450 nm using a microplate reader. Data are plotted as a ratio to solvent control calculated for each inhibitor. All three inhibitors decreased the absorbance ratio in a concentration-dependent manner (Fig. 26). The IC_{50} values were calculated from three independent experiments as described in the Materials and methods section 1-2-8 and showed as mean ± SD. Among the three inhibitors, crizotinib has a higher IC_{50} value, while TAE684 has the lowest one. This result indicates that H2228 cells were very sensitive to TAE684 but may be relatively resistant to crizotinib.

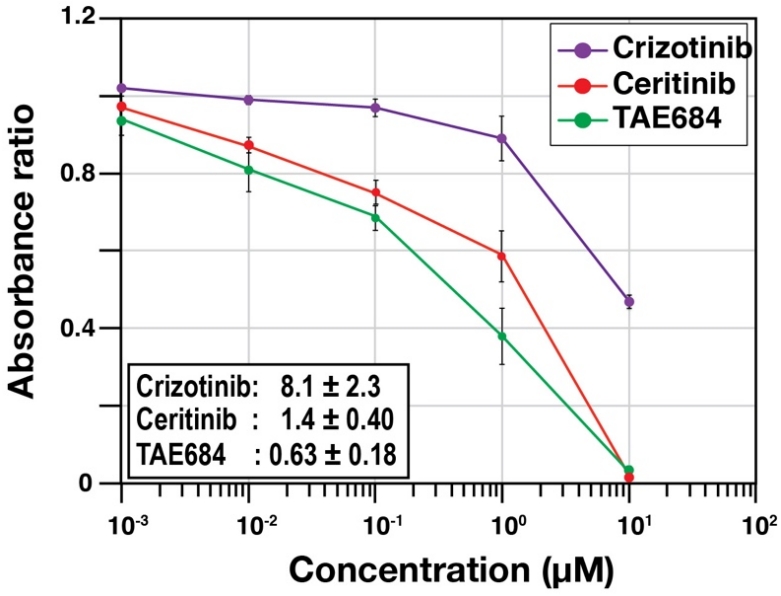

Figure 26. Inhibitors suppress the proliferation of H2228 cells. H2228 cells were seeded in a 96-well plate (1.2×10^4 cells per well) and then treated with crizotinib, ceritinib and TAE684 at different concentrations (0.001, 0.01, 0.1, 1, and 10 µM). After 3 days of incubation, WST-8 was added to the cells and absorbance was measured to determine viable cells. Relative values of absorbance to solvent control (DMSO) are shown as mean ± SD and calculated from three independent experiments. The IC_{50} value was calculated from three independent experiments.

3-3-2. Inhibitors suppress the phosphorylation of EML4-ALK

To examine whether ALK inhibitors suppressed autophosphorylation of EML4-ALK, H2228 cells were treated with three inhibitors for 1 h at around IC_{50} concentrations. Cells were lysed using SDS-sample buffer and denatured at 40°C for 20 min. The same amount of cell lysates was subjected to SDS-PAGE using 7% gel. The components of the lysates were transferred onto the PVDF membrane and sequentially exposed to anti-pALK, anti-ALK and anti-Lamin B antibodies. Inhibitor treatment completely decreased EML4-ALK phosphorylation but not total EML4-ALK protein levels (Fig. 27). This result suggests that ALK inhibitors suppress the auto-phosphorylation of EML4-ALK.

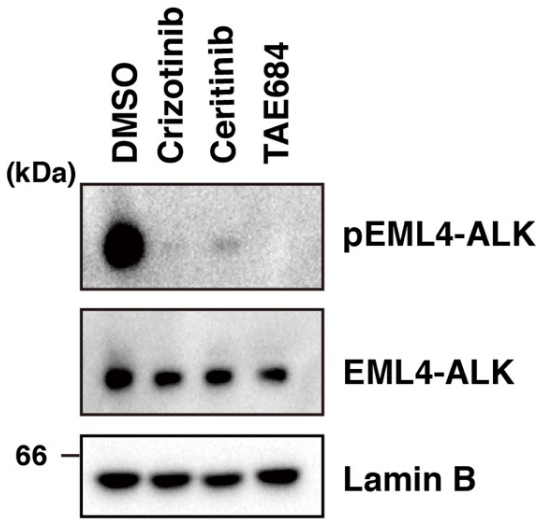

Figure 27. Inhibition of phosphorylation of EML4-ALK by inhibitors. H2228 cells were seeded in 35 mm dish and incubated for 24 h. Then, cells were treated with DMSO, 8.2 μM crizotinib, 1.4 μM ceritinib, and 0.7 μM TAE684 for 1h at 37°C. Whole-cell lysates were obtained and analyzed by Western blotting using anti-pEML4-ALK, anti-EML4-ALK, and anti-Lamin B (loading control) antibodies. pEML4-ALK and total EML4-ALK were detected at around 90 kDa position.

3-3-3. The M phase was prolonged due to EML4-ALK inhibition

To evaluate the effects of ALK inhibitors on the M phase, time-lapse imaging was performed. M-phase progression of H2228 cells was examined without synchronization of the cell cycle, as we were not able to synchronize the cell cycle of H2228 cells. Several approaches for synchronization, such as the double thymidine block, STLC- and RO-3306-treatment were applied. However, all these approaches failed to synchronize the desirable number of H2228 cells for examining the M-phase progression. H2228 cells were seeded in a 24-well plate and then treated with 0.7 μM TAE684 or DMSO as a solvent control. Hoechst 33342 was added to the culture medium to monitor chromosome movement. Live-cell images were obtained at 5-min intervals for 12 h using the Operetta imaging system. Representative brightfield images of cells treated with DMSO or TAE684 were shown in Figure 28A. The solvent control cells (DMSO) completed the M phase in 60 min. It took TAE-treated cells 50 and 225 min to complete P/PM and M, respectively, which is far longer than control cells.

M-phase cells were divided into three groups: prophase/prometaphase (P/PM), metaphase (M), and anaphase/telophase (A/T) based on the cell shape and chromosome morphology as described in Chapter 2. Moreover, cell death during M phase or mitotic exit without chromosome segregation was indicated by asterisk and hash. Bar graphs show the duration of each phase of individual cells (Fig. 28B). DMSO-treated cells took 30 min to complete P/PM. On the other hand, the duration of P/PM was prolonged to 130 min in TAE684-treated cells. Only 40% of TAE684-treated cells completed the M phase and 37% of cells failed to exit the M phase until the end of the analysis. Additionally, 13% and 10% of cells undergo mitotic cell death and prematurely exit upon TAE684 treatment. These results suggest that ALK inhibitors cause M-phase delay in H2228 cells possessing ALK fusion protein.

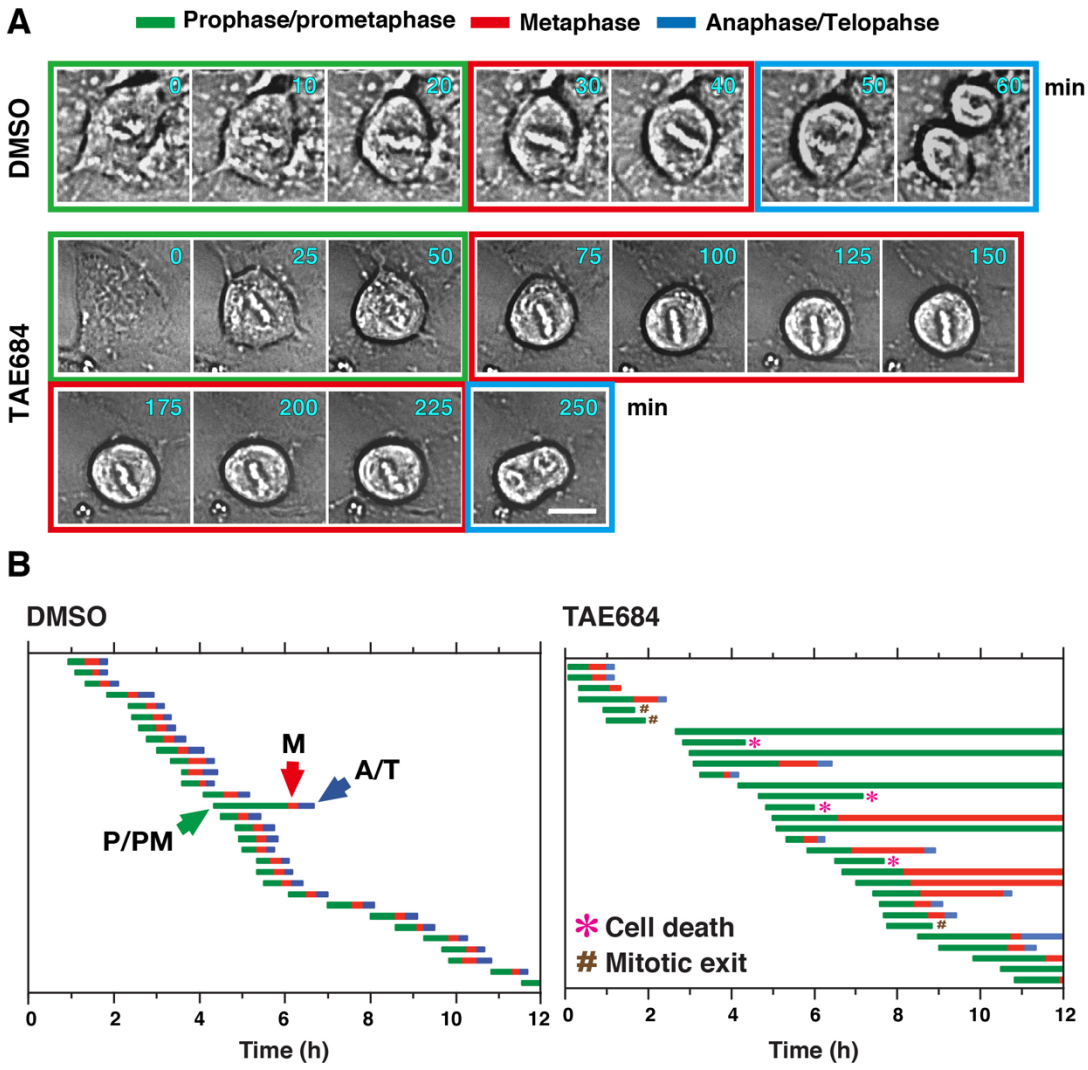

Figure 28. Inhibitor treatment prolongs the duration of P/PM and M. Asynchronous H2228 cells were treated with DMSO (solvent control) or 0.7 μM TAE684 and time-lapse imaging was performed for 12 h. (**A**) Representative images of DMSO- and TAE684-treated cells were shown at 10- and 25-min intervals, respectively. (**B**) Duration of P/PM (green), M (red), and A/T (blue) in individual cells were indicated (DMSO and TAE684, n=30) together with abnormal fates of cells (*, cell death; #, mitotic exit).

3-4. Discussion

Various studies showed that H2228 cells are sensitive to the ALK inhibitors crizotinib, ceritinib, alectinib, TAE684, and so on [104,106]. Some studies also reported that TAE684 can deplete EML4-ALK phosphorylation as well as downstream AKT phosphorylation in H2228 cells [32,34]. However, resistance against these drugs is frequently generated. One study screened 12,800 human ORFs and identified around 54 genes that confer resistance to crizotinib or TAE684 in H3122 cells, and half of these proteins can activate ERK or AKT pathways [107]. To overcome such inevitable resistance against these inhibitors is highly challenging. In this respect, understanding the novel molecular mechanisms underlying EML4-ALK-induced cell proliferation is required to combat the disease. The present study showed that inhibition of EML4-ALK affected M-phase progression through the extended duration of prophase/prometaphase and metaphase, leading to failure in anaphase onset and completion of M phase (Fig. 28B). While many cells remained in prophase/prometaphase and metaphase until 12 h of observation, few cells were dead or prematurely exited. This result suggests that EML4-ALK has a regulatory role in M phase and inhibition of this protein results in suppression of cell proliferation via a defect in the M phase, which is a novel mechanism underlying EML4-ALK inhibition-induced suppression of cell proliferation.

Inhibition of ALK and EML4-ALK showed similar effects on M-phase progression, although their mode of activation and localization are different. Activation of full-length ALK requires ligand-binding, whereas 140 kDa ALK and EML4-ALK reportedly remain in constitutively active form. The EML4 fragment of EML4-ALK fusion takes part in the dimerization and activation of this fusion protein. But the mechanism of ligand-independent activation of 140 kDa ALK is still unclear. However, it can be speculated that ALK may not require the ligand-binding for M-phase regulation. Although the different modes of activation, EML4-ALK fusion can activate many downstream signaling pathways via directly binding with the signaling molecules, both ALK and EML4-ALK trigger several common downstream signaling pathways such as Ras/MEK/ERK, PI3K/Akt and regulate cell proliferation and survival. In H2228 cells, EML4-ALK fusion can multimerize and trigger Ras/MEK/ERK activation via recruitment of RAS through the Grb2 adapter protein as well as full-length ALK. Thus, investigating a common signaling pathway trigger by all three different forms of ALK will provide the insight into the mechanism of M-phase regulation.

From these observations, it can be concluded that EML4-ALK has a role in M-phase regulation. Although the mechanism of TAE684-induced M-phase delay in H2228 cells is yet to be investigated, considering that SAC activation is involved in M-phase delay upon inhibition of

full-length ALK, I speculate that SAC might be involved in M-phase delay in H2228 cells. The summary of this chapter is illustrated in Figure 29.

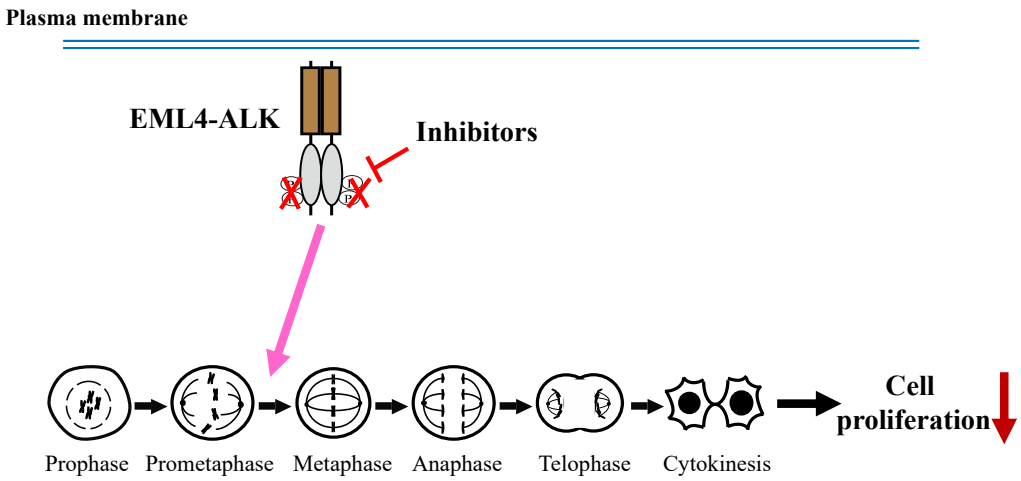

Figure 29. Summary of chapter 3. Inhibition of EML4-ALK with ATP-competitive inhibitors delays M-phase progression, mainly progression from prophase/ prometaphase to metaphase. Such M-phase delay contributes to the suppression of cell proliferation upon inhibitor treatment.

Continuous treatment with ALK inhibitors such as crizotinib or ceritinib causes focal amplification of the KRAS gene in EML4-ALK-positive lung cancer [22]. A clinical study also confirmed the focal amplification of KRAS in 3 out of 15 patients, resulting in acquired resistance against ALK inhibitors. ALK inhibition causes a defect in chromosome alignment that leads to abnormal chromosome segregation and may generate lower CIN that fails to induce cell death. This raises the possibility that resistance could be developed through generating genetically diverse cancer cells, including cancers having focal amplification of genes capable of driving cancer cell proliferation. It is of note that higher chromosome mis-segregation causes CIN beyond the threshold level and leads to cell death without causing genetic diversification. Based on the outcomes of this study, novel polytherapy approaches could be proposed. A combination of ALK inhibitors with agents that increase chromosome mis-segregation may provide higher therapeutic efficacy by causing severe errors in chromosome segregation and induce cell death. Such agents include microtubule-stabilizing drugs, inhibitors of mitotic kinases (PLK1, Aurora kinase inhibitors). Further studies are necessary to develop such effective polytherapy to combat highly heterogeneous cancers.

Conclusion

The present study reveals that inhibition of both ALK and EML4-ALK fusion causes delays in the early M phase, which leads to suppression of cell proliferation. Such delay in the M phase is achieved due to defect in chromosome alignment and/or spindle misorientation. These abnormalities trigger activation of the mitotic checkpoint SAC, which delays anaphase onset. Therefore, it can be concluded that ALK is a novel regulator of M phase and ALK inhibition-induced defect in chromosome alignment is a novel mechanism of suppression of cell proliferation.

The following illustration represents the overall outcome of this study.

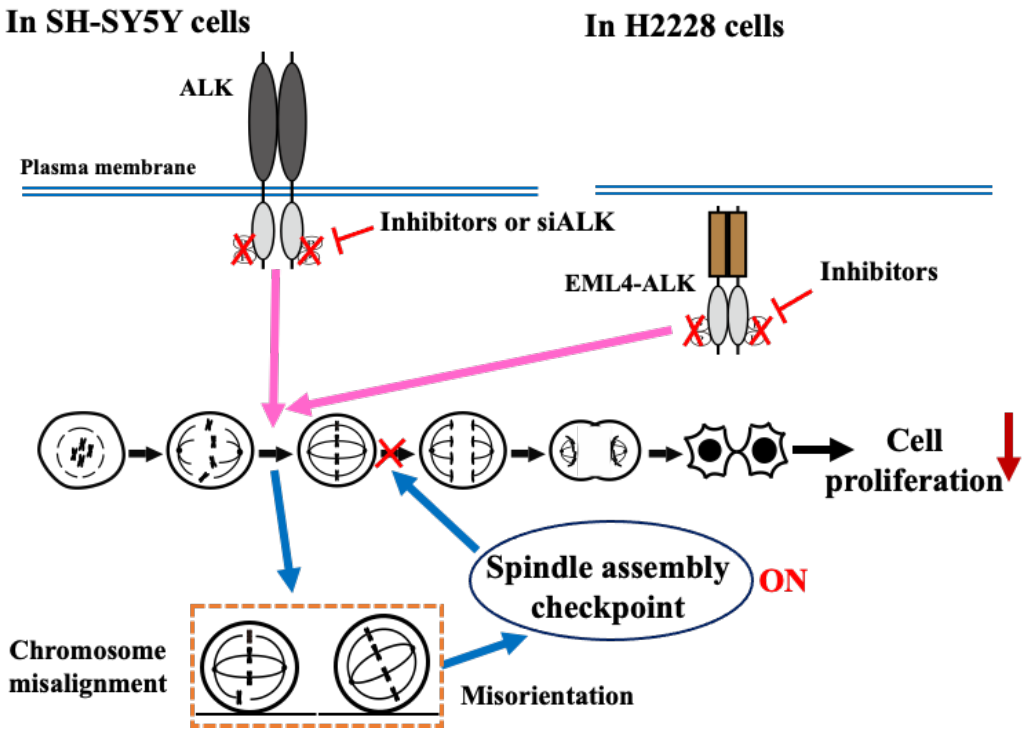

Acknowledgement

First of all, I would like to express my deepest gratitude to my supervisor Professor *Yuji Nakayama* for giving me the opportunity to be a Ph.D. student at Kyoto Pharmaceutical University. His great supervision, invaluable comments, and continuous supports regarding the successful completion of my research work, preparation of the thesis, and every aspect of my study are the most important key to the success of this dissertation.

I am very much grateful to Professor *Eishi Ashihara* and Professor *Masahiro Fujimuro* for their valuable suggestions, advice and comments on my Ph.D. thesis.

I would like to express my profound gratefulness to Associate Prof. *Youhei Saito* and Assistant Prof. *Ryuzaburo Yuki* for their guidance, support and encouragement in various aspects of my study.

I want to give appreciation to all of my past and present lab members and stuffs in the Laboratory of Biochemistry and Molecular Biology, Kyoto Pharmaceutical University for their assistance and friendly attitude that helped me to adjust with the new environment and to continue my journey. Especially, I want to acknowledge Dr. *Takahisa Kuga*, Dr. *Yuichiro Kaibori*, Dr. *Ayana Kakihana*, *Masayoshi Ikeuchi*, *Mari Hagino*, *Daiki Okumura*, *Natsumi Ueta* for their unconditional supports.

I would like to express my gratitude to the “Kyoto Pharmaceutical University” and “Tokyo Biochemical Research Foundation” for their financial supports during my study.

Lastly, I am very much grateful to my family members for their inspirations and supports during my very long period far away from home.

References

1. Iwahara, T.; Fujimoto, J.; Wen, D.; Cupples, R.; Bucay, N.; Arakawa, T.; Mori, S.; Ratzkin, B.; Yamamoto, T. Molecular characterization of ALK, a receptor tyrosine kinase expressed specifically in the nervous system. *Oncogene* **1997**, *14*, 439–449.
2. Morris, S.W.; Naeve, C.; Mathew, P.; James, P.L.; Kirstein, M.N.; Cui, X.; Witte, D.P. ALK the chromosome 2 gene locus altered by the t(2;5) in non-Hodgkin's lymphoma, encodes a novel neural receptor tyrosine kinase that is highly related to leukocyte tyrosine kinase (LTK). *Oncogene* **1997**, *14*, 2175–2188.
3. Lorén, C.E.; Scully, A.; Grabbe, C.; Edeen, P.T.; Thomas, J.; McKeown, M.; Hunter, T.; Palmer, R.H. Identification and characterization of DAlk: A novel Drosophila melanogaster RTK which drives ERK activation in vivo. *Genes to Cells* **2001**, *6*, 531–544.
4. Huang, H. Anaplastic lymphoma kinase (Alk) receptor tyrosine kinase: A catalytic receptor with many faces. *Int. J. Mol. Sci.* **2018**, *19*, 1–20.
5. Lamant, L.; Pulford, K.; Bischof, D.; Morris, S.W.; Mason, D.Y.; Delsol, G.; Mariamé, B. Expression of the ALK tyrosine kinase gene in neuroblastoma. *Am. J. Pathol.* **2000**, *156*, 1711–1721.
6. Webb, T.R.; Slavish, J.; George, R.E.; Look, A.T.; Xue, L.; Jiang, Q.; Cui, X.; Rentrop, W.B.; Morris, S.W. Anaplastic lymphoma kinase: Role in cancer pathogenesis and small-molecule inhibitor development for therapy. *Expert Rev. Anticancer Ther.* **2009**, *9*, 331–356.
7. Weiss, J.B.; Xue, C.; Benice, T.; Xue, L.; Morris, S.W.; Raber, J. Anaplastic Lymphoma Kinase and Leukocyte Tyrosine Kinase: Functions and genetic interactions in learning, memory and adult neurogenesis. *Pharmacol. Biochem. Behav.* **2012**, *100*, 566–574.
8. Bilsland, J.G.; Wheeldon, A.; Mead, A.; Znamenskiy, P.; Almond, S.; Waters, K.A.; Thakur, M.; Beaumont, V.; Bonnert, T.P.; Heavens, R.; et al. Behavioral and neurochemical alterations in mice deficient in anaplastic lymphoma kinase suggest therapeutic potential for psychiatric indications. *Neuropsychopharmacology* **2008**, *33*, 685–700.
9. Stoica, G.E.; Kuo, A.; Powers, C.; Bowden, E.T.; Sale, E.B.; Riegel, A.T.; Wellstein, A. Midkine binds to anaplastic lymphoma kinase (ALK) and acts as a growth factor for different cell types. *J. Biol. Chem.* **2002**, *277*, 35990–35998.
10. Perez-Pinera, P.; Zhang, W.; Chang, Y.; Vega, J.A.; Deuel, T.F. Anaplastic lymphoma kinase is activated through the pleiotrophin/receptor protein-tyrosine phosphatase β/ζ signaling pathway: An alternative mechanism of receptor tyrosine kinase activation. *J. Biol. Chem.* **2007**, *282*, 28683–28690.

11. Guan, J.; Umapathy, G.; Yamazaki, Y.; Wolfstetter, G.; Mendoza, P.; Pfeifer, K.; Mohammed, A.; Hugosson, F.; Zhang, H.; Hsu, A.W.; et al. FAM150A and FAM150B are activating ligands for anaplastic lymphoma kinase. *Elife* **2015**, *4*, 1–16.
12. BARBACID, M. Structural and Functional Properties of the TRK Family of Neurotrophin Receptors. *Ann. N. Y. Acad. Sci.* **1995**, *766*, 442–458.
13. Morris, S.W.; Kirstein, M.N.; Valentine, M.B.; Dittmer, K.G.; Shapiro, D.N.; Saltman, D.L.; Look, A.T. Fusion of a kinase gene, ALK, to a nucleolar protein gene, NPM, in non-Hodgkin's lymphoma. *Science (80-.).* **1994**, *263*, 1281–4.
14. Holla, V.R.; Elamin, Y.Y.; Bailey, A.M.; Johnson, A.M.; Litzenburger, B.C.; Khotskaya, Y.B.; Sanchez, N.S.; Zeng, J.; Shufean, M.A.; Shaw, K.R.; et al. ALK: a tyrosine kinase target for cancer therapy. *Mol. Case Stud.* **2016**, *21*, 139–148.
15. Soda, M.; Choi, Y.L.; Enomoto, M.; Takada, S.; Yamashita, Y.; Ishikawa, S.; Fujiwara, S.I.; Watanabe, H.; Kurashina, K.; Hatanaka, H.; et al. Identification of the transforming EML4-ALK fusion gene in non-small-cell lung cancer. *Nature* **2007**, *448*, 561–566.
16. George, R.E.; Sanda, T.; Hanna, M.; Fröhling, S.; Luther, W.; Zhang, J.; Ahn, Y.; Zhou, W.; London, W.B.; McGrady, P.; et al. Activating mutations in ALK provide a therapeutic target in neuroblastoma. *Nature* **2008**, *455*, 975–978.
17. Chen, Y.; Takita, J.; Choi, Y.L.; Kato, M.; Ohira, M.; Sanada, M.; Wang, L.; Soda, M.; Kikuchi, A.; Igarashi, T.; et al. Oncogenic mutations of ALK kinase in neuroblastoma. *Nature* **2008**, *455*, 971–974.
18. Sasaki, T.; Rodig, S.J.; Chirieac, L.R.; Jänne, P.A. The biology and treatment of EML4-ALK non-small cell lung cancer. *Eur. J. Cancer* **2010**, *46*, 1773–1780.
19. Wiesner, T.; Lee, W.; Obenauf, A.C.; Ran, L.; Murali, R.; Zhang, Q.F.; Wong, E.W.P.; Hu, W.; Scott, S.N.; Shah, R.H.; et al. Alternative transcription initiation leads to expression of a novel ALK isoform in cancer. *Nature* **2015**, *526*, 453–457.
20. Armstrong, F.; Duplantier, M.M.; Trempat, P.; Hieblot, C.; Lamant, L.; Espinos, E.; Racaud-Sultan, C.; Allouche, M.; Campo, E.; Delsol, G.; et al. Differential effects of X-ALK fusion proteins on proliferation, transformation, and invasion properties of NIH3T3 cells. *Oncogene* **2004**, *23*, 6071–6082.
21. Heuckmann, J.M.; Hölzel, M.; Sos, M.L.; Heynck, S.; Balke-Want, H.; Koker, M.; Peifer, M.; Weiss, J.; Lovly, C.M.; Grütter, C.; et al. ALK mutations conferring differential resistance to structurally diverse ALK inhibitors. *Clin. Cancer Res.* **2011**, *17*, 7394–7401.
22. Hrustanovic, G.; Olivas, V.; Pazarentzos, E.; Tulpule, A.; Asthana, S.; Blakely, C.M.; Okimoto, R.A.; Lin, L.; Neel, D.S.; Sabnis, A.; et al. RAS-MAPK dependence underlies a rational polytherapy strategy in EML4-ALK-positive lung cancer. *Nat. Med.* **2015**, *21*, 1038–1047.

23. Slupianek, A.; Nieborowska-Skorska, M.; Hoser, G.; Morrione, A.; Majewski, M.; Xue, L.; Morris, S.W.; Wasik, M.A.; Skorski, T. Role of phosphatidylinositol 3-kinase-Akt pathway in nucleophosmin/anaplastic lymphoma kinase-mediated lymphomagenesis. *Cancer Res.* **2001**, *61*, 2194–2199.
24. Schönherr, C.; Yang, H.L.; Vigny, M.; Palmer, R.H.; Hallberg, B. Anaplastic lymphoma kinase activates the small GTPase Rap1 via the Rap1-specific GEF C3G in both neuroblastoma and PC12 cells. *Oncogene* **2010**, *29*, 2817–2830.
25. Zamo, A.; Chiarle, R.; Piva, R.; Howes, J.; Fan, Y.; Chilosi, M.; Levy, D.E.; Inghirami, G. Anaplastic lymphoma kinase (ALK) activates Stat3 and protects hematopoietic cells from cell death. *Oncogene* **2002**, *21*, 1038–1047.
26. Hallberg, B.; Palmer, R.H. The role of the ALK receptor in cancer biology. *Ann. Oncol.* **2016**, *27*, 4–15.
27. Wan, W.; Albom, M.S.; Lu, L.; Quail, M.R.; Becknell, N.C.; Weinberg, L.R.; Reddy, D.R.; Holskin, B.P.; Angeles, T.S.; Underiner, T.L.; et al. Anaplastic lymphoma kinase activity is essential for the proliferation and survival of anaplastic large-cell lymphoma cells. *Blood* **2006**, *107*, 1617–1623.
28. Gu, T.L.; Tothova, Z.; Scheijen, B.; Griffin, J.D.; Gilliland, D.G.; Sternberg, D.W. NPM-ALK fusion kinase of anaplastic large-cell lymphoma regulates survival and proliferative signaling through modulation of FOXO3a. *Blood* **2004**, *103*, 4622–4629.
29. Voena, C.; Conte, C.; Ambrogio, C.; Erba, E.B.; Boccalatte, F.; Mohammed, S.; Jensen, O.N.; Palestro, G.; Inghirami, G.; Chiarle, R. The tyrosine phosphatase Shp2 interacts with NPM-ALK and regulates anaplastic lymphoma cell growth and migration. *Cancer Res.* **2007**, *67*, 4278–4286.
30. Ambrogio, C.; Voena, C.; Manazza, A.D.; Piva, R.; Riera, L.; Barberis, L.; Costa, C.; Tarone, G.; Defilippi, P.; Hirsch, E.; et al. p130Cas mediates the transforming properties of the anaplastic lymphoma kinase. *Blood* **2005**, *106*, 3907–3916.
31. Motegi, A.; Fujimoto, J.; Kotani, M.; Sakuraba, H.; Yamamoto, T. ALK receptor tyrosine kinase promotes cell growth and neurite outgrowth. *J. Cell Sci.* **2004**, *117*, 3319–3329.
32. Li, Y.; Ye, X.; Liu, J.; Zha, J.; Pei, L. Evaluation of eml4-alk fusion proteins in non-small cell lung cancer using small molecule inhibitors. *Neoplasia* **2011**, *13*, 1–11.
33. Koivunen, J.P.; Mermel, C.; Zejnullahu, K.; Murphy, C.; Lifshits, E.; Holmes, A.J.; Choi, H.G.; Kim, J.; Chiang, D.; Thomas, R.; et al. EML4-ALK fusion gene and efficacy of an ALK kinase inhibitor in lung cancer. *Clin. Cancer Res.* **2008**, *14*, 4275–4283.
34. McDermott, U.; Iafrate, A.J.; Gray, N.S.; Shioda, T.; Classon, M.; Maheswaran, S.; Zhou, W.; Hwan, G.C.; Smith, S.L.; Dowell, L.; et al. Genomic alterations of anaplastic

lymphoma kinase may sensitize tumors to anaplastic lymphoma kinase inhibitors. *Cancer Res.* **2008**, *68*, 3389–3395.

35. Kwak, E.L.; Bang, Y.J.; Camidge, D.R.; Shaw, A.T.; Solomon, B.; Maki, R.G.; Ou, S.H.I.; Dezube, B.J.; Jänne, P.A.; Costa, D.B.; et al. Anaplastic lymphoma kinase inhibition in non-small-cell lung cancer. *N. Engl. J. Med.* **2010**, *363*, 1693–1703.
36. Solomon, B.J.; Mok, T.; Kim, D.W.; Wu, Y.L.; Nakagawa, K.; Mekhail, T.; Felip, E.; Cappuzzo, F.; Paolini, J.; Usari, T.; et al. First-line crizotinib versus chemotherapy in ALK-positive lung cancer. *N. Engl. J. Med.* **2014**, *371*, 2167–2177.
37. Shaw, A.T.; Kim, D.W.; Nakagawa, K.; Seto, T.; Crinó, L.; Ahn, M.J.; De Pas, T.; Besse, B.; Solomon, B.J.; Blackhall, F.; et al. Crizotinib versus chemotherapy in advanced ALK-positive lung cancer. *N. Engl. J. Med.* **2013**, *368*, 2385–2394.
38. Shaw, A.T.; Engelman, J.A. ALK in lung cancer: Past, present, and future. *J. Clin. Oncol.* **2013**, *31*, 1105–1111.
39. Friboulet, L.; Li, N.; Katayama, R.; Lee, C.C.; Gainor, J.F.; Crystal, A.S.; Michellys, P.Y.; Awad, M.M.; Yanagitani, N.; Kim, S.; et al. The ALK inhibitor ceritinib overcomes crizotinib resistance in non-small cell lung cancer. *Cancer Discov.* **2014**, *4*, 662–673.
40. Gainor, J.F.; Dardaei, L.; Yoda, S.; Friboulet, L.; Leshchiner, I.; Katayama, R.; Dagogo-Jack, I.; Gadgeel, S.; Schultz, K.; Singh, M.; et al. Molecular mechanisms of resistance to first- and second-generation ALK inhibitors in ALK -rearranged lung cancer. *Cancer Discov.* **2016**, *6*, 1118–1133.
41. Choi, Y.L.; Soda, M.; Yamashita, Y.; Ueno, T.; Takashima, J.; Nakajima, T.; Yatabe, Y.; Takeuchi, K.; Hamada, T.; Haruta, H.; et al. EML4-ALK mutations in lung cancer that confer resistance to ALK inhibitors. *N. Engl. J. Med.* **2010**, *363*, 1734–1739.
42. Katayama, R.; Shaw, A.T.; Khan, T.M.; Mino-Kenudson, M.; Solomon, B.J.; Halmos, B.; Jessop, N.A.; Wain, J.C.; Yeo, A.T.; Benes, C.; et al. Cancer: Mechanisms of acquired crizotinib resistance in ALK-rearranged lung cancers. *Sci. Transl. Med.* **2012**, *4*, 120ra17.
43. Miyawaki, M.; Yasuda, H.; Tani, T.; Hamamoto, J.; Arai, D.; Ishioka, K.; Ohgino, K.; Nukaga, S.; Hirano, T.; Kawada, I.; et al. Overcoming EGFR bypass signal-induced acquired resistance to ALK tyrosine kinase inhibitors in ALK-translocated lung cancer. *Mol. Cancer Res.* **2017**, *15*, 106–114.
44. Di Paolo, D.; Yang, D.; Pastorino, F.; Emionite, L.; Cilli, M.; Daga, A.; Destafanis, E.; Di Fiore, A.; Piaggio, F.; Brignole, C.; et al. New therapeutic strategies in neuroblastoma: Combined targeting of a novel tyrosine kinase inhibitor and liposomal siRNAs against ALK. *Oncotarget* **2015**, *6*, 28774–28789.
45. Janoueix-Lerosey, I.; Lequin, D.; Brugières, L.; Ribeiro, A.; De Pontual, L.; Combaret, V.; Raynal, V.; Puisieux, A.; Schleiermacher, G.; Pierron, G.; et al. Somatic and germline

activating mutations of the ALK kinase receptor in neuroblastoma. *Nature* **2008**, *455*, 967–970.

46. Ou, S.H.I. Crizotinib: A novel and first-in-class multitargeted tyrosine kinase inhibitor for the treatment of anaplastic lymphoma kinase rearranged non-small cell lung cancer and beyond. *Drug Des. Devel. Ther.* **2011**, *5*, 471–485.
47. Lu, J.; Guan, S.; Zhao, Y.; Yu, Y.; Woodfield, S.E.; Zhang, H.; Yang, K.L.; Bieerkehazhi, S.; Qi, L.; Li, X.; et al. The second-generation ALK inhibitor alectinib effectively induces apoptosis in human neuroblastoma cells and inhibits tumor growth in a TH-MYCN transgenic neuroblastoma mouse model. *Cancer Lett.* **2017**, *400*, 61–68.
48. Zhang, S.; Anjum, R.; Squillace, R.; Nadworny, S.; Zhou, T.; Keats, J.; Ning, Y.; Wardwell, S.D.; Miller, D.; Song, Y.; et al. The potent ALK inhibitor brigatinib (AP26113) overcomes mechanisms of resistance to first- and second-generation ALK inhibitors in preclinical models. *Clin. Cancer Res.* **2016**, *22*, 5527–5538.
49. Nigg, E.A. Cyclin-dependent protein kinases: Key regulators of the eukaryotic cell cycle. *BioEssays* **1995**, *17*, 471–480.
50. Okumura, D.; Hagino, M.; Yamagishi, A.; Kaibori, Y.; Munira, S.; Saito, Y.; Nakayama, Y. Inhibitors of the VEGF Receptor Suppress HeLa S3 Cell Proliferation via Misalignment of Chromosomes and Rotation of the Mitotic Spindle, Causing a Delay in M-Phase Progression. *Int. J. Mol. Sci.* **2018**, *19*, 4014 (15 pages).
51. Vassilev, L.T.; Tovar, C.; Chen, S.; Knezevic, D.; Zhao, X.; Sun, H.; Heimbrook, D.C.; Chen, L. Selective small-molecule inhibitor reveals critical mitotic functions of human CDK1. *Proc. Natl. Acad. Sci. U. S. A.* **2006**, *103*, 10660–10665.
52. Yang, X.; Boehm, J.S.; Yang, X.; Salehi-Ashtiani, K.; Hao, T.; Shen, Y.; Lubonja, R.; Thomas, S.R.; Alkan, O.; Bhimdi, T.; et al. A public genome-scale lentiviral expression library of human ORFs. *Nat. Methods* **2011**, *8*, 659–661.
53. Moog-Lutz, C.; Degoutin, J.; Gouzi, J.Y.; Frobert, Y.; Brunet-De Carvalho, N.; Bureau, J.; Créminon, C.; Vigny, M. Activation and inhibition of anaplastic lymphoma kinase receptor tyrosine kinase by monoclonal antibodies and absence of agonist activity of pleiotrophin. *J. Biol. Chem.* **2005**, *14*, 439–449.
54. Mazot, P.; Cazes, A.; Dingli, F.; Degoutin, J.; Irinopoulou, T.; Boutterin, M.C.; Lombard, B.; Loew, D.; Hallberg, B.; Palmer, R.H.; et al. Internalization and down-regulation of the ALK receptor in neuroblastoma cell lines upon monoclonal antibodies treatment. *PLoS One* **2012**, *7*, e33581.
55. Miyazaki, M.; Otomo, R.; Matsushima-Hibiya, Y.; Suzuki, H.; Nakajima, A.; Abe, N.; Tomiyama, A.; Ichimura, K.; Matsuda, K.; Watanabe, T.; et al. The p53 activator

overcomes resistance to ALK inhibitors by regulating p53-target selectivity in ALK-driven neuroblastomas. *Cell Death Discov.* **2018**, *4*, 1 (17 pages).

56. Fernandes, M.; Duplaquet, L.; Tulasne, D. Proteolytic cleavages of MET: The divide-and-conquer strategy of a receptor tyrosine kinase. *BMB Rep.* **2019**, *52*, 239–249.
57. Cui, J.J.; Tran-Dubé, M.; Shen, H.; Nambu, M.; Kung, P.P.; Pairish, M.; Jia, L.; Meng, J.; Funk, L.; Botrous, I.; et al. Structure based drug design of crizotinib (PF-02341066), a potent and selective dual inhibitor of mesenchymal-epithelial transition factor (c-MET) kinase and anaplastic lymphoma kinase (ALK). *J. Med. Chem.* **2011**, *54*, 6342–6363.
58. Supriya Rajanna, A.S. c-Met: A Potential Target for Current Non-Small-Cell Lung Cancer Therapeutics. *Chemother. Open Access* **2014**, *3*, 1000136 (5 pages).
59. Peng, J.; Qi, S.; Wang, P.; Li, W.; Liu, C.; Li, F. Diagnosis and Prognostic Significance of c-Met in Cervical Cancer: A Meta-Analysis. *Dis. Markers* **2016**, *2016*, 1 (9 pages).
60. Hecht, M.; Papoutsi, M.; Tran, H.D.; Wilting, J.; Schweigerer, L. Hepatocyte growth factor/c-Met signaling promotes the progression of experimental human neuroblastomas. *Cancer Res.* **2004**, *64*, 6109–6118.
61. Factor, V.M.; Seo, D.; Ishikawa, T.; Kaposi-Novak, P.; Marquardt, J.U.; Andersen, J.B.; Conner, E.A.; Thorgeirsson, S.S. Loss of c-Met disrupts gene expression program required for G2/M progression during liver regeneration in mice. *PLoS One* **2010**, *5*, 1 (10 pages).
62. Lopez-Delisle, L.; Pierre-Eugène, C.; Louis-Brennetot, C.; Surdez, D.; Raynal, V.; Baulande, S.; Boeva, V.; Grossetête-Lalami, S.; Combaret, V.; Peuchmaur, M.; et al. Activated ALK signals through the ERK-ETV5-RET pathway to drive neuroblastoma oncogenesis. *Oncogene* **2018**, *37*, 1417–1429.
63. Marzec, M.; Kasprzycka, M.; Liu, X.; Raghunath, P.N.; Wlodarski, P.; Wasik, M.A. Oncogenic tyrosine kinase NPM/ALK induces activation of the MEK/ERK signaling pathway independently of c-Raf. *Oncogene* **2007**, *26*, 813–821.
64. Degoutin, J.; Vigny, M.; Gouzi, J.Y. ALK activation induces Shc and FRS2 recruitment: Signaling and phenotypic outcomes in PC12 cells differentiation. *FEBS Lett.* **2007**, *581*, 727–734.
65. Kaibori, Y.; Saito, Y.; Nakayama, Y. EphA2 phosphorylation at Ser897 by the Cdk1/MEK/ERK/RSK pathway regulates M-phase progression via maintenance of cortical rigidity. *FASEB J.* **2019**, *33*, 5334–5349.
66. Borysova, M.K.; Cui, Y.; Snyder, M.; Guadagno, T.M. Knockdown of B-Raf impairs spindle formation and the mitotic checkpoint in human somatic cells. *Cell Cycle* **2008**, *7*, 2894–2901.

67. Osajima-Hakomori, Y.; Miyake, I.; Ohira, M.; Nakagawara, A.; Nakagawa, A.; Sakai, R. Biological role of anaplastic lymphoma kinase in neuroblastoma. *Am. J. Pathol.* **2005**, *167*, 213–222.
68. Passoni, L.; Longo, L.; Collini, P.; Coluccia, A.M.L.; Bozzi, F.; Podda, M.; Gregorio, A.; Gambini, C.; Garaventa, A.; Pistoia, V.; et al. Mutation-independent anaplastic lymphoma kinase overexpression in poor prognosis neuroblastoma patients. *Cancer Res.* **2009**, *69*, 7338–7346.
69. He, D.; Chen, H.; Muramatsu, H.; Lasek, A.W. Ethanol activates midkine and anaplastic lymphoma kinase signaling in neuroblastoma cells and in the brain. *J. Neurochem.* **2015**, *135*, 508–521.
70. Tanaka, K. Dynamic regulation of kinetochore-microtubule interaction during mitosis. *J. Biochem.* **2012**, *152*, 415–424.
71. Maiato, H.; Gomes, A.M.; Sousa, F.; Barisic, M. Mechanisms of chromosome congression during mitosis. *Biology (Basel).* **2017**, *6*, 13 (56 pages).
72. Silva, P.; Barbosa, J.; Nascimento, A. V.; Faria, J.; Reis, R.; Bousbaa, H. Monitoring the fidelity of mitotic chromosome segregation by the spindle assembly checkpoint. *Cell Prolif.* **2011**, *44*, 391–400.
73. Foley, E.A.; Kapoor, T.M. Microtubule attachment and spindle assembly checkpoint signalling at the kinetochore. *Nat. Rev. Mol. Cell Biol.* **2013**, *14*, 25–37.
74. DeLuca, J.G.; Dong, Y.; Hergert, P.; Strauss, J.; Hickey, J.M.; Salmon, E.D.; McEwen, B.F. Hec1 and Nuf2 are core components of the kinetochore outer plate essential for organizing microtubule attachment sites. *Mol. Biol. Cell* **2005**, *16*, 519–531.
75. Kapoor, T.M.; Lampson, M.A.; Hergert, P.; Cameron, L.; Cimini, D.; Salmon, E.D.; McEwen, B.F.; Khodjakov, A. Chromosomes can congress to the metaphase plate before biorientation. *Science (80-.).* **2006**, *311*, 388–391.
76. Liu, D.; Lampson, M.A. Regulation of kinetochore-microtubule attachments by Aurora B kinase. *Biochem. Soc. Trans.* **2009**, *37*, 976–980.
77. Musacchio, A.; Salmon, E.D. The spindle-assembly checkpoint in space and time. *Nat. Rev. Mol. Cell Biol.* **2007**, *8*, 379–393.
78. Rieder, C.L.; Cole, R.W.; Khodjakov, A.; Sluder, G. The checkpoint delaying anaphase in response to chromosome monoorientation is mediated by an inhibitory signal produced by unattached kinetochores. *J. Cell Biol.* **1995**, *130*, 941–948.
79. Kakihana, A.; Oto, Y.; Saito, Y.; Nakayama, Y. Heat shock-induced mitotic arrest requires heat shock protein 105 for the activation of spindle assembly checkpoint. *FASEB J.* **2019**, *33*, 3936–3953.

80. Zhang, G.; Kruse, T.; López-Méndez, B.; Sylvestersen, K.B.; Garvanska, D.H.; Schopper, S.; Nielsen, M.L.; Nilsson, J. Bub1 positions Mad1 close to KNL1 MELT repeats to promote checkpoint signalling. *Nat. Commun.* **2017**, *8*, 1 (12 pages).
81. De Antoni, A.; Pearson, C.G.; Cimini, D.; Canman, J.C.; Sala, V.; Nezi, L.; Mapelli, M.; Sironi, L.; Faretta, M.; Salmon, E.D.; et al. The Mad1/Mad2 complex as a template for Mad2 activation in the spindle assembly checkpoint. *Curr. Biol.* **2005**, *15*, 214–225.
82. Skinner, J.J.; Wood, S.; Shorter, J.; Englander, S.W.; Black, B.E. The Mad2 partial unfolding model: Regulating mitosis through Mad2 conformational switching. *J. Cell Biol.* **2008**, *183*, 761–768.
83. Faesen, A.C.; Thanasoula, M.; Maffini, S.; Breit, C.; Müller, F.; Van Gerwen, S.; Bange, T.; Musacchio, A. Basis of catalytic assembly of the mitotic checkpoint complex. *Nature* **2017**, *542*, 498–502.
84. Han, J.S.; Holland, A.J.; Fachinetti, D.; Kulukian, A.; Cetin, B.; Cleveland, D.W. Catalytic assembly of the mitotic checkpoint inhibitor BubR1-Cdc20 by a Mad2-induced functional Switch in Cdc20. *Mol. Cell* **2013**, *51*, 92–104.
85. Sudakin, V.; Chan, G.K.T.; Yen, T.J. Checkpoint inhibition of the APC/C in HeLa cells is mediated by a complex of BUBR1, BUB3, CDC20, and MAD2. *J. Cell Biol.* **2001**, *154*, 925–936.
86. Howell, B.J.; McEwen, B.F.; Canman, J.C.; Hoffman, D.B.; Farrar, E.M.; Rieder, C.L.; Salmon, E.D. Cytoplasmic dynein/dynactin drives kinetochore protein transport to the spindle poles and has a role in mitotic spindle checkpoint inactivation. *J. Cell Biol.* **2001**, *155*, 1159–1172.
87. Lara-Gonzalez, P.; Westhorpe, F.G.; Taylor, S.S. The spindle assembly checkpoint. *Curr. Biol.* **2012**, *22*, R966–R980.
88. Tame, M.A.; Raaijmakers, J.A.; Afanasyev, P.; Medema, R.H. Chromosome misalignments induce spindle-positioning defects. *EMBO Rep.* **2016**, *17*, 317–325.
89. Kotak, S.; Busso, C.; Gönczy, P. Cortical dynein is critical for proper spindle positioning in human cells. *J. Cell Biol.* **2012**, *199*, 97–110.
90. Kuniyasu, K.; Iemura, K.; Tanaka, K. Delayed chromosome alignment to the spindle equator increases the rate of chromosome missegregation in cancer cell lines. *Biomolecules* **2019**, *9*, 10 (17 pages).
91. Potapova, T.; Gorbsky, G.J. The consequences of chromosome segregation errors in mitosis and meiosis. *Biology (Basel).* **2017**, *6*, 12 (33 pages).
92. Gascoigne, K.E.; Taylor, S.S. How do anti-mitotic drugs kill cancer cells? *J. Cell Sci.* **2009**, *122*, 2579–2585.

93. Hrustanovic, G.; Olivas, V.; Pazarentzos, E.; Tulpule, A.; Asthana, S.; Blakely, C.M.; Okimoto, R.A.; Lin, L.; Neel, D.S.; Sabnis, A.; et al. HHS Public Access. *Nat. Med.* **2015**, *21*, 1038–1047.

94. Monda, J.K.; Cheeseman, I.M. The kinetochore-microtubule interface at a glance. *J. Cell Sci.* **2018**, *131*, 214577 (7 pages).

95. Samora, C.P.; Mogessie, B.; Conway, L.; Ross, J.L.; Straube, A.; McAinsh, A.D. MAP4 and CLASP1 operate as a safety mechanism to maintain a stable spindle position in mitosis. *Nat. Cell Biol.* **2011**, *13*, 1040–1052.

96. Houtman, S.H.; Rutteman, M.; De Zeeuw, C.I.; French, P.J. Echinoderm microtubule-associated protein like protein 4, a member of the echinoderm microtubule-associated protein family, stabilizes microtubules. *Neuroscience* **2007**, *144*, 1373–1382.

97. Pollmann, M.; Parwaresch, R.; Adam-Klages, S.; Kruse, M.L.; Buck, F.; Heidebrecht, H.J. Human EML4, a novel member of the EMAP family, is essential for microtubule formation. *Exp. Cell Res.* **2006**, *312*, 3241–3251.

98. Chen, D.; Ito, S.; Yuan, H.; Hyodo, T.; Kadomatsu, K.; Hamaguchi, M.; Senga, T. EML4 promotes the loading of NUDC to the spindle for mitotic progression. *Cell Cycle* **2015**, *14*, 1529–1539.

99. P., S.; J., Z.; C., S.; L., Z. Alectinib treatment response in lung adenocarcinoma patient with novel EML4-ALK variant. *Thorac. Cancer* **2018**, *9*, 1327–1332.

100. Lin, E.; Li, L.; Guan, Y.; Soriano, R.; Rivers, C.S.; Mohan, S.; Pandita, A.; Tang, J.; Modrusan, Z. Exon array profiling detects EML4-ALK fusion in breast, colorectal, and non-small cell lung cancers. *Mol. Cancer Res.* **2009**, *7*, 1466–1476.

101. Young, L.C.; Takeuchi, K.; Soda, M.; Inamura, K.; Togashi, Y.; Hatano, S.; Enomoto, M.; Hamada, T.; Haruta, H.; Watanabe, H.; et al. Identification of novel isoforms of the EML4-ALK transforming gene in non-small cell lung cancer. *Cancer Res.* **2008**, *68*, 4971–4976.

102. Bayliss, R.; Choi, J.; Fennell, D.A.; Fry, A.M.; Richards, M.W. Molecular mechanisms that underpin EML4-ALK driven cancers and their response to targeted drugs. *Cell. Mol. Life Sci.* 2016, 1209–1224.

103. Heuckmann, J.M.; Balke-Want, H.; Malchers, F.; Peifer, M.; Sos, M.L.; Koker, M.; Meder, L.; Lovly, C.M.; Heukamp, L.C.; Pao, W.; et al. Differential protein stability and ALK inhibitor sensitivity of EML4-ALK fusion variants. *Clin. Cancer Res.* **2012**, *18*, 4682–4690.

104. Tanizaki, J.; Okamoto, I.; Takezawa, K.; Sakai, K.; Azuma, K.; Kuwata, K.; Yamaguchi, H.; Hatashita, E.; Nishio, K.; Janne, P.A.; et al. Combined effect of ALK and MEK inhibitors in EML4-ALK-positive non-small-cell lung cancer cells. *Br. J. Cancer* **2012**, *106*, 763–767.

105. Yamada, T.; Takeuchi, S.; Nakade, J.; Kita, K.; Nakagawa, T.; Nanjo, S.; Nakamura, T.; Matsumoto, K.; Soda, M.; Mano, H.; et al. Paracrine receptor activation by microenvironment triggers bypass survival signals and ALK inhibitor resistance in EML4-ALK lung cancer cells. *Clin. Cancer Res.* **2012**, *18*, 3592–3602.
106. Shaw, A.T.; Yeap, B.Y.; Mino-Kenudson, M.; Digumarthy, S.R.; Costa, D.B.; Heist, R.S.; Solomon, B.; Stubbs, H.; Admane, S.; McDermott, U.; et al. Clinical features and outcome of patients with non-small-cell lung cancer who harbor EML4-ALK. *J. Clin. Oncol.* **2009**, *27*, 4247–4253.
107. Wilson, F.H.; Johannessen, C.M.; Piccioni, F.; Tamayo, P.; Kim, J.W.; VanAllen, E.M.; Corsello, S.M.; Capelletti, M.; Calles, A.; Butaney, M.; et al. A Functional Landscape of Resistance to ALK Inhibition in Lung Cancer. *Cancer Cell* **2015**, *27*, 397–408.

Supplemental information

The followings are the full-length blots of the Western blotting analyses

Figure 6A

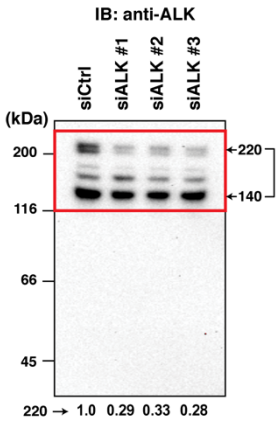

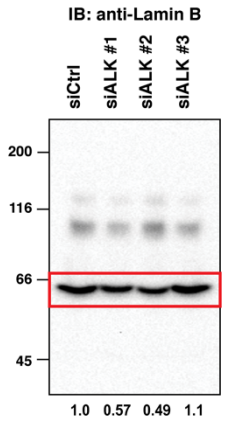

Figure 6C

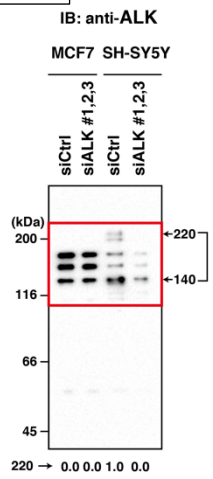

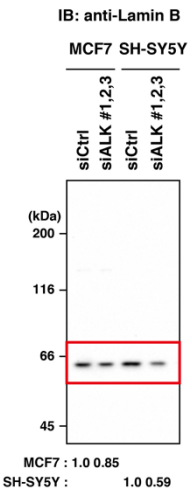

Figure 6B

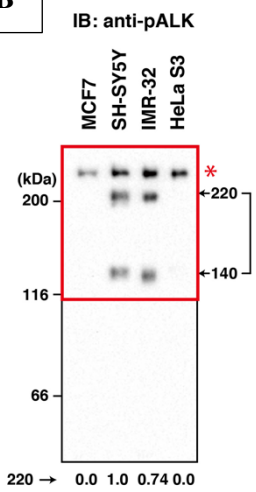

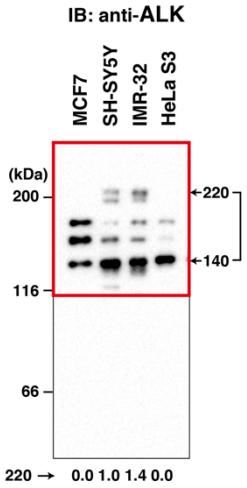

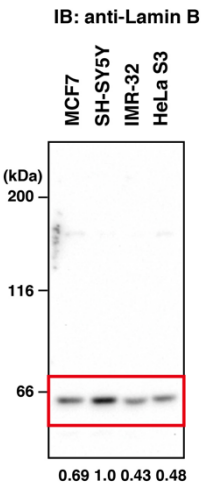

Figure 10

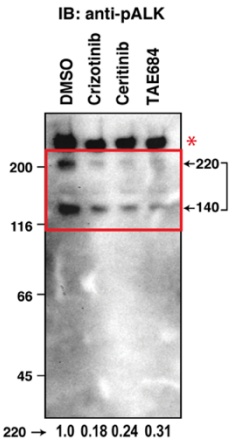

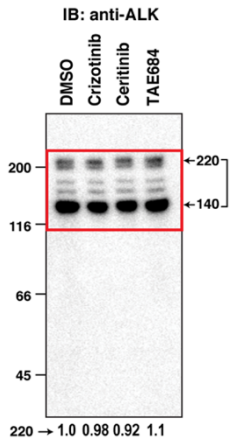

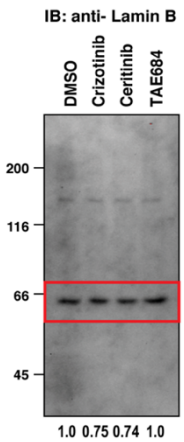

Figure 11B

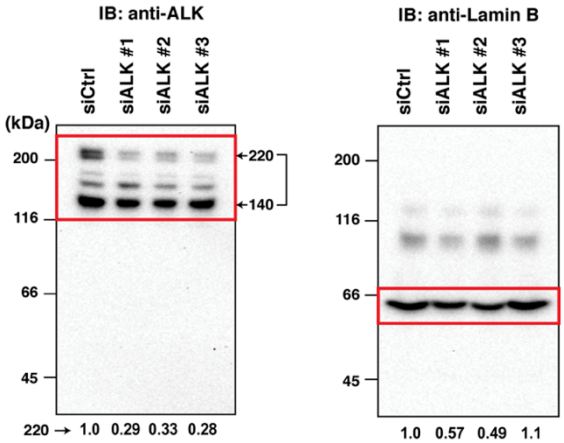

Figure 12B

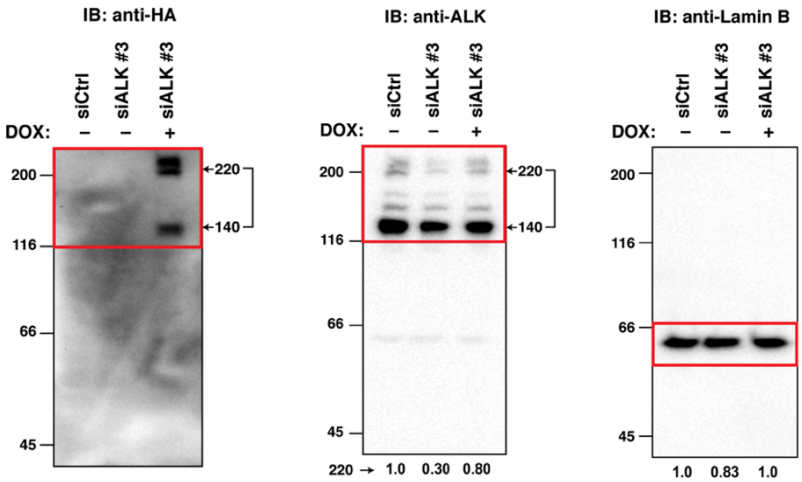

Figure 13

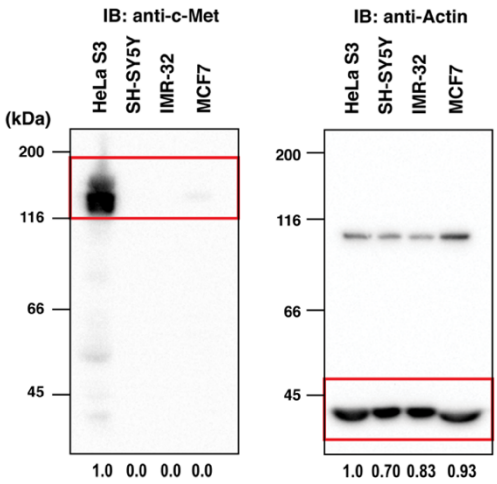

Figure 15B

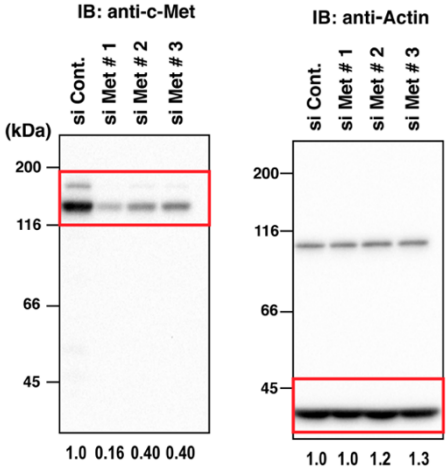

Figure 27

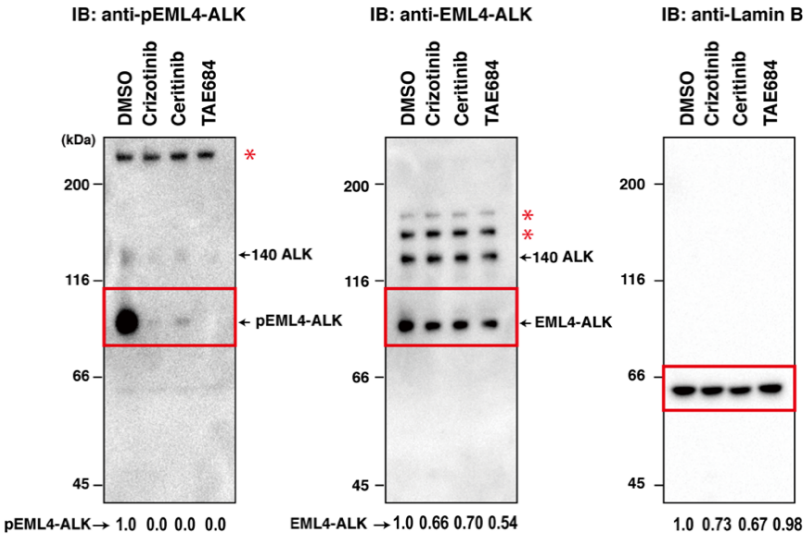
IB: anti-pEML4-ALK
IB: anti-EML4-ALK
IB: anti-Lamin B
DMSO
Crizotinib
Ceritinib
TAE684
(kDa)
200
116
66
45
*
**
←140 ALK
← pEML4-ALK
← EML4-ALK
pEML4-ALK→ 1.0 0.0 0.0 0.0
EML4-ALK →1.0 0.66 0.70 0.54
1.0 0.73 0.67 0.98